

**THE ROLE OF GLUTAREDOXIN-2 IN REGULATING
SUPEROXIDE/HYDROGEN PEROXIDE FORMATION FROM
LIVER AND CARDIAC TISSUE**

By © Julia Chalker

A Thesis submitted to the School of Graduate Studies in partial fulfilment of the
requirements for the degree of

Master of Science

Department of Biochemistry, Faculty of Science

Memorial University of Newfoundland

November 2017

St. John's

Newfoundland and Labrador

Abstract

S-glutathionylation has been found to control the production of mitochondrial reactive oxygen species (ROS), regulated by glutaredoxin-2 (GRX2). GRX2 deficiency is associated with heart disease, neurological deficits, and cataracts, which have all been linked to increased ROS production. Using GRX2^{+/-} and GRX2^{-/-} mice, we have shown that GRX2 controls the emission of superoxide (O₂^{•-}) /hydrogen peroxide (H₂O₂) from liver and cardiac mitochondria in a tissue and substrate dependant manner. In cardiac tissue, GRX2^{+/-} and GRX2^{-/-} mitochondria display increased O₂^{•-}/H₂O₂ production compared to WT when metabolizing succinate. In liver tissue, mitochondria isolated from GRX2^{-/-} mice show a significant decrease in O₂^{•-}/H₂O₂ emission when metabolizing pyruvate and 2-oxoglutarate. Our results show that GRX2 plays an important role in controlling mitochondrial ROS production in different tissues. Future work into the method of ROS control by GRX2 could highlight a method to control ROS production and prevent tissue damage from increased ROS.

Acknowledgements

I would foremost like to thank my supervisor, Dr. Ryan Mailloux. Without his guidance, advice, and expertise, the completion of this thesis would not have been possible.

I would also like to thank my supervisory committee, Dr. John Brosnan and Dr. John Robinson, for their help and supervision of my progress in this project.

Furthermore, I would like to thank our research assistant, Danielle Gardiner, who provided invaluable help with experimental work and kept the lab running smoothly, allowing for the completion of this thesis.

I would also like to thank the student members of the Mailloux lab group, past and present, for their help with this project. Thank you to Marisa O'Brien, Liam Slade, Adrian Young, and Nidhi Kuksal.

Table of Contents

| | |
|--|-------------|
| Abstract..... | II |
| Acknowledgements | III |
| Table of Contents | IV |
| List of Tables | VIII |
| List of Figures..... | IX |
| List of Abbreviations | XI |
| 1. Introduction..... | 1 |
| 1.1. Nutrient metabolism | 1 |
| 1.1.1. Glycolysis | 1 |
| 1.1.2. Beta-oxidation of fatty acids..... | 3 |
| 1.1.3. Protein oxidation..... | 4 |
| 1.1.4. The Krebs cycle | 6 |
| 1.1.5. Oxidative phosphorylation | 10 |
| 1.2. Reactive oxygen species in mitochondria | 17 |
| 1.3. Mitochondrial hydrogen peroxide clearing systems | 21 |
| 1.3.1. Glutathione antioxidant system | 21 |
| 1.3.2. Peroxiredoxin antioxidant system | 23 |
| 1.4. Control over ROS production..... | 24 |
| 1.4.1. Proton leak..... | 26 |
| 1.4.2. Supercomplexes..... | 27 |
| 1.4.3. Redox signals..... | 28 |
| 1.4.3.1. Sulfenylation..... | 28 |
| 1.4.3.2. Protein S-glutathionylation..... | 30 |

| | | |
|-------------|---|-----------|
| 1.5. | Glutaredoxin | 32 |
| 1.6. | S-Glutathionylation reactions in ROS formation..... | 36 |
| 1.6.1. | Complex I..... | 36 |
| 1.6.2. | Succinate dehydrogenase..... | 38 |
| 1.6.3. | OGDH and PDH..... | 38 |
| 1.6.4. | Uncoupling proteins 2 and 3..... | 41 |
| 1.7. | Research objectives | 42 |
| 1.7.1. | Hypothesis | 42 |
| 2. | Materials and Methods..... | 43 |
| 2.1. | Breeding | 43 |
| 2.2. | Genotyping..... | 44 |
| 2.2.1. | DNA extraction..... | 44 |
| 2.2.2. | Polymerase chain reaction | 44 |
| 2.2.3. | Gel electrophoresis | 44 |
| 2.3. | Mitochondrial isolation..... | 47 |
| 2.3.1. | Bradford assay | 48 |
| 2.4. | Amplex Ultra Red assay | 49 |
| 2.4.1. | Measurement of $O_2^{\bullet-}/H_2O_2$ formation during pyruvate and 2-oxoglutarate oxidation | 51 |
| 2.4.2. | Measurement of $O_2^{\bullet-}/H_2O_2$ formation during succinate oxidation | 54 |
| 2.4.3. | Examining the effect of membrane potential on ROS production | 55 |
| 2.5. | Polarographic measurement of oxygen consumption | 55 |
| 2.6. | Gel electrophoresis and Immunoblot | 59 |
| 2.7. | Data analysis | 64 |
| 3. | Results | 65 |
| 3.1. | Profile of GRX2 deficient mice | 65 |

| | | |
|-------------|--|------------|
| 3.1.1. | Mouse genotyping and confirmation of GRX2 deficiency | 65 |
| 3.1.2. | Effect of GRX2 deficiency on total body and organ weight | 65 |
| 3.1.3. | GRX2 deficiency does not induce a compensatory increase in GRX1 expression | 69 |
| 3.2. | Examination of the O₂[•]/H₂O₂ release potential of GRX2 deficient mitochondria..... | 69 |
| 3.2.1. | O ₂ [•] /H ₂ O ₂ release by liver mitochondria oxidizing Krebs cycle-linked substrates | 69 |
| 3.2.2. | O ₂ [•] /H ₂ O ₂ release by cardiac mitochondria oxidizing Krebs cycle-linked substrates | 78 |
| 3.2.3. | O ₂ [•] /H ₂ O ₂ release by liver and cardiac mitochondria supplemented with succinate | 80 |
| 3.2.4. | Tissue specific effect of substrates in O ₂ [•] /H ₂ O ₂ production..... | 84 |
| 3.2.5. | GRX2 loss on proton gradient driven O ₂ [•] /H ₂ O ₂ production | 86 |
| 3.3. | Mitochondrial respiration | 88 |
| 4. | Discussion..... | 92 |
| 4.1. | Summary | 92 |
| 4.2. | Importance of GRX2 in health and development | 94 |
| 4.2.1. | GRX2 is required to regulate cell metabolism and survival..... | 94 |
| 4.2.2. | Understanding the physiological function of GRX2 using mouse models | 96 |
| 4.2.3. | The role of GRX2 in embryogenesis | 99 |
| 4.3. | Production of O₂[•]/H₂O₂ during pyruvate/2-oxoglutarate oxidation | 100 |
| 4.3.1. | Liver mitochondria metabolizing pyruvate/2-oxoglutarate..... | 100 |
| 4.3.2. | Cardiac mitochondria metabolizing pyruvate/2-oxoglutarate | 103 |
| 4.4. | Production of O₂[•]/H₂O₂ during succinate supplementation | 104 |
| 4.4.1. | Liver mitochondria metabolizing succinate | 104 |
| 4.4.2. | Cardiac mitochondria metabolizing succinate..... | 106 |
| 4.5. | Proton gradient on O₂[•]/H₂O₂ production | 107 |
| 4.6. | Conclusions | 108 |
| 4.7. | Future Directions..... | 109 |

5. References..... 110

List of Tables

| | |
|---|----|
| Table 1.1: Known targets of S-glutathionylation..... | 31 |
| Table 2.1: DNA sequence of primers used for Grx2 genotyping | 45 |
| Table 2.2: Polymerase chain reaction protocol for Grx2 genotyping | 46 |
| Table 2.3: Immunoblot gel recipes | 61 |
| Table 2.4: Immunoblot specifications..... | 63 |

List of Figures

| | |
|--|----|
| Figure 1.1: The Krebs cycle..... | 7 |
| Figure 1.2: The pyruvate dehydrogenase complex | 8 |
| Figure 1.3: The electron transport chain | 11 |
| Figure 1.4: Sites of ROS production in mitochondria | 19 |
| Figure 1.5: Catalytic cycle and functions of the glutathione system | 22 |
| Figure 1.6: Peroxiredoxin catalytic cycle | 25 |
| Figure 1.7: Reactivity of thiols | 29 |
| Figure 1.8: The dithiol and monothiol mechanisms of GRX..... | 35 |
| Figure 2.1: Examples of Bradford assay standard curve for protein concentration determination | 50 |
| Figure 2.2: Examples of AUR assay standard curve for determination of O ₂ ^{•-} /H ₂ O ₂ concentration | 52 |
| Figure 2.3: Sites of action for different inhibitors of the Krebs cycle and ETC..... | 53 |
| Figure 2.4: The different states of respiration..... | 56 |
| Figure 2.5: Assembly of the Hansatech oxytherm electrode | 58 |
| Figure 3.1: Gel electrophoresis of PCR Grx2 gene amplification | 66 |
| Figure 3.2: Confirmation of GRX2 deficiency | 67 |
| Figure 3.3: Overall body weight of GRX2 deficient mice..... | 68 |
| Figure 3.4: Cardiac and liver weight in GRX2 deficient mice | 70 |
| Figure 3.5: There is no compensatory increase in GRX1 protein expression in GRX2 deficient mice..... | 71 |
| Figure 3.6: GRX2 deficiency increases the overall number and intensity of immunoreactive bands corresponding to PSSG adducts..... | 72 |

| | |
|---|----|
| Figure 3.7: O ₂ ^{•-} /H ₂ O ₂ production rates in liver mitochondria oxidizing pyruvate or 2-oxoglutarate | 74 |
| Figure 3.8: Protein abundance of OGDH and PDH in liver mitochondria of GRX2 deficient mice | 76 |
| Figure 3.9: Production of O ₂ ^{•-} /H ₂ O ₂ in liver mitochondria supplemented with pyruvate or 2-oxoglutarate normalized to enzyme content. | 77 |
| Figure 3.10: Production of O ₂ ^{•-} /H ₂ O ₂ in cardiac mitochondria supplemented with pyruvate or 2-oxoglutarate..... | 79 |
| Figure 3.11: Immunoblot of OGDH and PDH cardiac abundance between genotypes | 81 |
| Figure 3.12: Sources of O ₂ ^{•-} /H ₂ O ₂ production in succinate supplemented mitochondria | 82 |
| Figure 3.13: Tissue specific effects of different substrates on wildtype mice | 85 |
| Figure 3.14: Production of O ₂ ^{•-} /H ₂ O ₂ during state 3 respiratory conditions between genotypes. | 87 |
| Figure 3.15: Changes in respiratory states due to loss of GRX2 | 89 |
| Figure 3.16: Deregulated S-glutathionylation in the liver may lead to decreased proton leak..... | 91 |

List of Abbreviations

| | |
|-------------------|--|
| 4-HNE | 4-Hydroxynonal |
| Acn | Aconitase |
| ADP | Adenosine diphosphate |
| Ag | Silver |
| ANOVA | Analysis of variance |
| ANT | Adenine nucleotide transporter |
| APS | Ammonium persulfate |
| ATP | Adenosine triphosphate |
| AUR | Amplex Ultra Red |
| BCOADHC | Branched chain 2-oxoacid dehydrogenase complex |
| bp | Base pairs |
| BSA | Bovine serum albumin |
| c ₁ | c-type heme |
| CO ₂ | Carbon dioxide |
| CoA | Coenzyme A |
| CoQ | Coenzyme Q/Ubiquinone |
| CuSOD | Copper superoxide dismutase |
| Cys | Cysteine |
| Cyt c | Cytochrome c |
| Deglu | Deglutathionylation |
| DH | Dehydrogenase |
| DHODH | Dihydrooroate dehydrogenase complex |
| DNA | Deoxyribonucleic acid |
| DTT | Dithiothreitol |
| <i>E. coli</i> | <i>Escherichia coli</i> |
| E _H | Redox potential |
| ETC | Electron transport chain |
| ETF:QOR | Electron transferring flavoprotein:quinone oxidoreductase |
| FAD | Flavin adenine nucleotide |
| FADH ₂ | Reduced flavin adenine nucleotide |
| FCCP | Carbonylcyanide- <i>p</i> -trifluoromethoxyphenylhydrazone |
| Fe-S | Iron sulfur cluster |
| FMN | Flavin mononucleotide |
| g | Grams |
| GDP | Guanine diphosphate |
| Glu | Glutathionylated |
| GPx | Glutathione peroxidase |
| GR | Glutathione reductase |
| GRX | Glutaredoxin |

| | |
|-------------------------------|--|
| GRX1 | Glutaredoxin-1 |
| GRX2 | Glutaredoxin-2 |
| GRX2 ^{+/-} | Glutaredoxin-2 heterozygous |
| GRX2 ^{-/-} | Glutaredoxin-2 knockout |
| GRX-SS | Glutaredoxin with an intra-disulfide bond |
| GRX-SSG | Glutaredoxin with bound glutathione |
| GSH | Glutathione |
| GSSG | Glutathione disulfide |
| GST | Glutathione-S-transferase |
| GTP | Guanine triphosphate |
| h | Hour |
| H ⁺ | Proton |
| HCl | Hydrochloric acid |
| H ₂ O | Water |
| H ₂ O ₂ | Hydrogen peroxide |
| HRP | Horse radish peroxidase |
| I/R | Ischemia reperfusion |
| k | Rate of catalysis |
| KCl | Potassium chloride |
| KDa | Kilodalton |
| KJ | Kilojoules |
| KMV | α -keto- β -methyl-n-valeric acid |
| LSD | Least significant difference |
| M | Molar |
| mg | Milligram |
| mGPDH | Mitochondrial glycerol-3-phosphate dehydrogenase |
| min | Minute |
| mL | Millilitre |
| mM | Millimolar |
| MnSOD | Manganese superoxide dismutase |
| mol | Mole |
| MPTP | Mitochondrial permeability transition pore |
| N | Number |
| NaCl | Sodium chloride |
| NAD ⁺ | Nicotinamide adenine dinucleotide |
| NADH | Reduced nicotinamide adenine dinucleotide |
| NaN ₃ | Sodium azide |
| NH ₄ ⁺ | Ammonium ion |
| nm | Nanometer |
| nM | Nanomolar |
| Nrf2 | Nuclear factor (erythroid-derived 2)-like 2 |
| O ₂ | Molecular oxygen |
| O ₂ ^{•-} | Superoxide |
| OADHC | 2-oxoadipate dehydrogenase complex |

| | |
|-------------------|--|
| OGDH/OGDHC | 2-Oxoglutarate dehydrogenase complex |
| OH• | Hydroxyl radical |
| P | Phosphate |
| PCR | Polymerase chain reaction |
| PDH/PDHC | Pyruvate dehydrogenase complex |
| pH | Potential of hydrogen |
| pM | Picomolar |
| PMF | Proton motor force |
| PRX | Peroxiredoxin |
| PSSG | Protein glutathione mixed disulfide |
| Pt | Platinum |
| PVDF | Polyvinylidene difluoride |
| RCR | Respiratory control ratio |
| ROS | Reactive oxygen species |
| SDH | Succinate dehydrogenase |
| SDHA | Succinate dehydrogenase subunit A |
| SDS | Sodium dodecyl sulfate |
| SEM | Standard error of mean |
| Ser | Serine |
| SOD | Superoxide dismutase |
| SOH | Sulfenic acid |
| SO ₂ H | Sulfinic acid |
| SO ₃ H | Sulfonic acid |
| TBS | Tris-buffered saline |
| TBS-T | Tris-buffered saline + tween-20 |
| TEMED | Tetramethylethylenediamine |
| TMPD | N,N,N',N'-tetramethyl-phenylenediamine |
| TPP | Thiamine pyrophosphate |
| TR | Thioredoxin reductase |
| TRX | Thioredoxin |
| Tyr | Tyrosine |
| UCP | Uncoupling protein |
| UQ | Ubiquinone |
| UQH ₂ | Ubiquinol |
| V | Volts |
| v/v | Volume per volume |
| WT | Wildtype |
| w/v | Weight per volume |
| ZnSOD | Zinc superoxide dismutase |
| °C | Degrees Celsius |
| ∞ | Infinity |
| μg | Micrograms |
| μL | Microliters |
| μM | Micromolar |

1. Introduction

1.1. Nutrient metabolism

Nutrient metabolism encompasses the many chemical reactions that occur in the body which are responsible for converting food into usable energy. Digested food can be broken down into three types of macromolecules: carbohydrates, lipids and proteins. These macromolecules can undergo catabolism to provide energy for powering cellular processes, or can be used for anabolism, in which they are used to build necessary proteins, lipids, nucleic acids or carbohydrates. During catabolism, each type of macromolecule is processed through different metabolic pathways that ultimately converge on the Krebs cycle in the mitochondria. Exceptions include mitochondrial dehydrogenases that can transfer electrons from certain types of carbon directly to the ubiquinone (UQ) pool (*e.g.* electron transferring flavoprotein:quinone oxidoreductase, ETF:QOR) Once carbon reaches this point, it's electrons are converted to reducing equivalents that can be used by the electron transport chain (ETC) to form adenosine triphosphate (ATP). ATP is the energy currency of the cell, which is required to power the cellular reactions of the body.

1.1.1. Glycolysis

Carbohydrates ingested from dietary sources are first broken down into monosaccharide units, which most commonly include the hexose sugars glucose, fructose, and galactose, prior to absorption via the gut (1). After absorption, these monosaccharides are distributed throughout the body for energy metabolism and storage. The use of monosaccharides for energy metabolism requires their breakdown in the cytoplasm by glycolysis, a series of ten enzymatic reactions that convert one monosaccharide into two molecules of pyruvate. The first five steps of glycolysis are labelled as the preparatory phase. In these steps, glucose is broken down into two three carbon

sugars. This phase requires the input of energy, two ATP per molecule of glucose, to proceed. The first step of glycolysis is catalyzed by hexokinase, which expends ATP to phosphorylate glucose, forming membrane impermeable glucose-6-phosphate. (2). The hexokinase isozyme in liver, glucokinase, has a lower affinity for glucose which is integral for maintaining blood glucose levels (3). The next step converts glucose-6-phosphate to fructose-6-phosphate via phosphoglucose isomerase (4). This is also the entry point for phosphorylated fructose into glycolysis. Next, a second molecule of ATP in the preparatory phase is used by phosphofructokinase to phosphorylate fructose-6-phosphate, producing fructose-1,6-bisphosphate (5). In the two remaining steps, fructose-1,6-bisphosphate is cleaved, forming two molecules of glyceraldehyde-3-phosphate (1).

The second half of glycolysis is known as the payoff phase. This phase encompasses five steps which ultimately end in the production of two pyruvate molecules per glucose. The second half is labelled the payoff phase because it produces four ATP and two molecules of reduced nicotinamide adenine dinucleotide (NADH) per glucose molecule. The sixth step of glycolysis is the oxidation and phosphorylation of the glyceraldehyde-3-phosphate, producing NADH from nicotinamide adenine dinucleotide (NAD^+) (6). The phosphate on the carbon-1 position of 1,3-bisphosphoglycerate is then transferred to adenosine diphosphate (ADP) forming ATP by phosphoglycerate kinase via a process called substrate level phosphorylation (7). The eighth and ninth steps involve an isomerase and enolase reaction which form high energy phosphoenolpyruvate (1). The last step of glycolysis encompasses the second substrate level phosphorylation of the pathway, forming ATP and producing the end product, pyruvate (8). Overall, glycolysis produces a net amount of two ATP and two NADH per molecule of glucose. If the cell does not have access to oxygen, it can obtain its energy anaerobically via glycolysis. However, aerobic respiration, which is discussed in detail below, produces a much larger sum of

ATP per glucose. In theory, aerobic respiration produces 38 ATP per molecule of glucose, but the yield is likely closer to 30 ATP in the cell (9). Anaerobic respiration still occurs throughout the body, most notably in red blood cells or fast twitch muscle fibers, and involves the re-oxidation of NADH through lactic acid fermentation.

1.1.2. Beta-oxidation of fatty acids

Fatty acids that are obtained from the diet or from adipocyte storage can be oxidized to transform energy to a useable form. Fatty acids enter the mitochondrial matrix via the acyl-carnitine/carnitine antiporter (10). Once inside the matrix, fatty acids are systematically stripped of electrons through β -oxidation which drives ATP production. Fatty acids are shortened two carbons per cycle by removing one acetyl-CoA unit from the terminal carboxyl end of the molecule (1). This process is performed in four steps. The first step involves the formation of a double bond between the alpha and beta carbon of the fatty acid by acyl-CoA dehydrogenase, reducing flavin adenine dinucleotide (FAD) to form a molecule of reduced flavin adenine dinucleotide (FADH₂) (11). A molecule of water is added to the double bond by the enzyme enoyl-CoA hydratase, forming an alcohol group on the beta carbon of the fatty acid (12). In the third step, the alcohol is then dehydrogenated to a ketone by the enzyme β -hydroxyacyl-CoA dehydrogenase (1). The electrons from this step are used to form NADH. The final step of beta-oxidation involves the liberation of a two-carbon unit that combines with coenzyme A (CoA) to form acetyl-CoA, facilitated by the enzyme thiolase (1). These four steps are repeated until the fatty acid has been completely broken down into acetyl-CoA. If the fatty acid is unsaturated, an extra step is required for isomerization into a trans configuration double bond, which can then proceed with beta-oxidation (1). Overall, each pass of beta-oxidation produces one molecule of acetyl-CoA, FADH₂ and NADH. Acetyl-CoA can have many fates within the body. Acetyl-CoA produced from

oxidation of fatty acids in the mitochondria is mostly used to generate ATP via its entry into the Krebs cycle. However, it can also be used to make ketone bodies, a valuable source of energy for various tissues.

1.1.3. Protein oxidation

Unlike carbohydrates and fatty acids, amino acids obtained from the digestion of proteins cannot be stored in the body for later use. They are either used to build proteins or they are oxidized for energy (1). Protein from the diet is hydrolysed into free amino acids in the small intestine and then transported to the liver via the blood. Once they reach the liver, most amino acids undergo deamination by a transaminase enzyme, transferring the amino group to 2-oxoglutarate, forming glutamate and leaving behind an alpha-keto acid (1). Glutamate can then be transferred to the mitochondria and deaminated by glutamate dehydrogenase to release an ammonium ion (NH_4^+) into the urea cycle, leaving behind 2-oxoglutarate which can re-enter the Krebs cycle (13). Glutamate can also transfer its amino group to oxaloacetate by aspartate aminotransferase to form 2-oxoglutarate and aspartate, which can directly enter the urea cycle (14).

Amino acids degraded in extrahepatic tissues produce NH_4^+ , which is combined with glutamate by glutamate synthetase to form glutamine (15, 16) that can be transported to the liver. Once glutamine has reached the liver mitochondria, it can be cleaved back to glutamate by glutaminase, releasing NH_4^+ to the urea cycle (16). NH_4^+ can also be transported to the liver by the glucose-alanine cycle. Glutamate present in the tissue can transfer the NH_4^+ group to pyruvate via the enzyme alanine aminotransferase to form alanine which can travel through the blood to the liver (17). In the liver, alanine is then deaminated back to pyruvate, transferring NH_4^+ to 2-oxoglutarate to form glutamate (17).

Any nitrogen which is not used by the body for protein synthesis must be excreted. This is performed through the urea cycle, which consists of five enzymatically mediated reactions that convert hepatic ammonia to urea so that it may be excreted by the kidneys (1). The urea cycle occurs in the mitochondria and cytosol of liver cells, and ultimately results in the production of urea. To enter the urea cycle, free NH_4^+ is cleaved from glutamine and glutamate in the mitochondria. NH_4^+ must first combine with bicarbonate and two molecules of ATP to form carbamoyl phosphate, driven by the enzyme carbamoyl phosphate synthetase 1 (18). Carbamoyl phosphate can then enter the urea cycle. The urea cycle results in the production of fumarate, which can re-enter the Krebs cycle, as well as urea, which enters the blood stream to be filtered out and excreted by the kidneys.

Once the amino group has been separated from the amino acids, the carbon skeletons are now free to be oxidized for energy production. There are several different amino acid degradation pathways, depending on the structure of the amino acid carbon skeleton. Some amino acids are known as ketogenic amino acids. This means that they can only be converted to acetyl-CoA and therefore can either enter the Krebs cycle and be oxidized into carbon dioxide (CO_2) or they can be used to produce ketone bodies to feed the body during times of negative energy balance (1). Other amino acids are termed as gluconeogenic, meaning they can be converted back to glucose via the process of gluconeogenesis. These amino acids are converted to intermediates such as pyruvate, 2-oxoglutarate, succinyl-CoA, fumarate or oxaloacetate (1). These products are all intermediates of the Krebs cycle and can therefore enter at different points to be oxidized for fuel. Five amino acids exist that are classified as both gluconeogenic and ketogenic (1), and therefore can have different fates, depending on metabolic needs.

1.1.4. The Krebs cycle

The catabolism pathways of carbohydrates, fats, and amino acids ultimately form the common intermediates, acetyl-CoA, oxaloacetate, and 2-oxoglutarate, which enter the Krebs cycle for further oxidation. The Krebs cycle consists of eight enzymatically mediated reactions which function to oxidize carbon skeletons, forming CO₂ as a by-product, and producing reduced NADH and FADH₂, which can be further oxidized in the ETC to produce ATP. A diagram of the Krebs cycle can be found in Figure 1.1. The Krebs cycle is in the mitochondrial matrix and is required to produce fuel as dictated by the needs of the body.

For carbohydrates to enter the Krebs cycle, they must first undergo glycolysis, where they are used to produce pyruvate. Pyruvate is imported to the mitochondrial matrix by the symporter pyruvate translocase, which is powered by the symport of protons. Once inside the matrix, pyruvate is converted to acetyl-CoA by the pyruvate dehydrogenase complex (PDH). PDH is the gateway for carbohydrate oxidation in mitochondria since it is required to convert pyruvate to acetyl-CoA prior to its entry into the Krebs cycle. PDH is composed of three subunits, the first being pyruvate decarboxylase (E1 subunit), which facilitates the decarboxylation and transfer of pyruvate to thiamine pyrophosphate (TPP) (19). In the E2 subunit, dihydrolipoyl tranacetylase, the acetyl group and two electrons are transferred to the reduced lipoamide group, forming acyl lipoyllysine (19). A transesterification reaction occurs next, in which CoA replaces the lipoamide on the acetyl group, forming acetyl-CoA and leaving behind reduced lipoyllysine (19). The E3 subunit is termed dihydrolipoyl dehydrogenase and functions to re-oxidize the lipoyllysine group, passing the electrons on to a flavin group to form FADH₂ (19). The reduced FADH₂ then passes a hydride ion to NAD⁺ to form NADH (19). The enzyme is now returned to its original configuration and can proceed with further reactions. This can be visualized in Figure 1.2. Acetyl-CoA can now

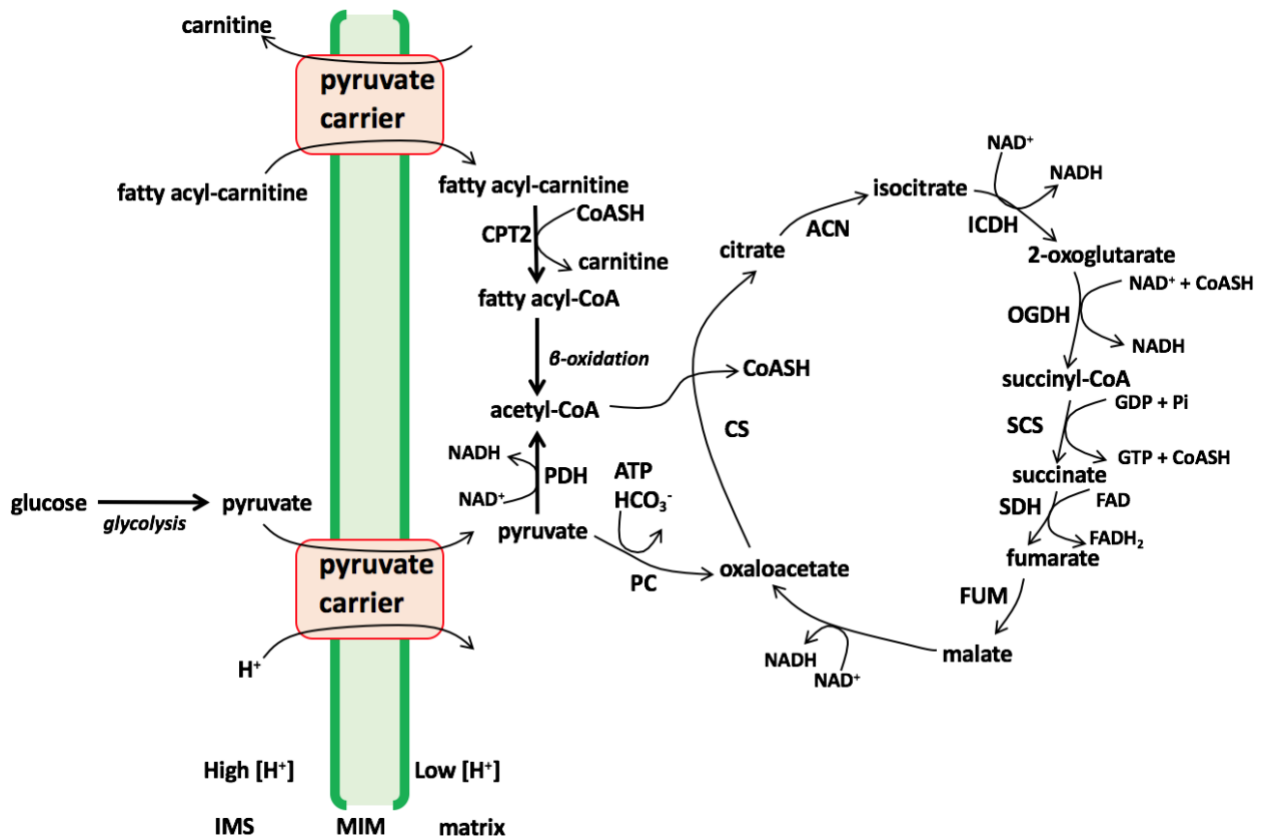


Figure 1.1: The Krebs cycle

This diagram shows the steps of the Krebs cycle, as well as its entry points. Acetyl-CoA is oxidized to CO₂, producing three NADH, one FADH₂, and one GTP/ATP.

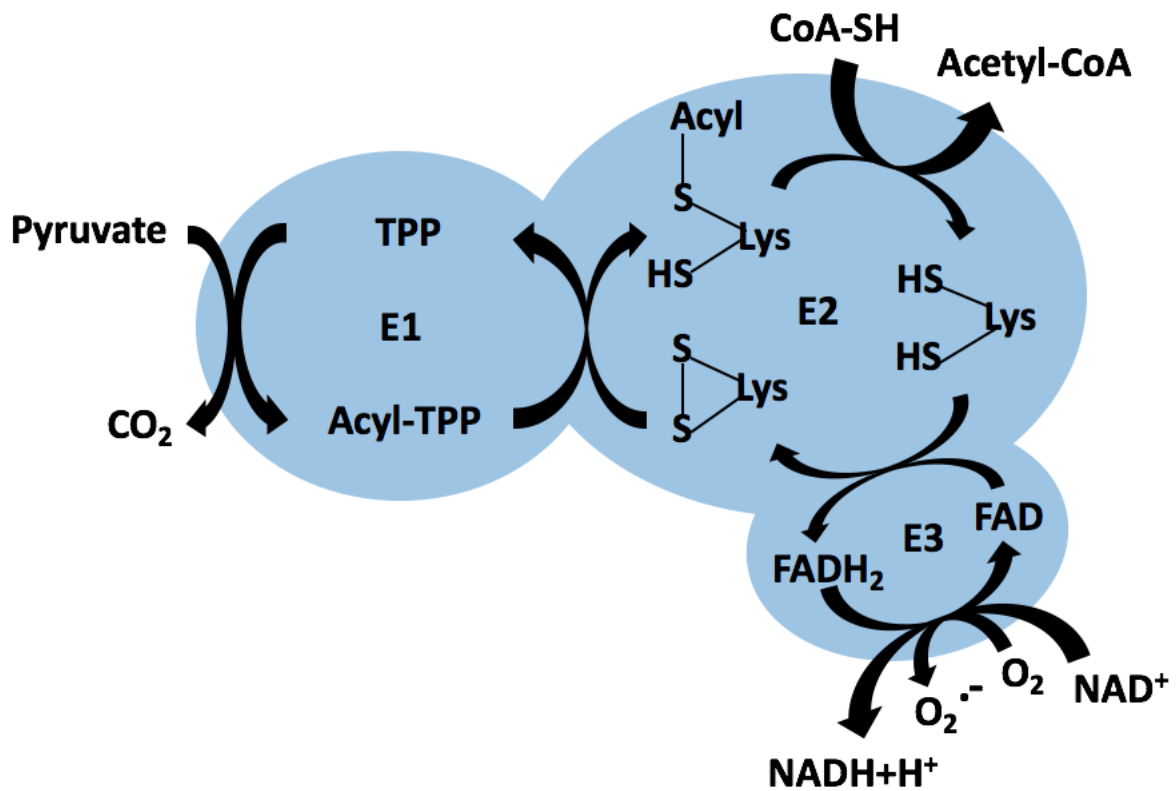


Figure 1.2: The pyruvate dehydrogenase complex

This diagram shows the overall reaction of PDH. (1) The decarboxylation of pyruvate by pyruvate decarboxylase, producing CO₂ and passing the acetyl group to TPP. (2) The acyl group is passed from TPP to lipoyllysine. (3) Acyl lipoyllysine reacts with CoA to release acetyl-CoA and produce reduced lipoyllysine. (4) The oxidation of lipoyllysine by FAD, producing FADH₂. (5) FADH₂ is re-oxidized by NAD⁺.

proceed directly to the Krebs cycle. PDH is an important regulatory enzyme of the Krebs cycle. It is allosterically inhibited by its own product, acetyl-CoA, as well as by high ratios of ATP/ADP and NADH/NAD⁺ and long chain fatty acids (1). PDH can also be covalently regulated by phosphorylation of a serine residue on the E1 subunit, mediated by pyruvate dehydrogenase kinase and pyruvate dehydrogenase phosphorylase (19).

Fatty acids, as well as ketogenic amino acids, also enter the Krebs cycle as acetyl-CoA. Acetyl-CoA combines with oxaloacetate in a claisen condensation reaction to form citrate, a reaction catalyzed by citrate synthase, releasing CoA (20). Aconitase then catalyzes the isomerization of citrate to isocitrate through a *cis*-aconitate intermediate (21). The conversion of isocitrate to 2-oxoglutarate via isocitrate dehydrogenase releases CO₂ and produces the first molecule of NADH in the cycle (1). 2-Oxoglutarate is a major entry point for amino acids into the Krebs cycle, specifically via the metabolism of glutamate by glutamate dehydrogenase. The next step of the cycle involves the oxidation of 2-oxoglutarate by the 2-oxoglutarate dehydrogenase complex (OGDH), producing succinyl-CoA, CO₂ and NADH (22). In terms of basic structure, OGDH is highly homologous to PDH, utilizing a similar mechanism for the oxidation of 2-oxoglutarate and the formation of NADH. The E1 subunit, 2-oxoglutarate decarboxylase, removes CO₂ from 2-oxoglutarate and attaches the succinyl group to the TPP cofactor (22). Dihydrolipoyl succinyltransferase, the E2 subunit, catalyzes the transfer of the succinyl group to the oxidized lipoamide group, which is then transferred to CoA, releasing succinyl-CoA (22). The E3 subunit, dihydrolipoyl dehydrogenase, is the same enzyme present in PDH, and functions in the same manner, to pass electrons from the reduced lipoamide to the flavin group and then to NAD⁺, producing NADH and returning the complex to its original conformation (22). OGDH, like PDH, is also an important regulatory step of the Krebs cycle. The enzyme complex is allosterically

inhibited by high ratios of ATP/ADP, NADH/NAD⁺ and increased concentrations of succinyl-CoA (1).

The sixth step of the Krebs cycle is catalyzed by succinyl-CoA synthetase, forming succinate from succinyl-CoA, with the substrate-level phosphorylation of ADP or guanine diphosphate (GDP) to ATP or guanine triphosphate (GTP), respectively (23). The next enzyme, succinate dehydrogenase, is both complex II of the ETC as well as the only membrane bound Krebs cycle enzyme, which catalyzes the conversion of succinate to fumarate and the production of FADH₂ (1). Fumarate then undergoes a hydration reaction to malate, catalyzed by fumarase (1). The final step of the Krebs cycle is the dehydrogenation of malate to oxaloacetate by malate dehydrogenase, producing the final NADH of the cycle (24). Overall, each molecule of acetyl-CoA that enters the Krebs cycle is oxidized to two molecules of CO₂ and produces three molecules of NADH, one FADH₂ and one substrate level phosphorylated GTP/ATP. The reducing equivalents generated in the Krebs cycle are oxidized by enzymes in the ETC to power the process of oxidative phosphorylation.

1.1.5. Oxidative phosphorylation

Oxidative phosphorylation is the method by which almost all aerobic organisms harness the energy derived from the metabolism of nutrients and use it to produce the universal energy currency, ATP. Oxidative phosphorylation is performed by a series of enzymes collectively called the respiratory complexes (also called the electron transport chain or ETC), which consists of enzyme complexes I-V, located in the mitochondrial inner membrane (Figure 1.3). Electron donors produced during the Krebs cycle and other metabolic pathways, donate their electrons to complexes in the ETC, which shuttle them along the chain to the terminal electron acceptor, molecular oxygen (O₂), forming water (H₂O) (note that the full reduction of O₂ to H₂O requires 4

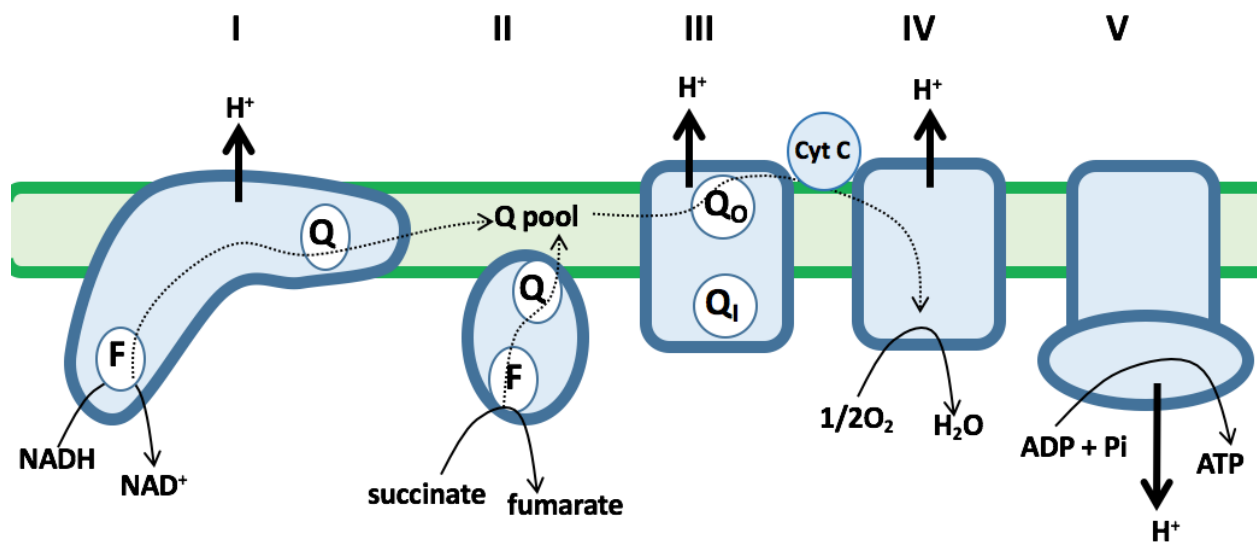


Figure 1.3: The electron transport chain

The flow of electrons through the ETC from NADH and succinate, to the terminal electron acceptor, O₂. During this process protons are pumped from the mitochondrial matrix to the intermembrane space.

electrons in total). The passage of electrons through the chain is coupled to the pumping of protons from inside the mitochondrial matrix to the intermembrane space. This process forms the proton gradient, which can then be harnessed for the formation of ATP by ATP synthase.

The first enzyme complex of the ETC is NADH:ubiquinone oxidoreductase, known more commonly as complex I, which catalyzes the transfer of electrons from NADH to the coenzyme UQ. Complex I is the largest ETC complex, containing 45 subunits, a flavin mononucleotide (FMN), and seven iron-sulfur (Fe-S) clusters (25). The complex is “L” shaped, with one arm anchored in the mitochondrial inner membrane, and the other hydrophilic arm located in the matrix. The hydrophilic section of the complex contains the binding site for NADH. Two electrons are liberated from the oxidation of NADH and are transferred to FMN, then through the Fe-S clusters to UQ, reducing it to ubiquinol (UQH₂) (26). During this process four protons are pumped from the matrix to the intermembrane space by complex I. UQH₂ then carries the electrons down the chain to complex III (26). Complex I can exist in two different conformations: the catalytically active “A” form, as well as the inactive “D” form, which can occur during pathological conditions such as ischemia (27).

Complex II of the ETC, succinate-ubiquinone oxidoreductase, is also known as succinate dehydrogenase (SDH) of the Krebs cycle. Its function is to oxidize succinate and transfer the electrons through the complex to UQ. Mammalian complex II is a ~120 KDa protein complex (28) composed of four subunits: subunit A and B are hydrophilic subunits that are present in the mitochondrial matrix, while the hydrophobic subunits C and D are anchored in the membrane (29). Subunit A contains the binding site for succinate, as well as a bound FAD. Electrons are passed from succinate to FAD, producing FADH₂ (30). Subunit B contains three Fe-S clusters, which tunnel electrons from FADH₂ to the UQ binding site, located in subunits C and D (30). UQH₂ is

produced which then transports electrons to complex III. Subunits C and D also contain a *b*-type heme that does not seem to be involved in the transfer of electrons, but may be involved in preventing their escape from the complex (29).

Electrons donated to UQ by complexes I and II are transported to complex III of the ETC, more formally known as ubiquinone:cytochrome *c* oxidoreductase. The function of this complex is to facilitate the transfer of electrons from UQH₂ to the heme protein cytochrome *c*, while pumping four protons from the matrix to the intermembrane space. The structure of complex III is a homodimer, with each monomer containing 11 subunits (31). Three of these subunits are known to be involved in the passage of electrons: cytochrome *b*, which contains two *b*-type heme groups (*b_L* and *b_H*), the Rieske iron-sulfur protein, which contains two Fe-S centers, and cytochrome *c*₁, which contains a *c*-type heme group (*c*₁) (31). To pass only one electron from UQH₂ to cytochrome *c*, complex III uses the Q cycle to recycle a lone electron back to UQ. The overall reaction involves the oxidation of two UQH₂ to UQ, the reduction of one UQ to UQH₂, the reduction of two cytochrome *c* molecules, the uptake of two protons from the matrix and the release of four protons into the intermembrane space (32). In the first round of the Q cycle, UQH₂ binds to the Q₀ site of complex III while UQ binds to the Q_i site. UQH₂ is oxidized, and its two protons are released to the intermembrane space (32). One electron is passed to the Fe-S center in the Rieske iron-sulfur cluster protein, then cytochrome *c*₁ and ultimately to cytochrome *c*, which can then bring the electron further down the ETC (32). The other electron is passed from the *b_L* to the *b_H* heme and then to the bound UQ, forming a ubisemiquinone (32). To fully reduce the ubisemiquinone, a second round of the Q cycle is performed by binding another UQH₂ and transferring one electron to the heme group of cytochrome *c*, releasing two more protons into the intermembrane space, and transferring the second electron to the ubisemiquinone, which also picks up two protons from the

matrix to become UQH₂ (32). The Q cycle explains how complex III can accommodate the transfer of electrons from the two-electron carrier, UQH₂, to the one electron carrier, cytochrome c.

Once cytochrome c has obtained an electron from complex III, it passes that electron on to the fourth complex of the ETC, complex IV. The function of complex IV, also known as cytochrome c oxidase, is to pass electrons from cytochrome c to the final electron acceptor of the ETC, O₂. Complex IV is composed of 14 subunits (33), with three critical ones that are known to be involved in electron transfer. They include: subunit I, which contains the heme groups a and a₃ and a copper ion, Cu₃, which complexes with a₃ to form the a₃:Cu₃ binuclear center, subunit II, which contains two copper ions complexed with two cysteine residues forming the binuclear center Cu_A, and subunit III (1). Electron transfer begins when two reduced cytochrome c molecules bind and donate one electron each to subunit II, which are transferred through the Cu_A center to heme a. Heme a transfers the electrons to the a₃:Cu₃ center (34). At this point, O₂ binds to heme a₃, and is reduced by the two electrons to O₂²⁻ (34). The delivery of two more electrons through the pathway, and the addition of four protons from the matrix, forms two molecules of H₂O. During this process four protons are transported into the intermembrane space (35).

One of the most notable aspects of the ETC is that electron movement from NADH or succinate down to the end of the chain to O₂ is an energetically favorable process. The energy obtained from the favorable “downhill” transfer is conserved as a transmembrane electrochemical gradient of protons which is formed by complexes I, III, and IV. It is important to note that complex II does not pump protons into the intermembrane space since it is not an integral membrane protein. In addition, the net Gibbs free energy change for electron transfer from succinate to UQ is ~0 KJ/mol. This gradient is known as the proton motive force (PMF). The PMF has two components: chemical energy due to the chemical gradient from the concentration difference of H⁺ between the

matrix and the intermembrane space, and electrical potential energy due to the charge separation from the transfer of a positive ion across the membrane, leaving behind a more negatively charged matrix. For every NADH oxidized by the ETC, ten protons are transferred to the intermembrane space, and for every succinate molecule oxidized, six protons are transferred (since complex II does not translocate protons). The chemiosmotic model, proposed by Peter Mitchell, states that the energy stored in the PMF is used to power the production of ATP (36). This is achieved by the flow of protons down their electrochemical gradient through a channel in ATP synthase (37). The oxidation of substrates is therefore tied to the phosphorylation of ADP, hence the term oxidative phosphorylation. If the PMF is disrupted, then production of ATP cannot occur. This is evident when the PMF is uncoupled from ATP synthesis with proton ionophores or by mitochondrial uncoupling proteins. Proton ionophores, such as carbonylcyanide-*p*-trifluoromethoxyphenylhydrazone (FCCP), are weak acids that are protonated in the intermembrane space allowing for diffusion into the matrix where a proton is released, dissipating the PMF (37). Uncoupling proteins are regulated proton channels located in the mitochondrial membrane that can also allow protons to diffuse down their gradient (38). When uncoupled, mitochondria can still oxidize substrates, but ATP production is diminished since uncoupling proteins return protons to the matrix, by-passing ATP synthase (38). Along with energizing the formation of ATP, the PMF is also used to transport vital substrates in and out of the mitochondrial matrix. The adenine nucleotide transporter transports ADP^{3-} into the matrix in exchange for ATP^{4-} , which is energetically favourable due to the negative charge of the matrix (39). Phosphate translocase also transports the symport of a phosphate group and a proton down the gradient into the matrix. Other various nutrient carriers, like the pyruvate carrier, also rely on the PMF to drive solute uptake (40).

ATP synthase, also known as complex V, is a large multi-subunit protein located in the mitochondrial inner membrane. The overall function of ATP synthase is to catalyze the phosphorylation of ADP to ATP, which is powered by the passage of protons down their electrochemical gradient through a channel in the enzyme. ATP synthase is composed of two functional domains: The F_0 domain, which is embedded in the mitochondrial inner membrane and contains the channel through which protons travel, and the F_1 domain, which is peripheral to the inner membrane on the matrix side, and contains the catalytic active sites (41). The F_1 domain contains five different subunits: α , β , γ , δ , and ϵ , with the composition $\alpha_3\beta_3\gamma\delta\epsilon$ (41). The three α and β subunits alternate in a circular structure, surrounding a γ shaft which associates with one of the β subunits. Although the β subunits are identical in composition, they differ in conformation due to their association with the γ subunit. At all times, the three β subunits are in three different conformations: β -empty, which contains no substrates, β -ADP, which binds ADP and phosphate (P), and β -ATP, which contains the recently formed ATP (42). The movement of protons down the F_0 section powers the rotation of the γ subunit of the F_1 section, a process known as rotational catalysis (41). When ADP and P bind to the β -ADP site, the conformation of the site changes to β -ATP, tightly binding the two substrates and bringing them close enough to undergo phosphorylation. Once ATP is formed, the subunit changes to the β -empty conformation, which releases the newly formed ATP due to a low affinity (42). Passage of the protons through the F_0 domain causes the rotation of the γ subunit by 120° , which allows it to associate with the next β subunit, changing its conformation (42). The β subunits are held in place during the rotation by the ϵ subunit of F_1 (1). The interaction between the three β subunits dictates that if one β -subunit is in the β -ADP form, its neighbours must be in the β -ATP and the β -empty forms (1). One complete rotation of the γ subunits allows the three β subunits to rotate through all three

conformations, catalyzing the production of three ATP molecules per full turn (1). These ATP molecules are then transferred out of the matrix to be used to power cellular processes.

1.2. Reactive oxygen species in mitochondria

Reactive oxygen species (ROS) are chemically reactive molecules produced by the incomplete reduction of molecular oxygen. The molecular structure of oxygen includes two unpaired electrons in its outer most anti-bonding orbitals, meaning that oxygen can only accept one electron at a time (43). Therefore, the reduction of O_2 to H_2O results in the formation of several oxygen radical intermediates, namely, superoxide ($O_2^{\bullet-}$), hydrogen peroxide (H_2O_2) and hydroxyl radical (OH^{\bullet}). $O_2^{\bullet-}$ and H_2O_2 are the two proximal ROS produced by mitochondria (44). Of all the oxygen consumed by the body for oxidative phosphorylation, it is estimated that approximately 0.02-0.2% is converted to $O_2^{\bullet-}$ (45, 46). H_2O_2 is a more stable form of ROS which, unlike $O_2^{\bullet-}$, is able to diffuse through membranes via aquaporin (47). Excess production of ROS is known to cause oxidative damage in cells, and has been associated with a wide array of diseases including cardiovascular, inflammatory, and degenerative diseases, as well as cancer (48). $O_2^{\bullet-}$ can cause enzyme inactivation by disassembling Fe-S clusters (49), while H_2O_2 disables proteins by irreversibly oxidizing cysteine residues (50). Even more damage can occur when $O_2^{\bullet-}$ and H_2O_2 interact with transition metal ions in the body, most notably free iron or copper, initiating Haber-Weiss and Fenton reactions which yields OH^{\bullet} (51). OH^{\bullet} is a very reactive molecule that can oxidize nucleotides, lipids, and amino acids, resulting in DNA, membrane, or protein damage culminating with cellular dysfunction and death.

Once thought to be unfortunate by-product of metabolism, ROS are now regarded as important secondary signalling molecules involved in modulating different cell functions. H_2O_2 has been found to affect enzyme activity by reversibly oxidizing thiol groups to sulfenic acid

(SOH) (52). This is referred to as “redox signaling” where cysteine switches are reversibly oxidized in response to fluctuations in the surrounding cellular redox environment. In fact, it is hypothesized that cysteine switches serve as a critical interface required to modulate cellular responses at the genomic, proteomic, and metabolomic levels in response to alterations in the surrounding cellular environment. For instance, H₂O₂ is implicated in stress signaling (Nrf2 activation (53), apoptosis (54)), T-cell activation (55), adipocyte differentiation (56), steroidogenesis (57), and insulin resistance and release (58).

ROS is currently known to have at least eleven sites of production within the mitochondria (Figure 1.4) (59). These ROS forming sites include respiratory complexes and dehydrogenases that are involved in substrate oxidation and the delivery of free electrons to O₂ in the respiratory chain. They include complexes I and III of the ETC, as well as 2-oxoacid dehydrogenase complexes and dehydrogenases that deliver electrons to UQ, such as complex II (59). Seven of these sites produce ROS from a flavin group which is associated with the unique radical chemistry of FAD and FMN groups in different respiratory complexes and dehydrogenases. The other five sites produce ROS from a UQ/UQH₂ binding site through the formation of ubisemiquinone radicals in different membrane bound dehydrogenases and respiratory complexes. Nine of the sites produce O₂[•] and H₂O₂ into the mitochondrial matrix, while two sites, complex III and glycerol-3-phosphate dehydrogenase, can produce ROS directly into the mitochondrial intermembrane space (59). Most work in discerning which enzymes serve as high capacity sites in mitochondria has been carried out in skeletal muscle mitochondria (59). It was found that complex III serves as the highest capacity site overall (59). Intriguingly, the 2-oxoacid dehydrogenase complexes, OGDH and PDH, were found to generate ~8x and ~4x more ROS than complex I during the oxidation of

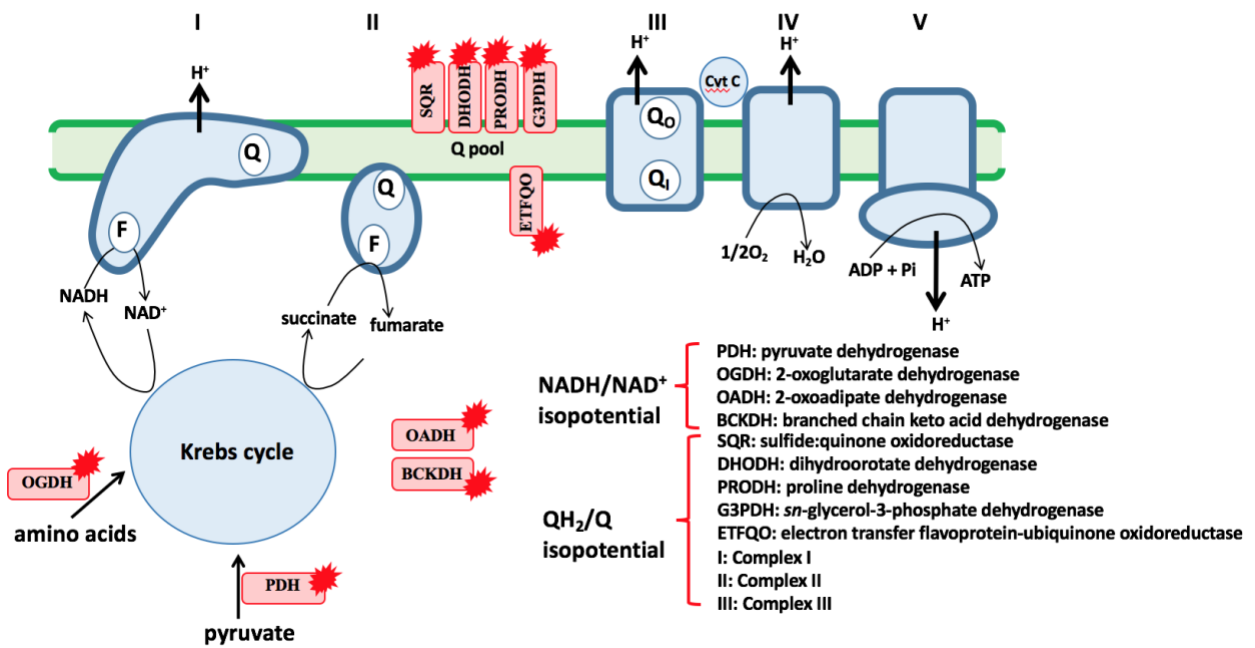


Figure 1.4: Sites of ROS production in mitochondria

The known sites of ROS production in the mitochondria. They are divided into the NADH/NAD⁺ isopotential sites and the QH₂/Q isopotential sites.

Kreb's cycle linked substrates (59). In addition, complex II was found to be an important source as well as complex I, but only under conditions of electron back flow from succinate (60). Our group recently started examining which enzymes serve as high capacity ROS production sites in liver and cardiac tissue mitochondria. It was found that complex III produces ~45% of the mitochondrial ROS in liver tissue and OGDH yields ~35% while sites like PDH and complex I account for the rest (61, 62). By contrast, complex I and III serve as the highest capacity sites in cardiac tissue, regardless of what substrate is being oxidized (Krebs cycle linked substrates or carbon that donates electrons directly to the respiratory chain) (63).

Levels of ROS in the mitochondria are closely regulated by a few different mechanisms. $O_2^{\bullet-}$ produced in the mitochondria is quickly dismutated to H_2O_2 by the enzyme superoxide dismutase (SOD). The kinetics for the dismutation of $O_2^{\bullet-}$ have been estimated to approach a rate constant of $2.3 \times 10^9 \text{ M}^{-1} \text{ s}^{-1}$, meaning that its concentration is very low, in the picomolar (pM) range (43). Within the mitochondrial matrix, $O_2^{\bullet-}$ is dismutated by manganese SOD (MnSOD), while the intermembrane space relies on copper SOD (CuSOD) and zinc SOD (ZnSOD) (64). There are many different mechanisms by which mitochondria H_2O_2 can be degraded into less harmful chemicals. The three main systems include catalase, which degrades H_2O_2 into H_2O and O_2 , and the glutathione (GSH) and thioredoxin (PRX) systems, which use their own mechanisms to quench H_2O_2 (62). Typically, the GSH and PRX systems are thought to be the major methods of clearance in mitochondria. However, catalase has recently been shown to play an important role in eliminating H_2O_2 (62).

1.3. Mitochondrial hydrogen peroxide clearing systems

1.3.1. *Glutathione antioxidant system*

GSH is a tripeptide molecule made up of glutamate, cysteine, and glycine. The synthesis of GSH occurs in the cytosol and is mediated by γ -glutamylcysteine synthetase, which catalyzes the addition of glutamate and cysteine, and then glutathione synthase, which adds glycine (65). GSH is transported from the cytosol into the mitochondria through a still unknown transporter (66). The concentration of GSH in the matrix of mitochondria is 1-10 mM (varies between different tissues, with liver containing the most and muscle having the least), while the oxidized form, glutathione disulfide (GSSG), occurs at 0.01-0.1 mM. The ratio of GSH:GSSG in mitochondria is typically kept at approximately 100:1, but can decrease during times of oxidative stress (67). This ratio is maintained by the activity of glutathione reductase (GR), which reduces GSSG to two molecules of GSH, using the cofactor nicotinamide adenine dinucleotide phosphate (NADPH). One of the major functions of the GSH system is the degradation of H_2O_2 to H_2O by the action of glutathione peroxidase (GPx). The reduction of H_2O_2 to two molecules of H_2O also causes the formation of GSSG from two molecules of GSH. GSSG is then converted back to GSH by the activity of GR and NADPH (Figure 1.5) (68). There exist different isozymes of GPx which catalyze the reduction of different peroxides. The above reaction is catalyzed by the mitochondrial matrix soluble GPx1 (68). GPx4 is located on the matrix side of the mitochondrial inner membrane and functions to reduce phospholipid hydroperoxides to alcohols, slowing the propagation of lipid peroxidation within the membrane (68).

The GSH system is also involved in the detoxification of xenobiotic substrates and products of endogenous oxidative damage such as α , β -unsaturated aldehydes, epoxides, and alkyl hydroperoxides (68). These reactions are catalyzed by glutathione-s-transferase (GST), which

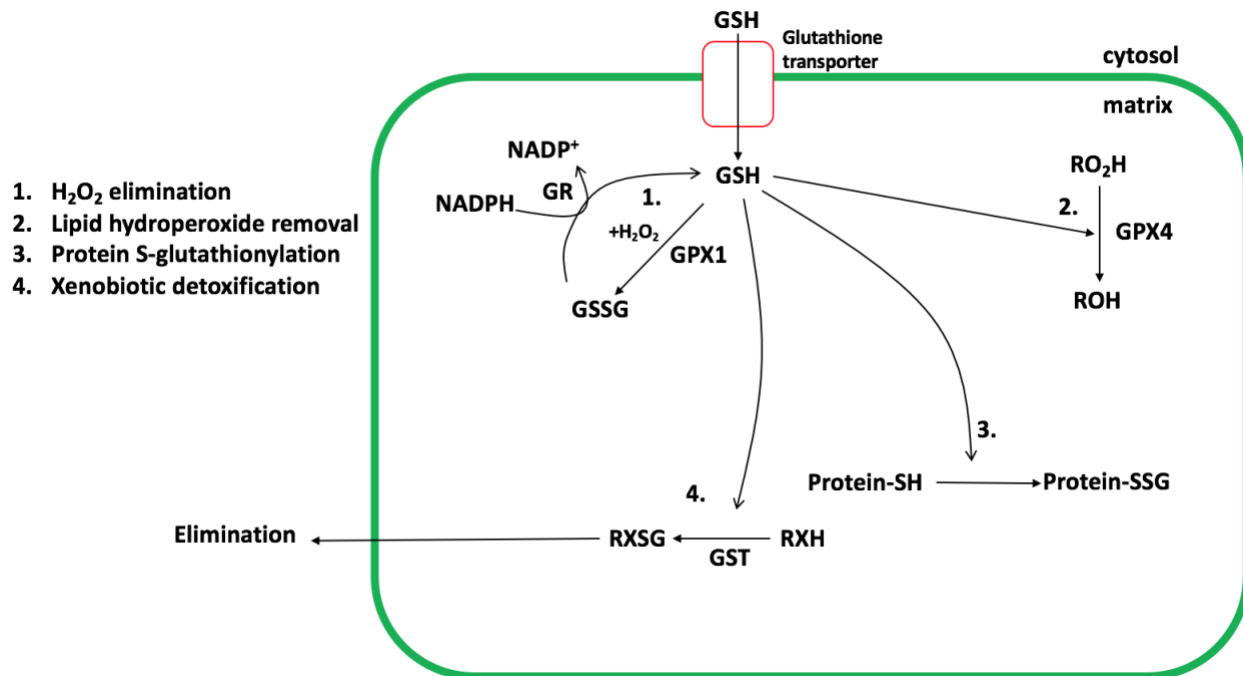


Figure 1.5: Catalytic cycle and functions of the glutathione system

This diagram illustrates the different functions of the glutathione system.

transfers GSH to the targeted substrates, producing a GSH thioester-xenobiotic conjugate which is effluxed from the mitochondria (68).

The third known function of glutathione is redox signaling through the addition of GSH to protein cysteine thiols in a mechanism called S-glutathionylation. Reversible S-glutathionylation is catalyzed by the enzyme glutaredoxin (GRX) (69). In the mitochondrial matrix and nucleus of the cell, glutaredoxin-2 (GRX2) catalyzes the addition and removal of GSH (note though that GRX2 has only been found to occur in the lumen of the nucleus in cancer cells) (70), while glutaredoxin-1 (GRX1) catalyzes this reaction in the cytosol and intermembrane space of mitochondria. S-glutathionylation of enzymes within the Krebs cycle and the ETC is a vital mechanism for control of ROS production, which will be discussed further in section 1.5.

1.3.2. Peroxiredoxin antioxidant system

To prevent toxic concentrations of H_2O_2 from accumulating within the cell, mitochondria contain a few different antioxidant systems, one of them being the peroxiredoxin system. Peroxiredoxins (PRX) are a family of thiol peroxidases which quench cellular H_2O_2 . The catalytic cycle begins when H_2O_2 reacts with a cysteine thiol residue called the “peroxidatic cysteine”, forming SOH (71). Mitochondrial PRX isoforms include PRX3 and PRX5 (71). Mitochondrial PRX3 is a typical 2-Cys PRX, meaning it is a homodimer oriented in a head to tail fashion, using cysteine thiol residues from both subunits for degradation of H_2O_2 (71). Reduction of one H_2O_2 molecule to H_2O causes both cysteine thiols on PRX3 to become oxidized to SOH (71). The two PRX3 units then condense to form an oxidized dimer with two intermolecular disulfide bonds, releasing two molecules of H_2O . The oxidized PRX3 is reduced by thioredoxin2 (TRX2), which in turn is reduced by thioredoxin reductase (TR) using the power of NADPH (71). PRX3 can be hyperoxidized to sulfinic acid (SO_2H) in the presence of excess H_2O_2 , causing it to be inactivated.

Hyperoxidized PRX3 can be reduced back to its active state by sulfiredoxin, but the reaction proceeds very slowly with a rate constant of $k=0.18 \text{ min}^{-1}$ (71). This mechanism of inactivation is thought to allow H_2O_2 to accumulate enough to exert signalling effects (64). This mechanism can be viewed in Figure 1.6.

Mitochondrial PRX5 proceeds via a different mechanism. It is an atypical 2-Cys PRX that exists as a monomer and forms an intramolecular disulfide bond when oxidized to SOH by H_2O_2 . PRX5 is then reduced by to its active state via the same pathway as PRX3. PRX3 is a more effective H_2O_2 scavenger than PRX5, with a rate constant that is about two orders of magnitude larger (71). However, PRX5 has been found to be a more effective scavenger of organic hydroperoxides, indicating that it may be more suited for repairing oxidative damage (72). It has been estimated that the bulk of mitochondrially produced H_2O_2 is degraded by the PRX antioxidant system, with around 90% reacting with PRX3. However, mitochondria would not be able to keep ROS levels in check with PRX only, as depletion of GSH or knockdown of GPx1 has been shown to cause increases in cell susceptibility to oxidative stress (73, 74).

1.4. Control over ROS production

The production of $\text{O}_2^{\bullet-}/\text{H}_2\text{O}_2$ by mitochondria depends on several factors including the concentration of the electron donating site, the redox state of the electron donor, and access to O_2 . While the degradation of $\text{O}_2^{\bullet-}/\text{H}_2\text{O}_2$ by antioxidant systems is an important method of ROS control, there exists other mechanisms by which mitochondria can exert control over the production of ROS from different sites. Three of the most important methods of control include: changes in proton leak, the formation of supercomplexes and the use of redox signals.

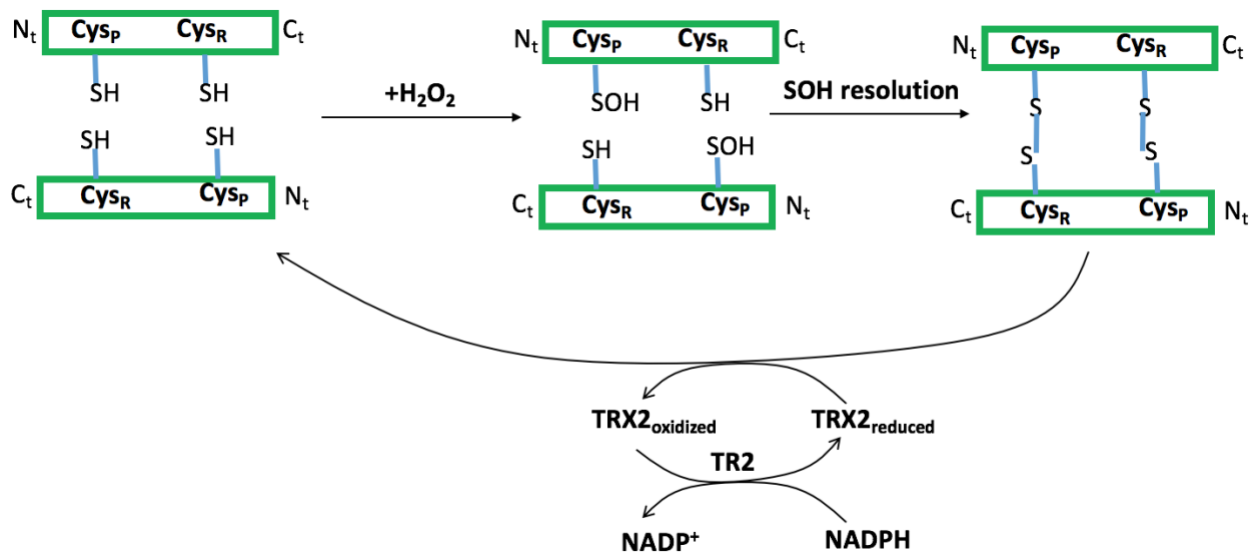


Figure 1.6: Peroxiredoxin catalytic cycle

This diagram illustrates the catalytic cycle of PRX3, showing its oxidation to a dimer, and then how it is reduced back to its active state by TRX2.

1.4.1. Proton leak

Proton leak is the return of protons to the mitochondrial matrix independently of ATP synthase. This causes depletion of the PMF used to power the phosphorylation of ADP. There are two types of proton leak that occur in mitochondria. The first is basal leak, which is minor, unregulated leak through the lipid bilayer as well as through the membrane protein adenine nucleotide translocase (ANT) (75). The second is called inducible leak and is regulated by specific mitochondrial inner membrane proteins such as uncoupling proteins (UCP) 1-3 (75). Notably, this may seem energetically wasteful but is likely the most studied mechanism for the prevention of mitochondrial ROS formation.

The production of ROS has been shown to be highly sensitive to changes in proton leak and to have a non-ohmic relationship with the PMF, meaning that small increases in the membrane potential can induce exponential increases in ROS production (54, 76). Induction of proton leaks has been shown to decrease the production of ROS from the ETC by preventing the over-reduction of electron donating sites for ROS formation (77). Indeed, loss of proton uncouplers like UCP2 or UCP3 is associated with the induction of oxidative stress and the overproduction of ROS by mitochondria (78, 79). Moreover, products of increased oxidative stress, such as 4-hydroxynonenal (4-HNE), have been found to induce proton leakage through UCPs, decreasing ROS production. A mechanism has been proposed which constitutes a negative feedback loop: increased concentration of ROS in the mitochondria leads to increased proton leakage, slowing down rate of ROS production (79).

UCP2 and UCP3 are thought to be major regulators of proton leakage in response to ROS. UCP2 is ubiquitously expressed throughout the body, while UCP3 is found mostly in skeletal muscle, cardiac muscle, and to a small extent in brown adipose tissue. Inhibition of UCP2 has been

found to cause increases in H₂O₂, while overexpression diminishes ROS production and protects from oxidative damage (80, 81). Similar trends have been found for UCP3. UCP3 knockout mice show increased levels of ROS and oxidative stress (82), while overexpression has been found to lower mitochondrial O₂[•]/H₂O₂ emission (83). Although numerous studies have shown that UCP2 and 3 play a role in decreasing oxidative stress, the exact mechanism is still up for debate. There have also been studies that provide evidence in contrary of their control of ROS production via changes in proton leak. Some studies have given evidence of alternate functions of UCP2 and 3 (84, 85), while other studies have concluded that changes in the PMF do not cause any effect on ROS production (86).

1.4.2. Supercomplexes

The complexes of the ETC were originally assumed to exist individually and be randomly distributed in the mitochondrial inner membrane. However, recent evidence has indicated that this is not the case. The theory of supercomplexes, also called respirasomes, was proposed in 2000 to explain why some complexes migrate together during polyacrylamide gel electrophoresis (87). The isolated respirasomes were found to consist of complexes I, III and IV (87). Later, it was discovered that isolated respirasomes were active and able to reduce O₂ in the presence of NADH (88). Complex I was found to form supercomplexes with other ETC complexes in many different combinations (88). The total evidence gathered about the nature of the ETC complexes cannot be completely explained by the supercomplex model, or by the free complex model and so, a model of complex plasticity has been proposed. The plasticity model postulates that complexes can exist as free units or as supercomplexes, depending on the nature of the environment (89, 90).

Supercomplex assembly has also emerged as a method for the control of ROS production. The loss of supercomplex assembly, and therefore the increase of free complex I, has been shown

to increase ROS production from the complex (91). Free complex I allows the FMN containing subunit to be more exposed, possibly increasing its chances of reacting with O₂ to form ROS (92). Another possibility is that free complex I experiences increased over-reduction of the FMN containing subunit due to decreased electron transfer to complex III. Further research is required to validate either of these hypotheses. However, it is possible that mitochondrial ROS levels may be controlled by facilitating the assembly of complex I into supercomplexes with other respiratory complexes.

1.4.3. Redox signals

1.4.3.1. Sulfenylation

Protein cysteine thiol residues in the mitochondria have been studied extensively as targets for redox signalling and control and can undergo many reactions (Figure 1.7). The oxidation of a thiol group to SOH by H₂O₂ is termed sulfenylation and its significance as a redox signal has been reviewed considerably. It has been suggested that sulfenylation could be a negative feedback mechanism used by H₂O₂ to limit ROS production from certain enzymes. The caveat to this hypothesis is that few enzymes in the mitochondria have been found to be sulfenylated. Also, sulfenylation has not been found to fit the conditions for an effective post-translational modification. For a redox signal to be efficient, it should meet certain criteria, much like other well-known modifications like phosphorylation. Redox modifications must be specific, reversible, rapid, and fulfill some physiological role (93). Sulfenylation of thiols is a very slow reaction (rate constant: $K=5-500 \text{ M}^{-1}\text{s}^{-1}$) and the reactions are not catalyzed by any known enzyme (93). Protein sulfonates are also strong nucleophiles and are thus very unstable and can form a number of different adducts (93). Sulfenic acids can be further oxidized by H₂O₂ to SO₂H, and even further to the irreversible sulfonic acid (SO₃H). Sulfenic and sulfinic acids can be reverted back to thiol

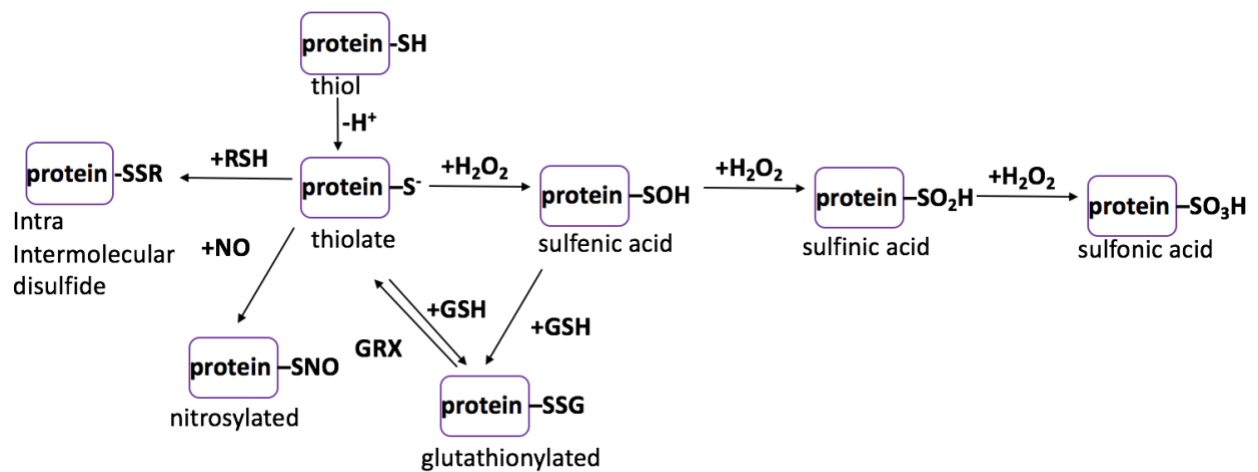


Figure 1.7: Reactivity of thiols

The many possible fates of free thiols in the mitochondria are illustrated including: [1] sulfonic acid, [2] sulfonamides, [3] disulfides, [4] S-glutathionylated thiols and [5] thiosulfinate.

groups via the action of sulfiredoxin (94), however this is thought to be a defense mechanism to prevent the irreversible deactivation of enzymes by oxidation to SO₃H. It has been proposed that sulfenylation may serve as a means to promote the formation of disulfide or sulfonamide bonds during protein folding (95).

1.4.3.2. *Protein S-glutathionylation*

Protein S-glutathionylation has emerged as a strong candidate for the redox-sensitive posttranslational modification of proteins. S-glutathionylation is the addition of a glutathione molecule to a protein cysteine thiol residue. As opposed to sulfenylation, S-glutathionylation fits all the outlined criteria for an effective post translational modification. Proteins have been found to contain S-glutathionylation motifs which are cysteine rich amino acid sequences that are accessible and surrounded by positively charged lysine residues (96). This latter characteristic is vital since it lowers the pKa of a protein cysteine residue, allowing easier deprotonation and the formation of a strongly nucleophilic thiolate anion that can attack GSH molecules. A number of proteins have been found to be S-glutathionylation targets (Table 1.1) (64). S-glutathionylation reactions are catalyzed by GRX, small heat stable thiol oxidoreductases that specialize in the conjugation and removal of GSH from a target protein. Notably, GRX mediated S-glutathionylation reactions are usually 10^2 - 10^5 M⁻¹s⁻¹ with the rate of the reaction increasing with a decreasing thiol pKa (96). The GST family has also been implicated in some cellular S-glutathionylation reactions (97).

Although S-glutathionylation can be enzymatically mediated, spontaneous S-glutathionylation is also able to proceed under the right conditions. During times of oxidative stress, when the 2GSH/GSSG ratio approaches 1, the increased concentrations of GSSG can lead to non-enzymatic

Table 1.1: Known targets of S-glutathionylation

| | Target | Effect |
|-------------------------------|------------------------------|--|
| Krebs cycle | Aconitase | Decreases activity |
| | Isocitrate dehydrogenase | Protects from oxidative damage |
| | 2-oxoglutarate dehydrogenase | Protects from oxidative damage Controls ROS release |
| | Succinyl-CoA synthetase | Oxidative stress |
| | Succinate dehydrogenase | Controls ROS release |
| | Pyruvate dehydrogenase | Redox sensing and controls ROS release |
| Respiratory chain | Complex I | Controls activity and ROS release |
| | Complex III | Unknown |
| | Complex V | Regulates phosphorylating respiration |
| Solute anion carrier proteins | UCP3 | Controls proton leaks |
| | UCP2 | Controls proton leaks for insulin release |
| | ANT | Regulates permeability transition |
| | CACT | Fatty acid metabolism |
| Mitochondrial shape | Mitofusins1, 2 | Mitochondrial elongation |
| Other | Cyclophilin D | Apoptosis |
| | SOD | Superoxide elimination |

This table lists mitochondria proteins that are known to be S-glutathionylated as of 2013.

protein S-glutathionylation (98). Non-enzymatic S-glutathionylation can also occur when cysteine is oxidized to SOH, which can then react with GSH (99). These are likely methods employed to protect proteins from irreversible oxidative inactivation when levels of H₂O₂ in the mitochondria are high. A third mechanism of spontaneous S-glutathionylation can also occur when cysteine forms a thiol radical that can react with GSH, forming a thiyl radical glutathionyl intermediate, which then passes an electron to O₂, leaving behind a protein glutathione mixed disulfide (PSSG) (99). Some enzymes in the mitochondria are known to show persisted S-glutathionylation during normal physiological conditions, such as SDH (100). Conditions that lead to S-glutathionylation of proteins in the mitochondria can vary widely, due to some proteins being more susceptible, and also due to the highly folded nature of cristae, which can form microenvironments that contain highly variable levels of GSSG as compared to the rest of the mitochondria (101).

The importance of S-glutathionylation reactions in the mitochondria extends past protection from oxidative stress. S-glutathionylation also has roles in energy metabolism, as seen by its extensive levels of protein S-glutathionylation found on Krebs cycle enzymes (102). Many other mitochondrial processes have also been shown to utilize S-glutathionylation such as apoptosis, mitochondrial shape, protein import, and proton leakage.

1.5. Glutaredoxin

GRXs are a family of GSH-dependent thiol oxidoreductases belonging to the thioredoxin fold superfamily (70). GRX was first discovered in *E. coli*, where it was found to catalyze the GSH-dependent reduction of ribonucleotide reductase (103). However, it was later found that the GSH-mediated modification of proteins was driven by GRX in mouse liver cells (104). This GRX isozyme was later identified as mammalian GRX1, a small 10-14 KDa protein located in the cytosol and the mitochondrial intermembrane space (103), which functions to keep thiols in the

reduced state, mainly by the reduction of PSSG adducts (105). The active site of GRX1 contains a Cys-Pro-Tyr-Cys sequence, with cysteine-22 harboring the requisite reductive power to deglutathionylate a target protein (105). Deglutathionylation forms a GRX1-SSG intermediate. In the second catalytic phase, GRX1-SSG binds GSH which is required to remove the glutathionyl moiety via a thiol disulfide exchange reaction that yields reactivated GRX1 and GSSG. GR and NADPH are then utilized to reduce GSSG reforming two GSH molecules. Other roles for GRX1 include dehydroascorbate reduction, cellular differentiation, and regulation of cell signaling and apoptosis (106).

GRX2 is the second GRX to be discovered in mammals. There are three GRX2 isoforms: GRX2a is localized to the mitochondria matrix, while GRX2b and GRX2c are localized to the nucleus (106). GRX2a is ubiquitously expressed in the body, while GRX2b and GRX2c are expressed exclusively in the testis or cancer cells (107). GRX2 shares about 36% homology with mammalian GRX1 (105), one of the most noticeable differences being the Cys-Ser-Tyr-Cys active site sequence (106). GRX2 also differs from GRX1 in that it is more resistant to oxidative inactivation. GRX1 contains additional protein surface Cys residues that are amenable to irreversible oxidation whereas GRX2 does not, allowing it retain activity during periods of increased oxidation (70). In addition, unlike GRX1, oxidized GRX2 can be reduced and reactivated by TR2 as well as GSH (69).

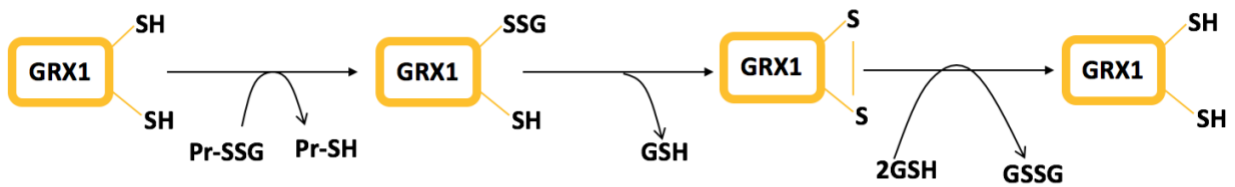
There exist two different mechanisms for the deglutathionylation of proteins by GRX1 and GRX2. In the dithiol mechanism, the N-terminal active site cysteine residue attacks a protein-glutathione disulfide bridge via a simple nucleophilic displacement reaction, releasing the reduced protein and a GRX-glutathione mixed disulfide, GRX-SSG (108). GRX-SSG immediately forms an intraprotein disulfide bond (GRX-SS), which is then reduced by two molecules of GSH,

reforming GRX and releasing GSSG (108). In the monothiol mechanism, the GRX-SSG adduct is reduced by GSH, reforming GRX and GSSG (108). These mechanisms can be viewed in Figure 1.8. To facilitate protein S-glutathionylation, GRX must form an intermediate GRX-SSG*, which can react with protein thiols to form PSSG (109).

GRX2 can exist in the mitochondria as an active monomer and an inactive dimer (106). Closer examination of the structure of GRX2 has revealed that the enzyme contains Fe(III) in a tetrahedral sulfur coordination consistent with the presence of an $[2\text{Fe-2S}]^{2+}$ cluster (106). A GRX2 dimer forms a $[2\text{Fe-2S}]^{2+}$ cluster stabilized by two active site protein cysteines and two cysteines from separate molecules of GSH (110). The role of the Fe-S cluster in GRX2 is to allow the enzyme to function as a redox sensor. When mitochondria have low levels of oxidation, GRX2 exists in the inactive dimer formation. However, during times of oxidative stress, the Fe-S cluster is degraded by $\text{O}_2^{\cdot-}$, releasing the active GRX2 monomers (106), which can then function to catalyze S-glutathionylation reactions to protect enzymes and modulate ROS production.

GRX2 has been proven to be an important enzyme in maintaining cellular function. Overexpression of GRX2 has been found to protect mice from doxorubicin induced cardiac injury (111), while silencing GRX2 in HeLa cells increases their sensitivity to the drug (112). Deletion of GRX2 was also shown to accelerate the onset and formation of cataracts in mice, due to increased formation of PSSG, leading to increases in proteins aggregates (113). GRX2 has also been identified to have an important function in embryogenesis, playing a role in both brain (114), vascular (115) and cardiac development (116). GRX2 deficiency in mice is associated with the development of hypertension, left ventricular hypertrophy, and fibrosis (117). Lastly, GRX2 may

Dithiol mechanism



Monothiol mechanism

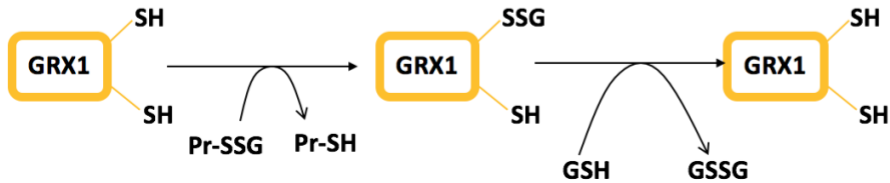


Figure 1.8: The dithiol and monothiol mechanisms of GRX

The dithiol mechanism of GRX shows protein deglutathionylation and subsequent oxidation of GRX, forming GSH, and next the reduction of GRX with GSH. The monothiol mechanism of GRX shows protein deglutathionylation, forming glutathionylated GRX via a thiol exchange. Next, the reduction of GRX with GSH via thiol exchange.

be required to control apoptosis. Overexpression of GRX2 in HeLa cells decreases doxorubicin mediated apoptosis by preventing the release of cytochrome c by cardiolipin, avoiding the initiation of the caspase cascade (118). This evidence points to the conclusion that the regulation of S-glutathionylation reactions is vital for normal development and function.

1.6. S-Glutathionylation reactions in ROS formation

The modification of enzyme function by S-glutathionylation has been found to be an important method of controlling ROS production from certain sites in the mitochondria. The addition of GSH causes a variety of outcomes depending on the enzyme and the site of S-glutathionylation. In some cases, S-glutathionylation can decrease $O_2^{\bullet-}/H_2O_2$ production, while in others it can augment $O_2^{\bullet-}/H_2O_2$ emission. Some enzymes are only S-glutathionylated when local redox buffering networks are more oxidized (*e.g.* GSSG levels are higher due to increased H_2O_2 production), while some are consistently S-glutathionylated during normal physiological conditions. So far, S-glutathionylation has been proven to occur on number of vital mitochondrial enzymes, altering oxidative phosphorylation and the production of ROS in response to redox signals.

1.6.1. Complex I

One of the most studied sites of S-glutathionylation is complex I of the ETC. The effects of thiol modification of complex I were first noticed by Balijepalli *et al.*, who found that diethyl maleate and iodoacetamide, which binds to protein cysteine thiols, can inhibit its activity (119). Notably, this effect could be reversed with the reductant dithiothreitol (DTT). Complex I was also found to be inhibited by nitric oxide, due to thiol S-nitrosylation, which could be reversed by the addition of GSH (120). This evidence indicated the possibility of a mechanism which controls complex I activity by modulating its thiol groups. Complex I was found to contain thiol residues

in the NDUSF1 (~75 KDa) and NDUFV1 (~51 KDa) subunits which were able to become reversibly S-glutathionylated in the presence of GSSG (117, 121, 122). These subunits are located on the arm of complex I which protrudes into the matrix (121). Taylor *et al.* also found that S-glutathionylation of these complexes correlated with an increase in the concentration of mitochondrial ROS (121). In response to decreasing GSH/GSSG ratios, Beer *et al.* found complex I to be one the most persistently S-glutathionylated proteins in the mitochondria (123). Beer *et al.* also discovered that the S-glutathionylation of complex I could be reversed by the addition of purified GRX2 (123). The overall effect of complex I S-glutathionylation on its ROS predicting capabilities has shown mixed results. While some studies have shown that S-glutathionylation of complex I increases $O_2^{\bullet-}/H_2O_2$ emission from the enzyme (117, 121), another study has provided evidence that it causes decreased ROS production (122). Decreases in ROS production could be caused by S-glutathionylation of the NDUSF1 and NDUFV1 subunits in complex I, blocking the transfer of hydride ions from NADH to FMN and decreasing the formation of the FMN semi-radicals and fully reduced flavin molecules that produce ROS (99). S-glutathionylation could also block the flow of electrons to the UQ binding site, also lowering the production of ROS. There are also possible mechanisms that could explain increases in ROS. S-glutathionylation of ND3 subunit in the UQ binding pocket could block electron flow and lead to a buildup of electrons at the FMN site, increasing the likelihood of ROS formation (27). During long term complex I S-glutathionylation, ROS production may also be increased from other sites due the increased levels of NADH caused by decreased complex I activity (99). It has been proposed that the S-glutathionylation of complex I is ultimately more complex than originally thought, and that different S-glutathionylation states of complex I can cause different outcomes in response to different stimuli (99). This hypothesis, also known as the “complex I cysteine code”, suggests that

S-glutathionylation of certain thiols can cause changes in ROS emission in response to changes in the environment.

1.6.2. Succinate dehydrogenase

SDH, also known as complex II of the ETC, is also a significant site of ROS production in the mitochondria. SDH has been found to produce ROS from its FAD prosthetic group in the SDHA subunit during forward and reverse electron flow through the complex (124). During normal physiological conditions SDH is persistently S-glutathionylated on the 70 KDa FAD binding subunit, at Cys90 (100). Deglutathionylation of the enzyme causes decreased activity and increased production of ROS (100). One hypothesis is that S-glutathionylation of the specified residue causes a conformational change in the FAD binding site which increases electron transfer away from the flavin site, decreasing electron leakage (100). During ischemia in cardiac tissue, the highly reduced environment causes deglutathionylation of SDH, decreasing its activity and increasing ROS production (100). Increased levels of oxidation can also inactivate the enzyme, suggesting that S-glutathionylation may also act as a protective mechanism (100).

1.6.3. OGDH and PDH

Although in the past complex I was considered the most important source of ROS production in the mitochondria, evidence has shown that several other enzymes in mitochondria can serve as high capacity sites for $O_2^{\bullet-}/H_2O_2$ formation. For instance, it was found that Krebs cycle enzymes, OGDH (125, 126) and PDH (127), can generate far more $O_2^{\bullet-}/H_2O_2$ than complex I. In skeletal muscle, the OGDH and PDH complexes have been found to produce eight and four times as much ROS than complex I, respectively, when NADH is the source of electrons (128). Similar observations have been made in cardiac and liver tissue, with OGDH producing more ROS than PDH (44). Moreover, it has been found in liver mitochondria that OGDH accounts

for ~35% of the ROS formed whereas PDH and complex I generate negligible amounts (62). These enzymes have also been shown to produce ROS during reverse electron transfer (*e.g* NADH is oxidized by PDH and OGDH and electrons flow backwards through the enzyme complex) (44). This can occur at physiological concentrations of NADH, indicating that reverse electron flow through these enzymes is a source of ROS even during normal mitochondrial function (44). Both enzymes complexes are likely to be important sites of redox signaling due to the evidence that they are major sources of ROS and because they are both essential entry sites for carbon into the Krebs cycle.

Initial studies have identified OGDH as a redox sensor, meaning that it undergoes changes in function in response to levels of ROS in the mitochondria. Nulton-Persson *et al.* found that treatment of mitochondria with H₂O₂ caused a decrease in oxidative phosphorylation, which was linked to a decrease in the activity of OGDH (129). This inactivation was reversed by either DTT or GRX1, demonstrating that H₂O₂ must cause some sort of modification of the sulfhydryl groups of OGDH (129). The discovery that OGDH is a source of ROS led to the hypothesis that production of ROS from the complex can negatively feedback and inhibit further production (22). Further inquiries into the modification of OGDH during oxidative stress showed that the lipoic acid residues of the E2 subunit were reversibly S-glutathionylated (130, 131). Since the lipoic acid residues of OGDH are susceptible to oxidation by H₂O₂, S-glutathionylation may be a method to keep them protected during times of increased oxidative stress (22). Initially, diminished ROS production seen during OGDH S-glutathionylation was considered to be caused by decreased NADH production, reducing its oxidation at complex I (22). However, it has been shown that S-glutathionylation of OGDH can modulate the emission of ROS from the enzyme complex itself (44, 61, 132). Depending on where OGDH is S-glutathionylated, production of ROS can be either

decreased or increased. S-glutathionylation of the lipoic acid residues of the E2 subunit by GSSG leads to decreased O_2^{\bullet}/H_2O_2 production by blocking the transfer of electrons to the E3 flavin group, also coinciding with decreased production of NADH (44, 132). Conversely, when OGDH is incubated with increased concentrations of GSH, the E1 subunit becomes S-glutathionylated, leading to increased O_2^{\bullet}/H_2O_2 emission (132). OGDH does generate O_2^{\bullet}/H_2O_2 from its E1 and E3 subunits and thus it is possible that S-glutathionylation of the E1 subunit leads to the accumulation of thiamine radicals, which can increase ROS production (132). The accumulated evidence indicates that OGDH can serve as a mitochondrial redox sensor that can increase or decrease ROS production in response to changes in the GSH/GSSG ratio.

Recent work from our laboratory has indicated that like OGDH, ROS production by PDH is also controlled by S-glutathionylation (61). Using the S-glutathionylation catalysts, diamide and disulfiram, during the forward oxidation of pyruvate, PDH has been found to show decreased O_2^{\bullet}/H_2O_2 emission (61). S-glutathionylation of PDH has been confirmed on all three enzyme subunits, with the E2 subunit being the most persistently S-glutathionylated (61). This indicates that like OGDH, PDH can also be S-glutathionylated on the E2 subunit to decrease ROS emission from the complex. PDH has also been shown to facilitate reverse electron flow through the complex, during which ROS is produced (44). Incubation of PDH with GSSG caused amplified ROS production through reverse electron transport when supplemented with NADH (61). This effect was reversed by the addition of GRX2, indicating it was driven by S-glutathionylation (61). S-glutathionylation of the E2 subunit of PDH during reverse electron transfer may block the flow of electrons from the E3 to the E1 subunit. This may allow for increased passage of electrons from the flavin group of the E3 subunit, to O_2 , increasing the production of ROS (61). During times of increased oxidative stress leading to high levels of GSSG and NADH, GRX2 may be an important method

to prevent S-glutathionylation of PDH and thereby prevent further increases in ROS production from the complex.

1.6.4. Uncoupling proteins 2 and 3

Uncoupling proteins in the mitochondria have also been suggested to influence the production of ROS. These proteins can decrease the membrane potential in mitochondria by allowing protons to return to the matrix independently of ATP synthase, decreasing the membrane potential, which may decrease ROS production. UCP2 and UCP3, which are 73% homologous to each other, are integral proteins embedded in the mitochondrial inner membrane and part of the solute anion carrier superfamily. ROS production from complex I and III is known to be very sensitive to the PMF, therefore it was hypothesized that mitochondrial uncoupling may be a possible method of decreasing ROS production by the ETC (78). Over a decade ago, it was found that proton leakage through the mitochondrial UCPs can be activated by O_2^{\bullet} (133). This indicated that ROS may be able to regulate its own production through a negative feedback loop that involved activation of proton leaks through the UCPs. Inhibition or knockout of UCP2 and UCP3 has been found to increase production ROS, while overexpression of these proteins has the opposite effect (80, 82, 83). More recent work has identified that UCP2 and UCP3 can be S-glutathionylated, which is thought to be required for the regulation of proton return to the matrix and the modulation of mitochondrial ROS production (77). UCP2 and UCP3 both contain reactive cysteine sites that can be S-glutathionylated, specifically Cys25 and Cys259 in UCP3 (77). S-glutathionylation of UCP3 causes a decrease in UCP3 mediated proton leak (77). S-glutathionylation of UCP3 was also discovered to be catalyzed by the enzyme GRX2 (134). In GRX2 knock out mice UCP3 was less glutathionylated and proton leak was increased in skeletal muscle mitochondria (134). The evidence may suggest a mechanism in which S-glutathionylation

of UCPs can alter proton leak, modifying the proton gradient and therefore altering ROS production by the ETC.

1.7. Research objectives

The goal of this project was to further characterize the functionality of S-glutathionylation reactions in the mitochondria and how this redox sensitive covalent modification alters ROS production in liver and cardiac mitochondria metabolizing different substrates and subjected to different bioenergetic conditions. Using GRX2 homozygous knock out mice (GRX^{-/-}) and mice heterozygous for GRX2 (GRX2^{+/-}), changes in mitochondrial ROS production were measured and compared to wildtype (WT) C57BL/6N littermates. Since S-glutathionylation reactions are mediated by GRX2 in the mitochondria, the loss of the enzyme would lead to altered S-glutathionylation states of important ROS production enzymes in the mitochondria. Changes in ROS emission from specific sites in the mitochondria was measured using site specific inhibitors.

1.7.1. Hypothesis

My hypothesis is that the loss of GRX2 will lead to deregulated S-glutathionylation in the mitochondria, which will cause alteration in ROS emission from key sites, in particular, complexes I and II of the ETC and PDH and OGDH of the Krebs cycle. Specific aims for this project will include:

1. Characterizing the production of ROS in liver and cardiac mitochondria isolated from GRX2 deficient mice when supplemented with malate and pyruvate or 2-oxoglutarate.
2. Characterizing the production of ROS in liver and cardiac mitochondria isolated from GRX2 deficient mice, when supplemented with succinate.
3. Characterizing the change in ROS production in liver and cardiac mitochondria isolated from GRX2 deficient mice, when the membrane potential of the mitochondria is altered.

2. Materials and Methods

2.1. Breeding

Male and female GRX2^{+/-} mice were a gift from Dr. Mary-Ellen Harper (University of Ottawa). GRX2^{+/-} mice were generated using the C57BL/6N mouse strain as described in Wu *et al.* 2011 (135). Mice were housed in the animal care unit at room temperature (~23 °C, 12 hour (h) dark/12 h light cycle, lights on at 0700 h) and given free access to water and chow (Teklad Global 18% Protein Rodent Diet, 2018). Age-matched male and female GRX2^{+/-} mice were paired for breeding and the generation of litters containing WT, GRX2^{+/-}, GRX2^{-/-} animals. Male mice were removed once it was confirmed female mice were pregnant. After birth, the male pups were weaned at 3 weeks of age and ear notched for genotyping. Ear notches were stored at -20 °C. Female pups were either kept for future breeding or culled. Male mice were fed a standard grain based chow diet (Teklad Global 18% Protein Rodent Diet, 2018) *ad libitum* and given free access to water for up to 10 weeks. Mice were weighed and examined routinely from the age of 4-8 weeks to ascertain if GRX2 deficiency caused any alterations in linear growth (change in weight over time). It is important to note that two previous studies found that deletion of the GRX2 gene does not alter linear growth, food and water consumption, or result in the development of any adverse phenotypes that may affect physiological function(s) (117, 134). Animals were cared for in accordance with the principles and guidelines of the Canadian Council on Animal Care and the Institute of Laboratory Animal Resources (National Research Council). All procedures using mice were approved by the Animal Care and Use Committee at Memorial University of Newfoundland.

2.2. Genotyping

2.2.1. DNA extraction

Mouse genotyping was conducted as described in Mailloux *et al.* and Wu *et al.* (117, 135). DNA extraction from ear notches was performed using the REDExtract-N-Amp Tissue PCR Kit (Sigma-Aldrich) according to the manufacturer's instructions. Ear notches were placed in separate 1.5 mL microcentrifuge tubes and treated with 100 μ L Extraction Solution and 25 μ L Tissue Prep Solution. Samples were then incubated at room temperature for 10 mins followed by a second incubation at 95 °C for 3 mins. This was followed by the addition of 100 μ L of Neutralization Solution to each tube. Samples were then vortexed and used for polymerase chain reaction (PCR). Alternatively, samples were stored at -20 °C for later use.

2.2.2. Polymerase chain reaction

Primers for *Grx2* were obtained from Integrated DNA Technologies (Table 2.1). Primer sequences were provided by Dr. Mary-Ellen Harper (University of Ottawa) and were generated based on previously published studies by Mailloux *et al.* and Wu *et al.* (134, 135). In a PCR tube the following contents were added: 1 μ L of 0.5 μ M *Grx2* forward primer, 1 μ M of 0.5 μ M *Grx2* reverse primer, 1 μ L of 0.5 μ M *Grx2* neo primer, 4 μ L of DNA solution, 3 μ L nuclease-free water and 10 μ L of REDExtract-N-Amp Tissue PCR Kit Reaction Mixture, giving a final volume of 20 μ L. DNA sequences were then amplified using an Eppendorf Mastercycler pro PCR System. The PCR sequence is shown in Table 2.2.

2.2.3. Gel electrophoresis

PCR samples were electrophoresed on a 1.5 % agarose gel which was made by dissolving 0.75 g of agarose powder (Fisher Scientific) in 0.5X Tris-Borate-EDTA (TBE, 10X solution diluted to 0.5X in analytical water) under heat. SYBR Safe DNA Gel Stain (Fisher Scientific)

Table 2.1: DNA sequence of primers used for *Grx2* genotyping

| Primer | Sequence |
|--------------|---|
| Grx2 Forward | 5'-GAC CTA GCC TAC CAG ACT TGG CTG AAA TTT ATT C-3' |
| Grx2 Reverse | 5'-CAT AGA CAC TCT TCA CTT TCA AGC CCA CCC TC-3' |
| Grx2 Neo | 5'-CCT ACA TTT TGA ATG GAA GGA TTG GAG CTA CGG G-3' |

Table 2.2: Polymerase chain reaction protocol for *Grx2* genotyping

| | Temperature (°C) | Time |
|---------------------|------------------|--------|
| Step 1 | 94 | 5 min |
| Step 2 30 Cycles | 94 | 30 sec |
| | 63 | 1 min |
| | 72 | 1 min |
| Step 3 | 72 | 7 min |
| Hold | 4 | ∞ |

was added to the molten agarose (1/10,000 dilution), which was then poured into the gel molding and allowed to solidify. The gel was then set up in a Fisher Biotech Horizontal Electrophoresis Systems gel box. Trackit 100 bp DNA Ladder (Fisher Scientific) was used to estimate DNA fragment size. Samples were electrophoresed for 40 mins at 90 V. Nucleotide sequences corresponding to the amplified *Grx2* gene were visualized with the Alpha Innotech ChemiImager Ready System. WT mice produced a single nucleotide sequence that was 729 base pairs (bp) in length while *GRX2^{-/-}* mice produced a fragment 510 bp in size. Samples collected from *GRX2^{+/-}* mice contained both nucleotide fragments (510 bp and 729 bp).

2.3. Mitochondrial isolation

All steps were performed on ice or at 4°C. Prior to experiments 2 liters of MESH buffer (220 mM mannitol, 1 mM EGTA, 70 mM sucrose, and 20 mM HEPES, pH 7.4) was made and stored at 4 °C. Note that all substrates and reagents utilized for mitochondrial assays were prepared in MESH buffer. Mitochondrial isolation buffer (MESH-B; MESH + 0.5% (w/v) fatty acid-free bovine serum albumin (BSA) (Sigma-Aldrich)) was made fresh the day of experiments. Mitochondria were isolated from the livers and cardiac tissue of 8-10-week-old mice. Mice were deeply anesthetized using isoflurane and euthanized by cervical dislocation. Livers and hearts were then harvested and placed in MESH-B buffer, washed of any excess blood, dabbed dry, and weighed. Tissues were then cut into small pieces and washed in MESH-B. Tissue pieces were then minced with a razor blade and homogenized using the Potter-Elvjham method in 15 mL MESH-B (~15 passes with the pestle). Before homogenizing cardiac tissue, 1 unit of subtilisin A (Sigma-Aldrich), a protease, was added to MESH-B to ensure proteolytic degradation of myofibers and the release of intermyofibrillar mitochondria. The amount of protease required was calculated using Equation 2.1:

Equation 2.1: Calculation of subtilisin A addition

$$\text{Volume of } 1 \frac{\text{mg}}{\text{mL}} \text{ subtilisin A} = \frac{\text{mass of muscle (g)}}{1 \frac{\text{mg}}{\text{mL}} \times 11.7 \frac{\text{mg}}{\text{unit}}}$$

Liver mitochondria were isolated by first centrifuging the homogenate at 800 x g for 9 minutes to remove nuclei and any undisrupted tissue. The pellet was discarded and the supernatant collected and centrifuged at 10,000 x g for 9 mins. The supernatant was then discarded and the pellet was resuspended in 20 mL MESH-B and centrifuged again at 10,000 x g for 9 mins. The wash step is vital for the removal of any contaminating organelles. The supernatant was discarded and the pellet was resuspended in 500 μ L MESH buffer devoid of BSA. For cardiac mitochondria, the homogenate was centrifuged at 10,000 x g for 9 mins and the supernatant was discarded to remove subtilisin A. The pellet was resuspended in 15 mL MESH-B and centrifuged at 800 x g for 9 mins to remove contaminating organelles and undisrupted myofibers. The supernatant was collected and centrifuged at 10,000 x g for 10 mins. The supernatant was discarded and the pellet was resuspended in 100 μ L MESH buffer. Note that BSA was omitted to ensure accurate determination of protein equivalents to mitochondria.

2.3.1. Bradford assay

The concentration of the mitochondrial samples was determined with the Bradford assay (Sigma-Aldrich) using BSA (Sigma-Aldrich) as the standard, with a concentration range of 0 to 1.875 mg/mL. An aliquot of mitochondrial suspension was diluted by 1000 times in analytical water and then vortexed for ~ 5 seconds. Two hundred microliters of Bradford reagent was added to a 1.5 mL microcentrifuge tube followed by 50 μ L of diluted mitochondrial protein solution. The volume was then adjusted to 1 mL with analytical water. After a brief vortex 200 μ L aliquots of the Bradford mixture was added to individual wells of a clear bottom black 96-well plate (Greiner

Bio-One) in duplicate. The final concentration of liver and cardiac mitochondria was calculated using the slope of the line and the equation $y = mx + b$ (Figure 2.1). The final concentration of liver and cardiac mitochondria was approximately 15-20 mg/mL and 6-10 mg/mL, respectively. Samples were then stored on ice for assays. Once assays were completed, remaining samples were stored at -80 °C for immunoblot analysis.

2.4. Amplex Ultra Red assay

$O_2^{\bullet-}$ is often considered the proximal ROS formed by mitochondria. However, it is now well documented that flavin sites (either FAD or FMN) form a mixture of $O_2^{\bullet-}$ and H_2O_2 (44). In addition, any $O_2^{\bullet-}$ formed is quickly dismutated to H_2O_2 by endogenous SOD. The production of ROS by mitochondria oxidizing different substrates was examined using the Amplex Ultra Red (AUR) assay which selectively measures H_2O_2 levels. However, AUR cannot discriminate between H_2O_2 formed during nutrient oxidation or by the dismutation of $O_2^{\bullet-}$. Thus, for this study any measures of ROS emission by mitochondria was denoted as $O_2^{\bullet-}/H_2O_2$ to account for 1) any H_2O_2 generated directly by sites of production and 2) any H_2O_2 formed as a consequence of $O_2^{\bullet-}$ dismutation. Prior to assays, liver and cardiac samples were diluted to 3 mg/mL and 1 mg/mL in MESH-B, respectively, and stored on ice. Twenty microliters of liver or cardiac mitochondria suspension was then transferred into individual chambers of a black 96-welled plate containing MESH-B. Mitochondria were allowed to equilibrate for a few minutes and then AUR assay reagents, enzyme inhibitors, and substrates were added. The final volume in each reaction chamber was 200 μ L and the final concentration of liver and cardiac mitochondria was 0.3 mg/mL and 0.1 mg/mL protein equivalent to mitochondria, respectively. For all assays, changes in fluorescence were tracked at 565/600 nm every 30 seconds for 5 minutes using a SpectraMax M5 plate reader at room temperature.

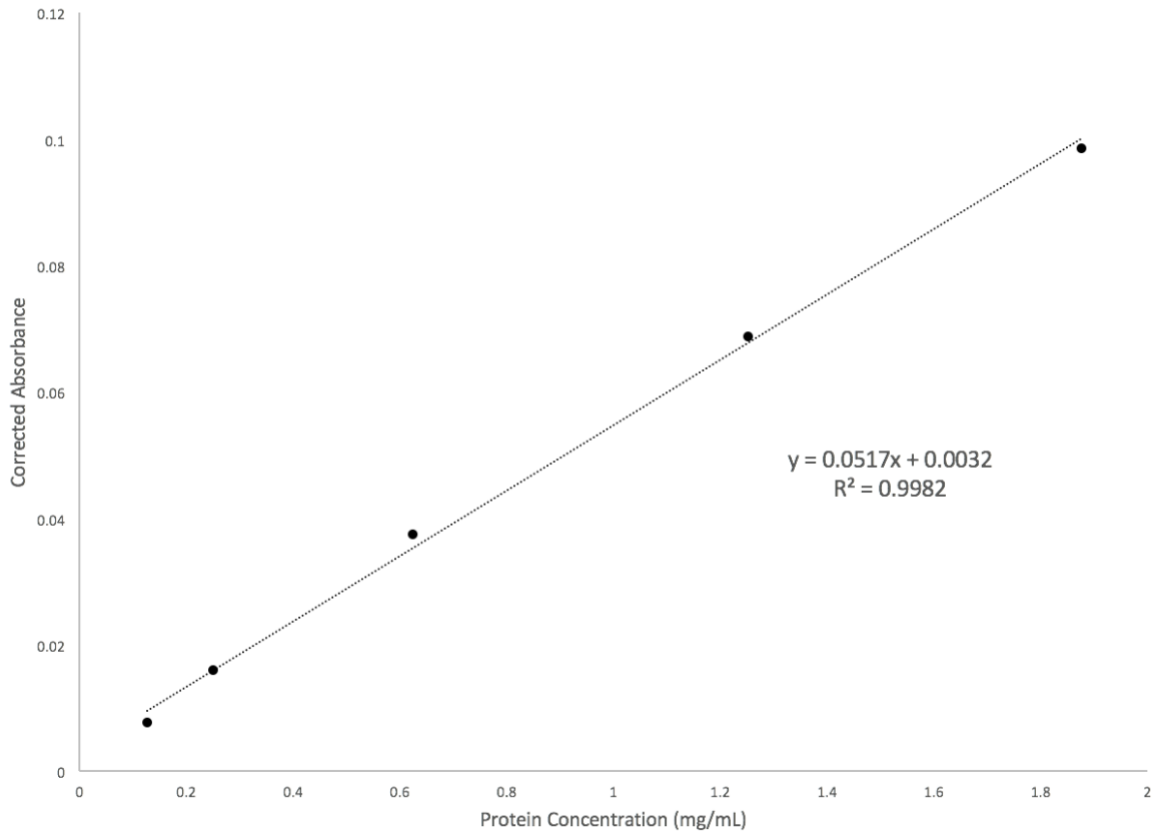


Figure 2.1: Examples of Bradford assay standard curve for protein concentration determination

Increasing concentrations of BSA were mixed with the Bradford reagent at a constant volume and absorbance was measured. This allows for samples with unknown protein concentration to be determined via absorbance.

Rates of production were calculated using standard curves generated with different concentrations of H₂O₂ (30 % stock solution at 12.8 M, Sigma-Aldrich) ranging from 20-400 nM (Figure 2.2).

Rates of O₂^{•-}/H₂O₂ production were calculated using Microsoft Excel 2013.

2.4.1. Measurement of O₂^{•-}/H₂O₂ formation during pyruvate and 2-oxoglutarate oxidation

Mitochondria have been documented to contain up to 11 sources of ROS during nutrient metabolism. This includes Krebs cycle enzymes, respiratory complexes I, II, and III, and several enzymes that feed electrons directly into the UQ pool. In order to ascertain the effect of GRX2 deficiency on O₂^{•-}/H₂O₂ from the different sites of production, different substrate and inhibitor combinations are used (Figure 2.3). Substrates that feed directly into the Krebs cycle can induce ROS production by OGDH, PDH (if pyruvate is present), and the ETC (Figure 2.3). By contrast other substrates like succinate or glycerol-3-phosphate donate electrons directly to the UQ pool, bypassing the Krebs cycle (Figure 2.3). To determine if GRX2 alters ROS production during Krebs cycle metabolism, O₂^{•-}/H₂O₂ emission from liver and cardiac mitochondria was examined using either pyruvate (50 μM) or 2-oxoglutarate (50 μM) in combination with malate (50 μM). These concentrations were chosen because the physiological concentrations of the substrates are known to be in the μM range. In addition, our group has shown previously that μM concentration of substrate can induce a measurable rate of ROS production (61, 62). Prior to initiating the assay, samples were incubated in 10 mM α-keto-β-methyl-n-valeric acid (KMV) (Sigma-Aldrich) or 4 μM myxothiazol (Sigma-Aldrich) for 5 mins at 25 °C. KMV is a structural analog for 2-oxoglutarate and thus selectively inhibits ROS production by OGDH (62). Myxothiazol is a selective inhibitor for ROS production by Complex III (62). Briefly, myxothiazol binds to the UQ binding pocket near the outer leaflet of the inner membrane (Q_o site) preventing the formation of

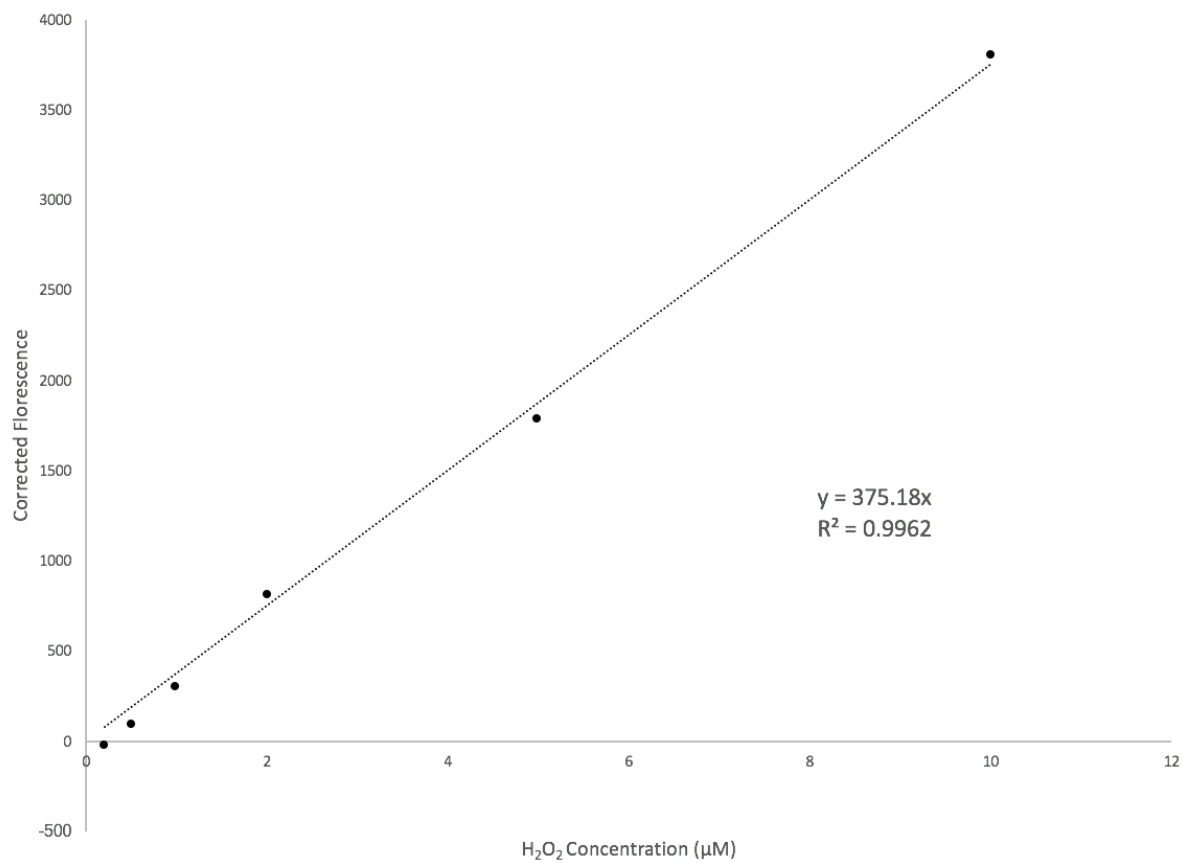


Figure 2.2: Examples of AUR assay standard curve for determination of $O_2^{\bullet-}/H_2O_2$ concentration

The fluorescence of increasing known concentrations of H_2O_2 in MESH buffer was measured with the AUR assay in order to produce a standard curve, allowing for the concentration of unknown H_2O_2 to be determined when fluorescence is measured.

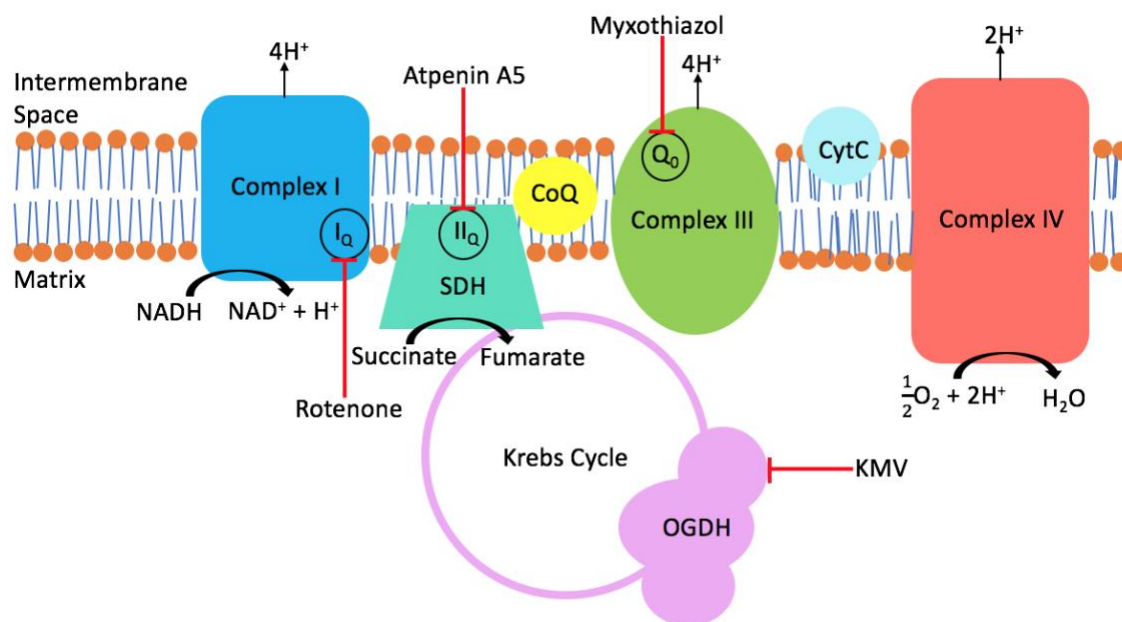


Figure 2.3: Sites of action for different inhibitors of the Krebs cycle and ETC

Rotenone blocks the flow of electrons between the UQ site (I₀) of complex to UQ (CoQ). Atpenin A5 blocks electrons from travelling between the UQ site of SDH and CoQ. Myxothiazol blocks electrons from UQH₂ to the UQH₂ site of complex III (Q₀). KMV is a competitive inhibitor of OGDH, blocking electron movement through the complex, decreasing ROS production.

semiquinone which drives $O_2^{\bullet-}$ formation. The following reagents were then added to all reaction chambers: horseradish peroxidase (HRP, 3 U/mL, Sigma-Aldrich), superoxide dismutase (SOD, 25 U/mL, Sigma-Aldrich), AUR (10 μ M, Invitrogen) and malate (50 μ M). SOD was added to convert any $O_2^{\bullet-}$ present in the intermembrane space into H_2O_2 . Assays were then initiated by the addition of either 50 μ M pyruvate or 50 μ M 2-oxoglutarate.

2.4.2. Measurement of $O_2^{\bullet-}/H_2O_2$ formation during succinate oxidation

Succinate oxidation bypasses the Krebs cycle and Complex I, donating electrons directly to the UQ pool in mitochondria (Figure 2.1). Experimental conditions that employ succinate can be manipulated to allow for the measurement of ROS production by the ETC only. This can be advantageous since it eliminates $O_2^{\bullet-}/H_2O_2$ production from the Krebs cycle allowing one to zero in on which respiratory complex forms the most ROS. To ensure that we were measuring ROS formation by only the respiratory complexes, experimental conditions were manipulated to avoid priming ROS production by the Krebs cycle. This was achieved by excluding pyruvate which, after conversion to acetyl-CoA, can condense with oxaloacetate from succinate metabolism to yield citrate. To determine which site produces the most ROS several ETC inhibitors were used (Figure 2.3). Liver and cardiac mitochondrial samples were incubated with either 40 μ M Atpenin A5 (Santa Cruz), 4 μ M myxothiazol or 4 μ M rotenone (Sigma-Aldrich) for 20 mins at 25 °C. Atpenin A5 is a selective inhibitor for Complex II where it blocks the UQ binding pocket preventing electron flow to Complex I or III (136). Rotenone is a selective inhibitor for Complex I which blocks electron flow from Complex II to the ROS forming FMN prosthetic group. After the incubation, AUR assay reagents were added to each well as described in section 1.4.1. The assay was initiated by the addition of 50 μ M succinate.

2.4.3. Examining the effect of membrane potential on ROS production

The polarity of the mitochondrial inner membrane and the rate of proton extrusion and return can influence mitochondrial ROS production (76). The rate of proton extrusion and return and the strength of the PMF can be manipulated by artificially inducing different states of respiration or by short circuiting proton return by adding chemical uncouplers. Manipulation of the different states of respiration was achieved by exposing mitochondria to four different experimental conditions: (1) substrate alone (state 2 respiration), (2) substrate + 1 mM ADP (state 3 respiration), (3) substrate + 1 mM ADP + 4 $\mu\text{g/mL}$ oligomycin (ATP synthase inhibitor, state 4 respiration, Sigma-Aldrich), and (4) substrate + 1 mM ADP + 4 $\mu\text{g/mL}$ oligomycin + 4 μM FCCP (uncoupled respiration, Sigma-Aldrich). The addition of ADP promotes proton return through Complex V of the respiratory chain which lowers the membrane potential. Oligomycin is a specific inhibitor for Complex V and thus impedes proton return and ATP production allowing for the hyperpolarization of the mitochondrial inner membrane. FCCP is a protonophore that “short circuits” the proton gradient by diffusing protons back into the matrix bypassing Complex V. After mitochondria were exposed to the four different conditions, assays were initiated by the addition of malate (50 μM) and pyruvate (50 μM) were added to all chambers.

2.5. Polarographic measurement of oxygen consumption

The different states of mitochondrial respiration were measured using a Hansatech Oxytherm Electrode. Respiratory states were defined as; state 1: mitochondria only, state 2: mitochondria + substrate, state 3: mitochondria + substrate + ADP, state 4: mitochondria + substrate + ADP + oligomycin, and inhibition of respiration: mitochondria + substrate + ADP + oligomycin + antimycin A (Figure 2.4). The electrode was assembled according to the manufacturer’s instructions. First, the silver (Ag) anode is inspected for any oxidation (depicted

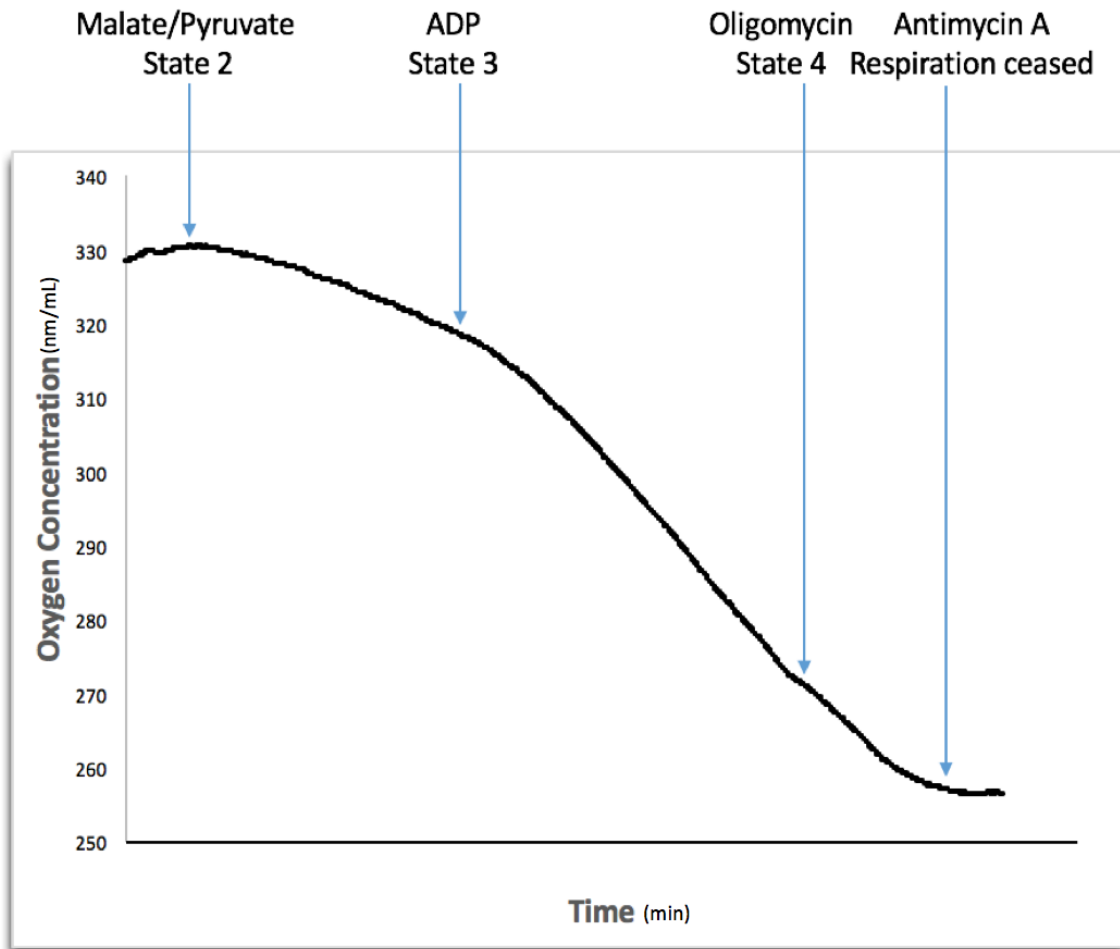


Figure 2.4: The different states of respiration

State 2 respiration of mitochondria is initiated by the addition of malate and pyruvate. State 3 respiration occurs once ADP had been added. Oligomycin is added to block ATP synthase and induce state 4 respiration which allows the estimation of how much respiration can be attributed to proton leakage. Respiration is halted by the addition of antimycin A which binds to complex III, blocking the flow of electrons and collapsing the proton gradient.

by brown spots). manufacturer's instructions. First, the silver (Ag) anode is inspected for any oxidation (depicted by brown spots). If any oxidation was detected, the Ag anode was polished with specialized electrode polish provided by the manufacturer. The electrode was then rinsed well and dabbed dry. One drop of KCl (2.3 M, prepared by dissolving 17.5 g of KCl in 100 mL of analytical water) was first placed on the platinum (Pt) cathode which was then covered with a piece of filter paper and O₂-permeant polyvinylidene difluoride (PVDF) membrane. The membrane/filter paper composite was then saturated with KCl solution and then held in place by a small O-ring which fits snugly around the Pt cathode. The large O-ring was then applied to the outer most part of the disk creating a small chamber on top of the Ag anode which was filled with KCl. This can be visualized in Figure 2.5. The completed electrode system was then attached to the Oxytherm chamber. The chamber was filled with 2 mL of fully oxygenated analytical water and heated to 37 °C with constant stirring. The system was then calibrated by establishing a 100% oxygen saturation condition followed by a 0% oxygen condition which was achieved by adding a few crystals of sodium dithionite (Sigma-Aldrich) to the chamber. For experiments, the chamber was rinsed 5 times with water prior to adding buffer and samples. Mitochondrial samples were diluted to 0.5 mg/ml for liver and 0.1-0.2 mg/ml for cardiac in mitochondrial respiration buffer (220 mM mannitol, 70 mM sucrose, 1 mM EGTA, 2 mM Hepes, 10 mM KH₂PO₄, 2 mM MgCl₂, pH: 7.4). Samples were added to the chamber and equilibrated until oxygen consumption stabilized. State 2 respiration was initiated with the addition of 2 mM malate and 10 mM pyruvate. State 3 respiration was initiated with the addition of 1 mM ADP. State 4 respiration was initiated by adding 4 mg/ml oligomycin. Respiration was ceased with the addition of 4 μM antimycin-A (Sigma-Aldrich). Respiratory control ratios (RCR) were calculated as the ratio of state 3 to state 4 respiration which serves as a proxy measure for the efficiency of mitochondrial ATP production.

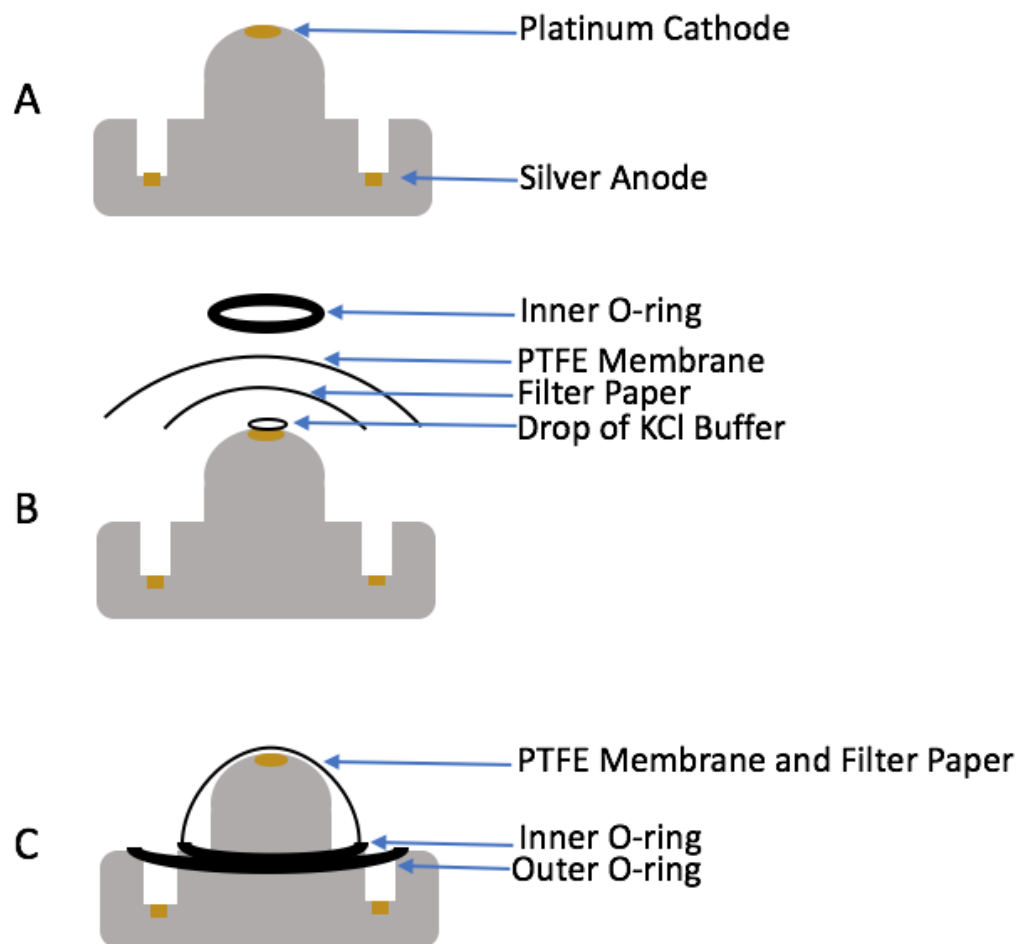


Figure 2.5: Assembly of the Hansatech oxytherm electrode

(A) The electrode disk showing the positions of the Pt cathode and Ag anode. (B) The order of assembly: a drop of KCl buffer overlayed with filter paper and PTFE membrane. The inner O-ring was placed on top and pushed down into place. (C) The assembled electrode. The outer O-ring is placed in the groove, which is then filled with KCl buffer.

Respiration states were measured in WT, GRX2^{+/-} and GRX2^{-/-} mice. WT, GRX2^{+/-} and GRX2^{-/-} mitochondrial samples were performed 4 times in duplicate. Respiration rates were then normalized to the concentration of protein equivalent to mitochondria.

2.6. Gel electrophoresis and Immunoblot

Mitochondria stored at -80 °C were thawed, vortexed vigorously, and then placed on ice. Samples were diluted to 1-6 mg/ml in analytical water containing Laemmli buffer (2X stock diluted to 1X in water, Bio-Rad) and heated for 10 minutes at 100°C. The variable dilution of protein samples depended on the amount required to afford proper detection of enzymes of interest (*e.g.* 40 µg of protein was required to detect GRX2 whereas only 10 µg was needed for OGDH). Reducing conditions, if used, were induced by adding 2% v/v β-mercaptoethanol to each sample. Electrophoresis buffer was prepared as a 10X solution in analytical water (25 mM Trizma base, 1920 mM glycine and 1% (v/v) sodium dodecyl sulfate (SDS)) and stored at room temperature. On the day of experiments electrophoresis buffer was diluted to 1X in analytical water (100 mL 10X electrophoresis buffer + 900 mL analytical water). Samples were electrophoresed in 10% SDS resolving gel for proteins with a molecular weight > 40 KDa and a 12% SDS resolving gel for proteins < 40 KDa. Resolving gels were prepared by first adding 40% acrylamide solution (36.7% w/v acrylamide/3.3 % w/v bis-acrylamide, Biorad) to a 50 mL conical tube followed by the addition of 4X Trizma/SDS resolving gel solution (1.5 M Trizma base + 0.4% (w/v) SDS in 100 mL of analytical water, pH 8.8 with 6 N hydrochloric acid (HCl)). The volume was then adjusted to 20 mL with analytical water. Gel polymerization was initiated by adding N,N,N',N'-tetramethylethane-1,2-diamine (TEMED, Biorad) and 1% (w/v) ammonium persulfate solution

(APS, Biorad). The exact recipes for each gel can be found in Table 2.3. The gel solution was then quickly poured into the gel cast filling the chamber three quarters of the way from the top of the small glass plate. The gel solution was then overlaid with 100% isopropyl alcohol. Once the gel had polymerized, the isopropyl alcohol was removed and the top of the gel carefully dabbed dry and overlaid with a stacking gel. The stacking gel was prepared by first adding acrylamide solution to a 15 mL conical tube (for a 4% (v/v) acrylamide concentration only 1 mL was required). This was followed by the addition of 2.5 mL of 4X Trizma/SDS stacking gel solution (0.5 M Trizma Base + 0.4% (w/v) SDS in 100 mL, pH 6.8). The volume was adjusted to 10 mL with analytical water and then gel polymerization was initiated by the addition of TEMED and APS. The gel solution was then quickly placed on top of the resolving gel and then a 1 mm wide 15 well comb was inserted into the stacking gel. Once polymerized the comb was removed and the wells were dabbed dry.

Samples were loaded into the gel and the Mini-protean Tetra System (Bio-Rad) apparatus was filled with electrophoresis buffer (2.5 mM Trizma base, 192 mM glycine and 0.1% v/v SDS). Samples were electrophoresed at 80 V through the stacking gel. Once the running front penetrated the resolving gel the voltage was increased to 240 V. Fifteen microliters of PageRuler Plus Prestained protein ladder (Fisher Scientific) was also loaded into each gel to track protein migration, gel transfer efficiency, and confirm the molecular weight of proteins of interest detected by immunoblot. Gels were stopped once the running front reached the bottom of the gel. Gels were then removed from the electrophoresis apparatus and equilibrated for at least 15 minutes in 1X transfer buffer. A 10X transfer buffer solution was prepared in advance and stored at room temperature (500 mM Trizma, 380 mM glycine, 10% w/v SDS). One times transfer buffer solution was prepared the day of experiments by diluting 100 mL of buffer in 800 mL of analytical water

Table 2.3: Immunoblot gel recipes

| | 4X Tris/SDS 8.8 Buffer (mL) | 4X Tris/SDS 6.8 Buffer (mL) | 40% Acrylamide/Bis Solution (mL) | Analytical water (mL) | TEMED (μL) | APS (μL) |
|-------------------|-----------------------------|-----------------------------|----------------------------------|-----------------------|-------------------------|-----------------------|
| 10% Resolving Gel | 5 | 0 | 5 | 10 | 150 | 75 |
| 12% Resolving Gel | 5 | 0 | 6 | 9 | 150 | 75 |
| 4% Stacking Gel | 0 | 2.5 | 1 | 6.5 | 75 | 50 |

and 100 mL methanol. Extra thick blotting paper (Bio-Rad), electroblotting sponges (Bio-Rad), and nitrocellulose membranes (Bio-Rad) were also equilibrated for at least 15 mins in transfer buffer. Proteins were electroblotted onto a nitrocellulose membranes (Bio-Rad) for one hour at 120 V at room temperature in transfer buffer with the Mini Trans-Blot Electrophoretic Transfer Cell (Bio-Rad). Successful transfer was confirmed with Ponceau-S (Sigma-Aldrich) staining. Membranes were then blocked at room temperature for at least one hour under constant agitation in a blocking solution consisting of Tris-buffered saline (TBS; 1mM Trizma base and 68 mM NaCl) containing 0.1% (v/v) Tween-20 (Bio-Rad) (TBS-T) and 5% (w/v) non-fat skim milk (Lab Scientific). After three, 5 min room temperature washes in TBS-T, membranes were probed with primary antibodies diluted in TBS-T + 5% (w/v) BSA + 2% (w/v) NaN₃ (Sigma-Aldrich). Primary antibodies used included anti-OGDH (Abcam, catalogue #ab137773), anti-PDH cocktail (Mitoscience, catalogue #ab110416), anti-GRX1 (Abcam, catalogue #ab45953), anti-GRX2 (Abcam, catalogue #ab191292), anti-GSH (Abcam, catalogue #ab19534), anti-SOD (Santa-Cruz, catalogue #sc-30080) and anti-SDHA (Santa-cruz, catalogue #sc-377302). Further details on the dilution factor for each antibody and the amount of protein utilized for detection can be found in Table 2.4. The membrane was incubated in the primary antibody solution overnight at 4°C while shaking continuously. The membranes were rinsed 3 times with TBS-T for 5 mins at room temperature. Membranes were then incubated in secondary goat antibody conjugated to HRP diluted in blocking solution, either anti-mouse or anti-rabbit, depending on the primary antibody, for 70 mins while shaking at room temperature. Immunoreactive bands were visualized using WestPico Super Signal Chemiluminescent substrate and the ImageQuant LAS 4000 system. Band intensities were quantified using ImageJ software. Blots were performed in triplicate.

Table 2.4: Immunoblot specifications

| Immunoblot (Primary Ab) | Tissue | Amount of protein loaded per well (μg) | Acrylamide gel percentage (%) | Primary Ab dilution (μL) | Secondary Ab-HRP conjugate dilution (μL) | Loading control and dilution (μL) | Secondary Ab-HRP conjugate dilution (μL) |
|-------------------------|---------|---|-------------------------------|---------------------------------------|---|--|---|
| OGDH (polyclonal) | Liver | 20 | 10 | 1/3000 | Goat anti-rabbit 1/3000 | SOD 1/2000 (polyclonal) | Goat anti-rabbit 1/3000 |
| | Cardiac | 10 | 10 | | | | |
| PDH (monoclonal) | Liver | 20 | 10 | 1/3000 | Goat anti-mouse 1/3000 | | |
| | Cardiac | 10 | 10 | | | | |
| GRX1 (polyclonal) | Liver | 30 | 12 | 1/2000 | Goat anti-rabbit 1/3000 | SDHA 1/3000 (monoclonal) | Goat anti-mouse 1/3000 |
| | Cardiac | 60 | 12 | | | | |
| GRX2 (polyclonal) | Liver | 40 | 12 | 1/500 | Goat anti-rabbit 1/3000 | | |
| GSH (monoclonal) | Liver | 20 | 10 | 1/500 | Goat anti-mouse 1/3000 | None | N/A |
| | Cardiac | | | | | | |

2.7. Data analysis

All data analysis was performed with Graphpad Prism 6 software. Unpaired T-tests were used for comparison between two groups, one-way analysis of variance (ANOVA) with Fischer's least significant difference (LSD) test was used for comparison between multiple groups. A one-way ANOVA test was used to test for significant difference in ROS production between the genotypes. The significance within the genotypes when using inhibitors was not tested, as these inhibitors have already been proven to significantly inhibit ROS production. LSD is an appropriate post-hoc test for this data as the experiments are well controlled and do not contain many variables. Values are presented as mean + standard error of mean (SEM). Statistical significance was calculated and indicated (****P < 0.0001, ***P < 0.001, **P < 0.01 and *P < 0.05).

3. Results

3.1. Profile of GRX2 deficient mice

3.1.1. Mouse genotyping and confirmation of GRX2 deficiency

Successful deletion of GRX2 was achieved by the elimination of the second exon of the gene encoding the enzyme (135). This resulted in the production of a shortened *Grx2* gene that is 510 bp in length. This is in contrast to the WT *Grx2* gene product, which is 729 bp long. Mice heterozygous or homozygous for the truncated *Grx2* gene were identified by PCR amplification and agarose gel electrophoresis. As shown in Figure 3.1, amplification of the *Grx2* gene by PCR allowed for easy identification of WT, GRX2^{+/-}, and GRX2^{-/-} mice in different litters. WT mice contain a *Grx2* gene sequence that is 729 bp while GRX2^{-/-} mice have a truncated form that is 510 bp long (Figure 3.1). Mice heterozygous for GRX2 contain both bands at 510 and 729 bp, respectively. GRX2 enzyme deficiency was confirmed by immunoblotting for the thiol oxidoreductase in mitochondria prepared from liver (Fig. 3.2). GRX2 protein expression was completely abolished in the knockout mice, while GRX2^{+/-} mice did not show a significant difference in GRX2 expression from that of WT mice (Fig. 3.2).

3.1.2. Effect of GRX2 deficiency on total body and organ weight

Mice deficient in GRX2 were monitored for changes in overall body weight and liver and cardiac weight. It was shown in a previous study that GRX2^{-/-} mice displayed a very small decrease in total body weight when compared to WT littermates fed a standard chow diet *ad libitum* (134). In this study, GRX2^{-/-} and GRX2^{+/-} mice did not show any significant differences in body weight from 4-8 weeks of age (Fig. 3.3). Previous studies have also shown an increase in cardiac weight in GRX2^{-/-} and GRX2^{+/-} mice, which is associated with increased cardiomyocyte size, left ventricular hypertrophy, and fibrosis (117). However, excised hearts from 8-10-week-old

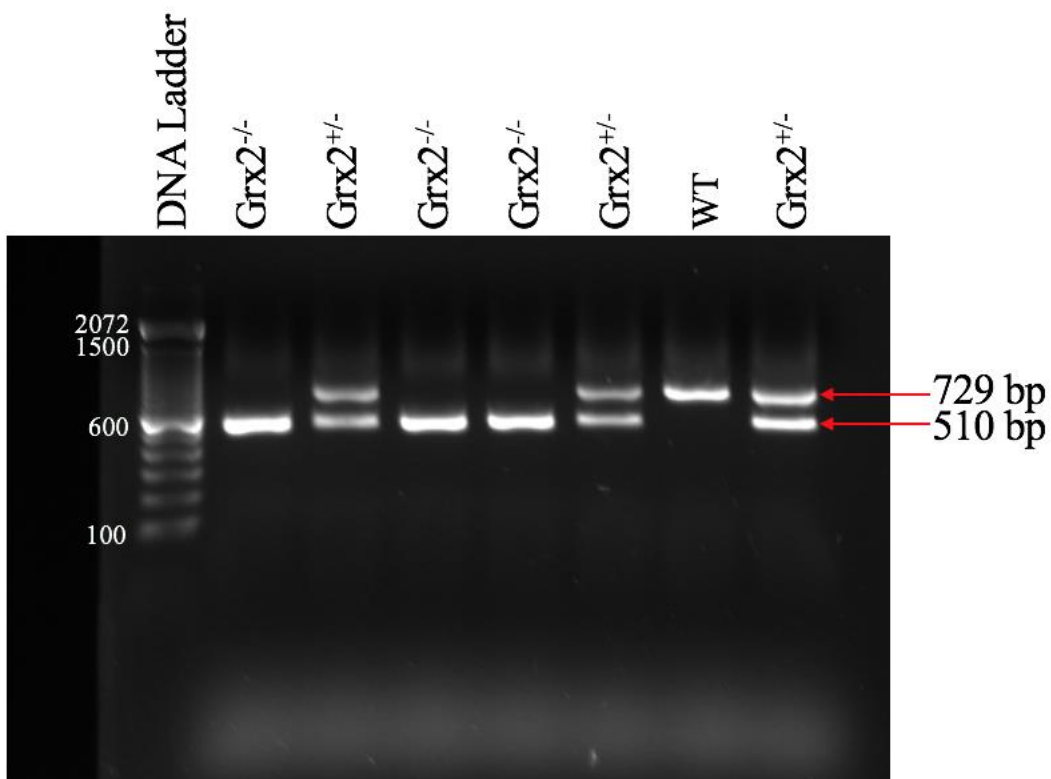


Figure 3.1: Gel electrophoresis of PCR *Grx2* gene amplification

The 729 bp band represents full length *Grx2* product (WT) and the 510 bp band corresponds to *Grx2* devoid of exon 2 (*GRX2*^{-/-}). Mice harboring both bands are *GRX2*^{+/-}.

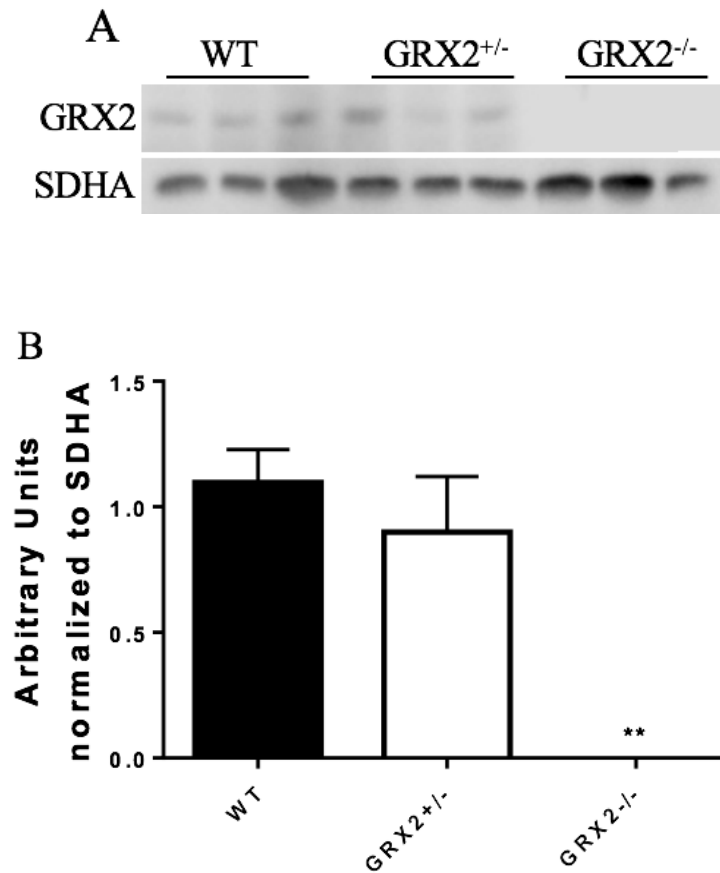


Figure 3.2: Confirmation of GRX2 deficiency

Protein abundance of GRX2 was measured in liver mitochondria samples from WT, GRX2^{+/-}, and GRX2^{-/-} mice. (A) Immunoblot of GRX2 abundance in each genotype. (B) Densitometry analysis of GRX2 immunoblot using ImageJ software. GRX2 was found to be significantly decreased in GRX2^{-/-} mice, as compared to WT mice. Succinate dehydrogenase subunit A (SDHA) was used as the loading control. N=3, mean + SEM. This blot was completed by my supervisor, Dr. Ryan Mailloux.

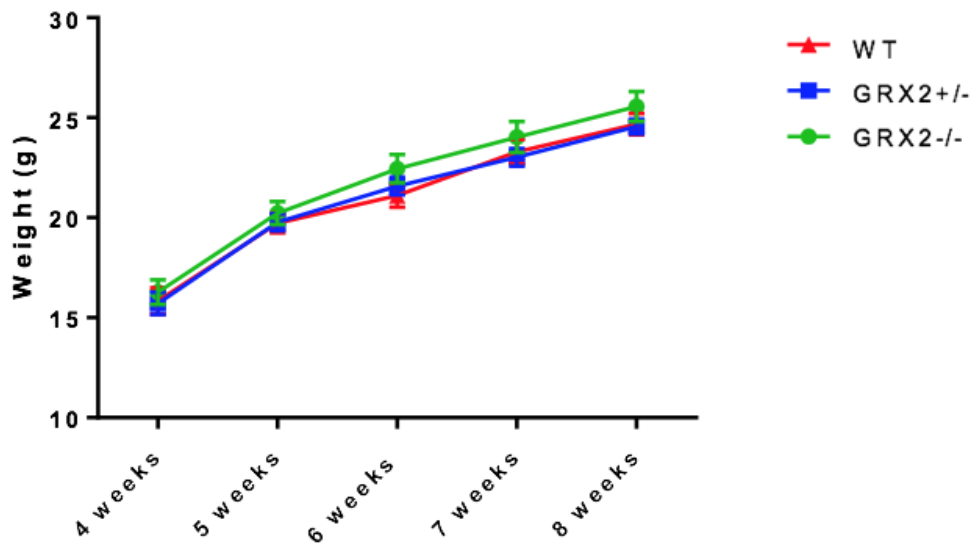


Figure 3.3: Overall body weight of GRX2 deficient mice

WT, GRX2^{+/-}, and GRX2^{-/-} mice were weighed weekly from 4 to 8 weeks of age. No significant difference in weight was noticed between genotypes at any age. N=12-21, mean \pm SEM, one-way ANOVA with a Fischer's LSD post-hoc test.

GRX2^{-/-} and GRX2^{+/-} mice did not show any significant changes in heart weight (Fig. 3.4A). Livers from GRX2 deficient mice also did not show any differences in weight as compared to WT mice, an observation that is consistent with previous findings (Fig. 3.4B) (134).

3.1.3. *GRX2 deficiency does not induce a compensatory increase in GRX1 expression*

GRX1 is a GRX2 isoform that localizes to the cytosol and mitochondrial intermembrane space. The abundance of the GRX1 thiol oxidoreductase in mitochondria isolated from liver and cardiac tissue was examined by immunoblot to determine if GRX2 deficiency caused any compensatory increases in GRX1 abundance. GRX2^{-/-} and GRX2^{+/-} mice did not show any significant increases in the protein abundance of GRX1 when compared to WT mice (Fig 3.5). The densities of the bands in Figure 3.5 were still within the quantitative range of the antibody. GRX2 plays a vital role in conjugating and removing GSH from protein cysteine thiols. It was reported in two previous studies that complete ablation of the *Grx2* gene results in a significant increase in the overall number of S-glutathionylated proteins in mitochondria (134, 135). As shown in Figure 3.6, GRX2^{+/-} mice also displayed a significant increase the total number of mitochondrial proteins modified by GSH. Electrophoresis was carried out under nonreducing conditions to preserve the S-glutathionylated proteome. To confirm antibody specificity, samples were also treated with β -mercaptoethanol, a strong reducing agent known to reverse protein S-glutathionylation. Figure 3.6 demonstrates that conducting the electrophoresis under reducing conditions almost completely abolishes the presence of immunoreactive bands corresponding to S-glutathionylated proteins.

3.2. Examination of the O₂[•]/H₂O₂ release potential of GRX2 deficient mitochondria

3.2.1. *O₂[•]/H₂O₂ release by liver mitochondria oxidizing Krebs cycle-linked substrates*

Protein S-glutathionylation is known to alter O₂[•]/H₂O₂ production from different sites in mitochondria including complex I, OGDH, and PDH (61, 121). However, whether or not GRX2

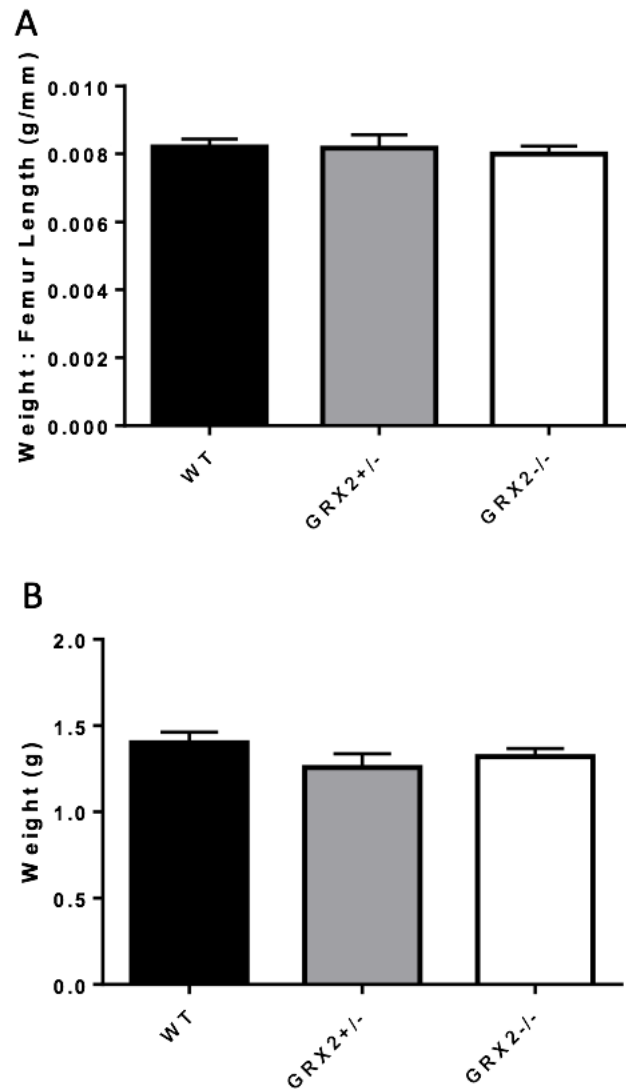


Figure 3.4: Cardiac and liver weight in GRX2 deficient mice

(A) Hearts and (B) livers were excised from mice of each genotype at 8-10 weeks of age and weighed. Cardiac weight was normalized to femur length. No significant difference in weight was noticed in either organ between the three genotypes. N=12-21, mean + SEM, one-way ANOVA with Fischer's a LSD post-hoc test.

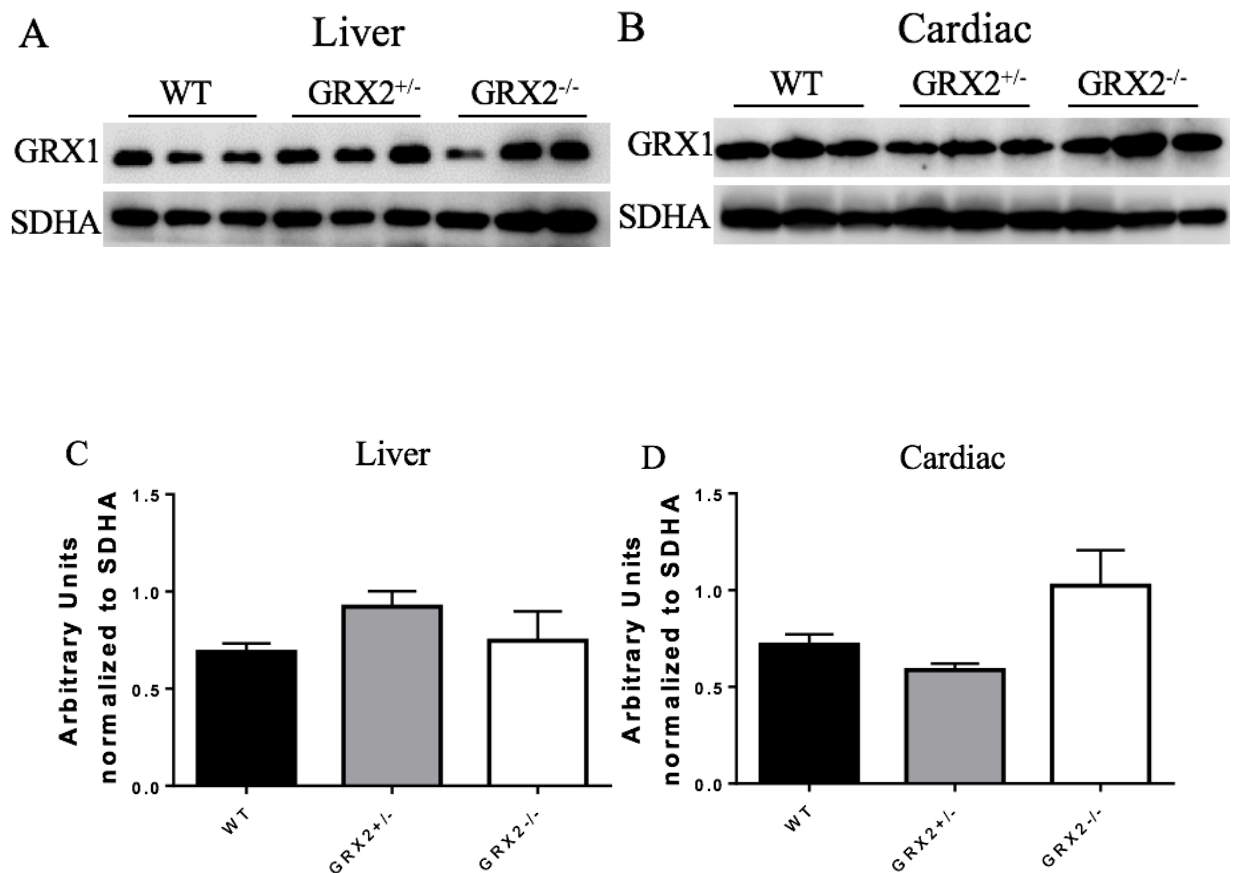


Figure 3.5: There is no compensatory increase in GRX1 protein expression in GRX2 deficient mice

The relative protein abundance of GRX1 was measured by immunoblot in mitochondrial samples from (A) liver and (B) cardiac tissue in each genotype. Densitometry analysis (C & D) was performed on the resulting bands with ImageJ software. No significant changes in protein abundance was noted compared to WT mice. N=3, mean + SEM, one way ANOVA with a Fischer's LSD post-hoc test.

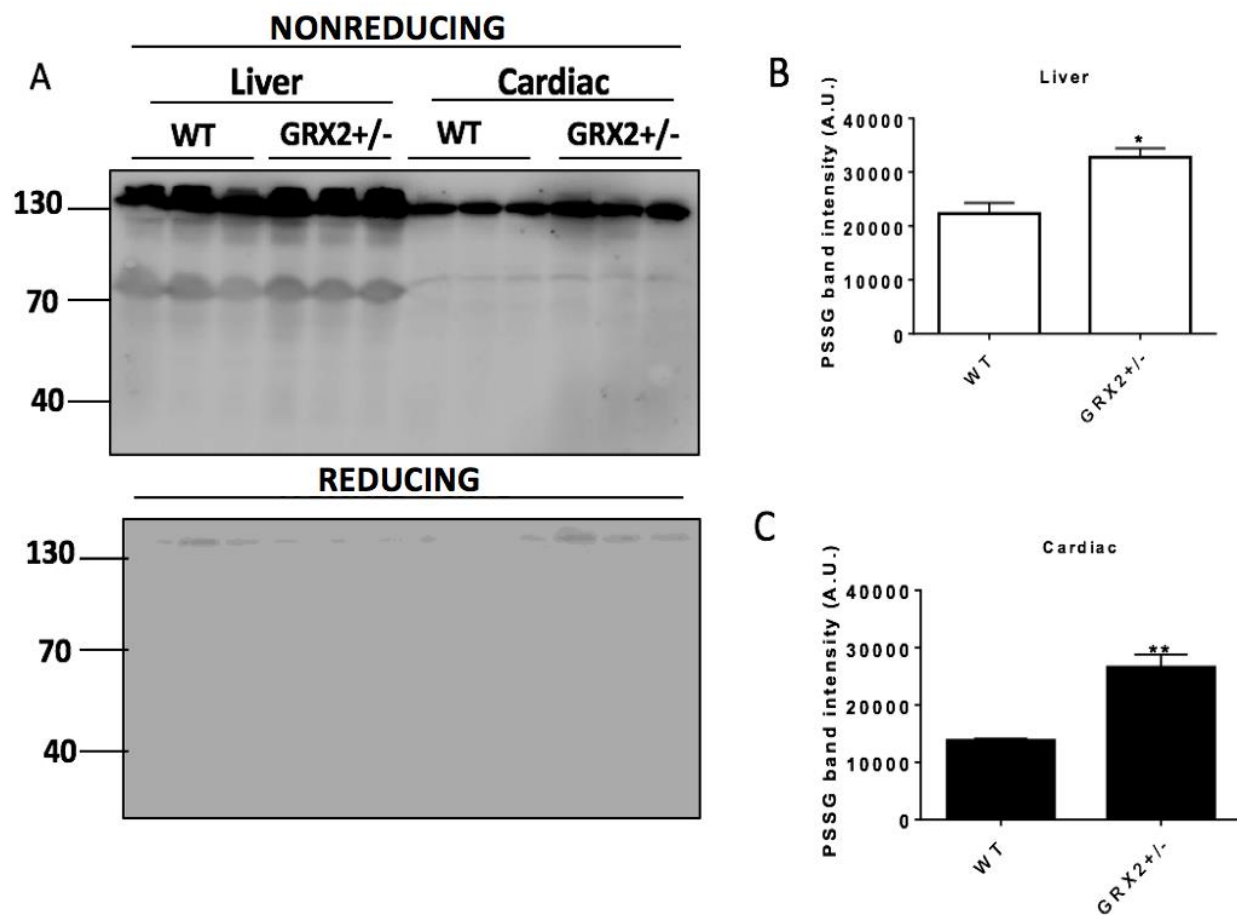


Figure 3.6: GRX2 deficiency increases the overall number and intensity of immunoreactive bands corresponding to PSSG adducts

(A) The abundance of PSSG adducts was measured by immunoblot in WT and GRX2^{+/-} mitochondria isolated from liver and cardiac tissue. Non-reducing conditions were initiated with β -mercaptoethanol. (B) Densitometry analysis of the resulting liver bands was performed with ImageJ software. (C) Densitometry analysis of the resulting cardiac bands was performed with ImageJ software. N=3, mean + SEM, unpaired t-test.

controls $O_2^{\bullet-}/H_2O_2$ release from these sites has not been studied. Thus, we decided to profile the $O_2^{\bullet-}/H_2O_2$ forming capacity of liver and cardiac mitochondria oxidizing different substrates. The rate of $O_2^{\bullet-}/H_2O_2$ production was first examined in liver mitochondria treated with or without KMV or myxothiazol, two potent inhibitors for ROS production by OGDH and complex III, respectively. Mitochondria were supplemented with 50 μ M malate, to replenish Krebs cycle intermediates, and then treated with either 50 μ M pyruvate (Fig. 3.7A) or 50 μ M 2-oxoglutarate (Fig. 3.7B) to stimulate Krebs cycle metabolism and ROS production. Liver mitochondria prepared from GRX2^{+/-} and GRX2^{-/-} mice displayed no significant change in $O_2^{\bullet-}/H_2O_2$ release when compared to WT mitochondria regardless of which substrate was being oxidized (Fig 3.7A and Fig 3.7B). In addition, no differences were observed with mitochondria treated with KMV or myxothiazol. Notably, KMV, a structural analog of 2-oxoglutarate and site-specific inhibitor for OGDH, induced a ~85% decrease in $O_2^{\bullet-}/H_2O_2$ emission from liver mitochondria isolated from WT, GRX2^{+/-}, and GRX2^{-/-} mice metabolizing either pyruvate or 2-oxoglutarate (Fig 3.7A and Fig 3.7B). This indicates that OGDH, not PDH, is a high capacity site for $O_2^{\bullet-}/H_2O_2$ production in liver mitochondria, even when pyruvate and malate serve as substrates. Myxothiazol, on the other hand, induced a ~30% decrease in $O_2^{\bullet-}/H_2O_2$ production by mitochondria metabolizing pyruvate or 2-oxoglutarate (Fig 3.7A and Fig 3.7B). It is important to point out that the concentrations of inhibitors used represent the amount required to achieve maximal inhibition of ROS production by either site of $O_2^{\bullet-}/H_2O_2$ formation (62). Myxothiazol has been shown to cause inhibition of complex I, but the effect is small (137) and likely does not affect these results. Overall, these results confirm findings from a previous study that showed OGDH and Complex III were the highest capacity sites for $O_2^{\bullet-}/H_2O_2$ release in liver mitochondria (62).

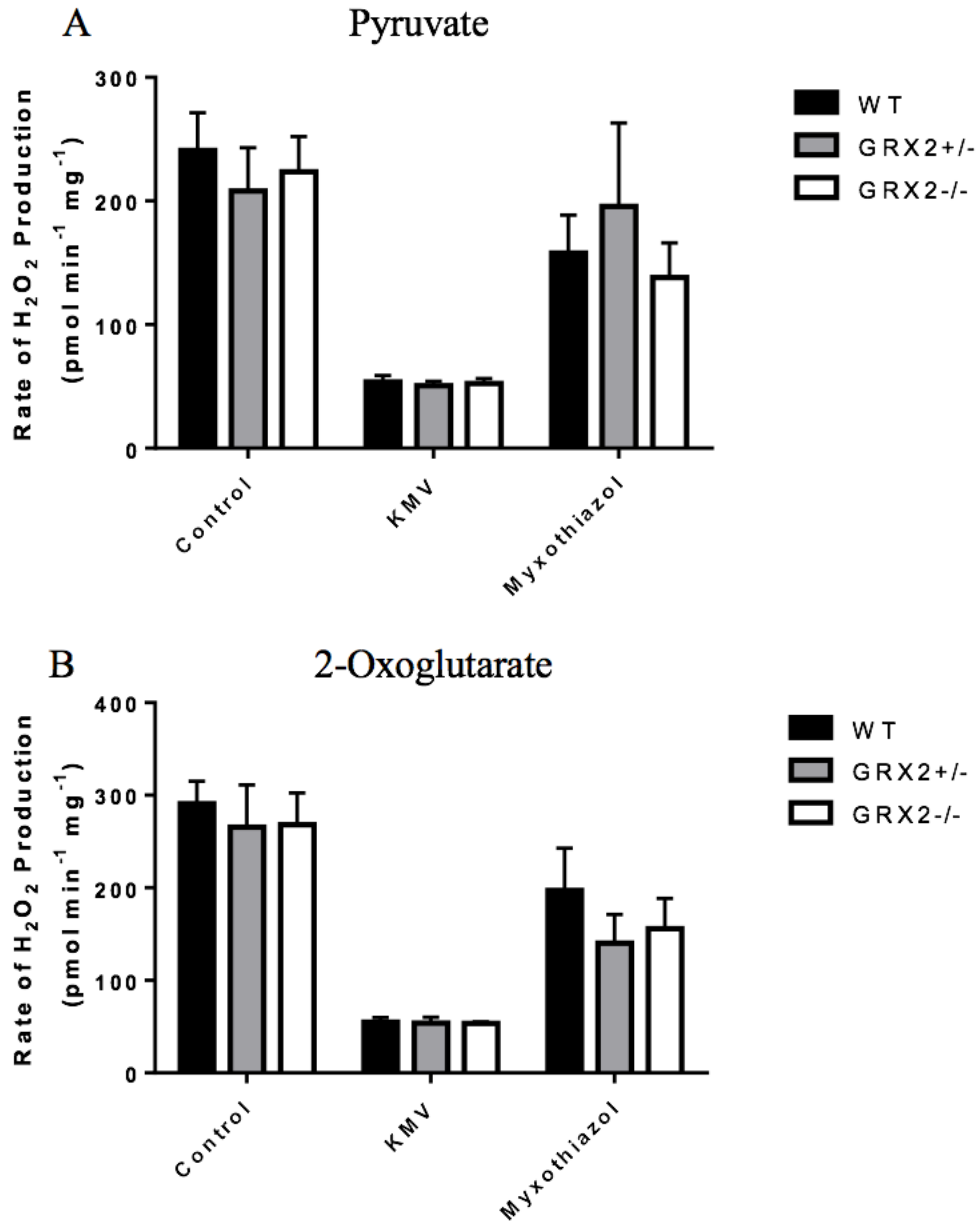


Figure 3.7: $O_2^{\bullet-}/H_2O_2$ production rates in liver mitochondria oxidizing pyruvate or 2-oxoglutarate

Liver mitochondria (0.3 mg/ml) were supplemented with 50 μ M malate and either 50 μ M (A) pyruvate or (B) 2-oxoglutarate. Mitochondria were treated with 10 mM KMV or 4 μ M myxothiazol to examine the source of $O_2^{\bullet-}/H_2O_2$. The rate of $O_2^{\bullet-}/H_2O_2$ production was measured using AUR at 565/600 nm. N=4-6, mean + SEM, one-way ANOVA with a Fisher's LSD post-hoc test.

Enzyme concentration plays a vital role in dictating in how much $O_2^{\bullet-}/H_2O_2$ will be formed by a particular site of production (*e.g.* as the [electron donating site] increases, so will the potential for ROS production). Thus, the overall abundance of PDH and OGDH in WT, GRX2^{+/-}, and GRX2^{-/-} liver mitochondria was assayed by immunoblot. OGDH displayed a significant increase in abundance in GRX2^{-/-} mitochondria when compared to WT (Fig. 3.8). Large differences are seen in the abundance of PDH subunits in the WT mice due to E1, E2, and E3 being present in a 40:40:20 ratio (138). In addition, all three subunits for PDH were significantly higher in liver mitochondria isolated from GRX2^{-/-} mice (Fig. 3.8). These findings prompted us to normalize the $O_2^{\bullet-}/H_2O_2$ production rates in Figure 3.6 to the relative abundance of OGDH and PDH. Normalization of the results to the relative abundance of an enzyme complex is a commonly accepted method (139). In Figure 3.9A, the rate of $O_2^{\bullet-}/H_2O_2$ production from pyruvate supplemented mitochondria was normalized to the abundance of the E2 subunit of PDH. Normalization of the rate of $O_2^{\bullet-}/H_2O_2$ production to PDH levels revealed that liver mitochondria from GRX2^{-/-} mice displayed a significant decrease in $O_2^{\bullet-}/H_2O_2$ emission when compared to WT (Fig. 3.9A). Similar observations were made with liver mitochondria metabolizing 2-oxoglutarate (Fig. 3.9B). Indeed, a decrease in $O_2^{\bullet-}/H_2O_2$ production was observed in GRX2 deficient mitochondria following the normalization of $O_2^{\bullet-}/H_2O_2$ production rates to OGDH abundance (Fig. 3.9B). These observations confirm previously published studies showing that the protein S-glutathionylation of OGDH and PDH decreases $O_2^{\bullet-}/H_2O_2$ emission from either enzyme complex (44, 61). Moreover, these findings show that GRX2 is required to modulate the reversible S-glutathionylation of both proteins, an observation our group has made in two separate publications (44, 61).

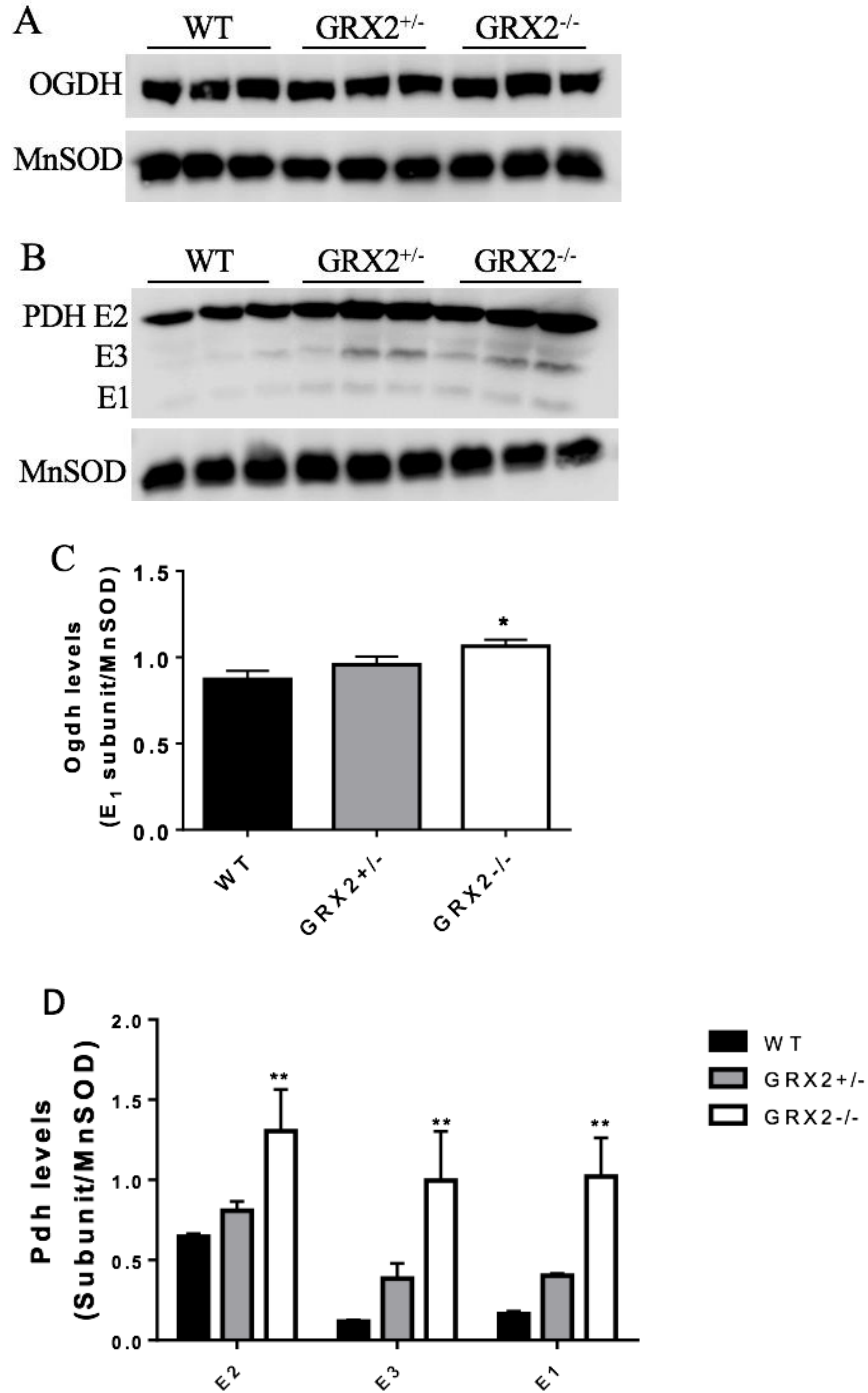


Figure 3.8: Protein abundance of OGDH and PDH in liver mitochondria of GRX2 deficient mice

(A) Immunoblot with liver mitochondrial samples using anti-OGDH (B) Immunoblot with liver mitochondrial samples using anti-PDH cocktail. Note that the loading control was performed on a separate blot with the same concentrations and conditions. (C) Densitometry analysis was performed on OGDH blot with ImageJ analysis. (D) Densitometry analysis was performed on PDH blot with ImageJ analysis MnSOD was used as a loading control. N=3, mean + SEM, one-way ANOVA with a Fischer's LSD post-hoc test.

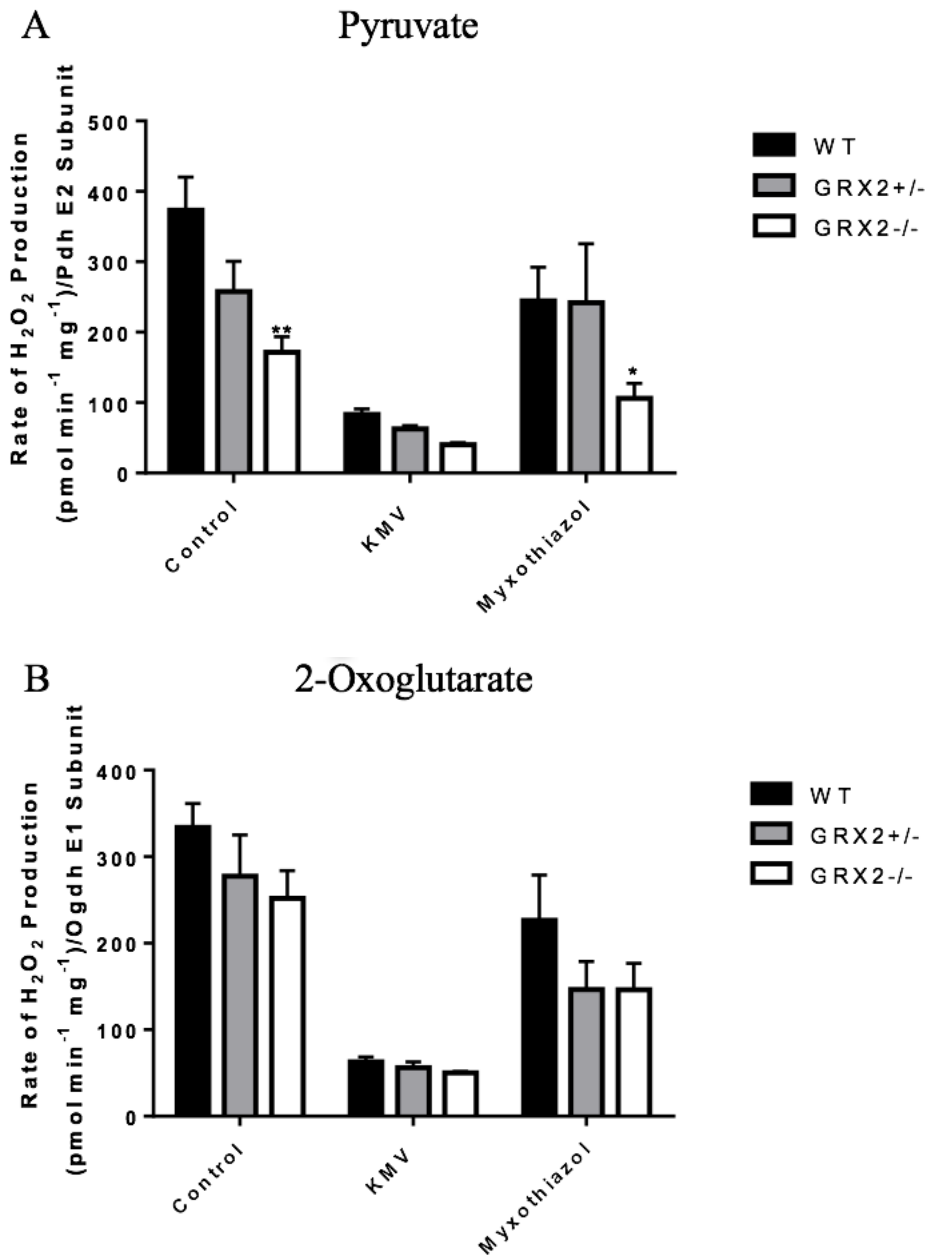


Figure 3.9: Production of O₂[•]/H₂O₂ in liver mitochondria supplemented with pyruvate or 2-oxoglutarate normalized to enzyme content.

Liver mitochondria (0.3 mg/ml) were supplemented with 50 μM malate and with either 50 μM (A) pyruvate or (B) 2-oxoglutarate. Mitochondria were treated with either 10 mM KMV or 4 μM myxothiazol to examine the source of O₂[•]/H₂O₂. The rate of O₂[•]/H₂O₂ production was measured using AUR at 565/600 nm. N=4-6, mean + SEM, one-way ANOVA with a Fisher's LSD post-hoc test. Results were normalized to either the expression of the PDH E2 subunit or the OGDH E1 subunit as determined from immunoblotting.

3.2.2. $O_2^{\bullet-}/H_2O_2$ release by cardiac mitochondria oxidizing Krebs cycle-linked substrates

Mice deficient for GRX2 develop left ventricular hypertrophy and fibrosis, hypertension, and metabolic inflexibility (117), indicating that deregulation of S-glutathionylation reactions in mitochondria can potentially cause cardiovascular disease. On a molecular level, the loss of GRX2 in cardiac mitochondria induces an increase in overall mitochondrial ROS production, an effect that is associated with a ~50% decrease in oxidative phosphorylation (117). It is important to point out though that the $O_2^{\bullet-}/H_2O_2$ release capacity of GRX2 deficient cardiac mitochondria was never profiled. Thus, we decided to examine the impact of GRX2 deficiency on $O_2^{\bullet-}/H_2O_2$ production in WT and GRX2 deficient cardiac mitochondria oxidizing either 50 μ M pyruvate or 50 μ M 2-oxoglutarate with 50 μ M malate. KMV and myxothiazol were used to pinpoint the location of $O_2^{\bullet-}/H_2O_2$ production. No significant differences in the rate of $O_2^{\bullet-}/H_2O_2$ production between the GRX2 deficient and WT mice were noticed when the mitochondria were oxidizing either substrate (Fig. 3.10A and Fig. 3.10B). The inhibitors, KMV and mxyothiazol, had the opposite effect on $O_2^{\bullet-}/H_2O_2$ release rates in cardiac mitochondria when compared to results collected with liver mitochondria (Fig. 3.7). In mitochondria metabolizing pyruvate, KMV and myxothiazol both elevated $O_2^{\bullet-}/H_2O_2$ emission from cardiac mitochondria isolated from WT and GRX2 deficient mice (Fig. 3.10A). Collectively, these findings indicate that high capacity sites for $O_2^{\bullet-}/H_2O_2$ production differ between liver and cardiac mitochondria. Indeed, in this and a previous study, it was found that OGDH and complex III represent the major sources for $O_2^{\bullet-}/H_2O_2$ production in liver mitochondria (62). By contrast, complex I and III have been documented to serve as chief sources of $O_2^{\bullet-}/H_2O_2$ in cardiac mitochondria (43, 63).

Due to the significant changes in PDH and OGDH abundance in GRX2 deficient liver mitochondria, we also decided to look for any changes in the protein abundance levels of both

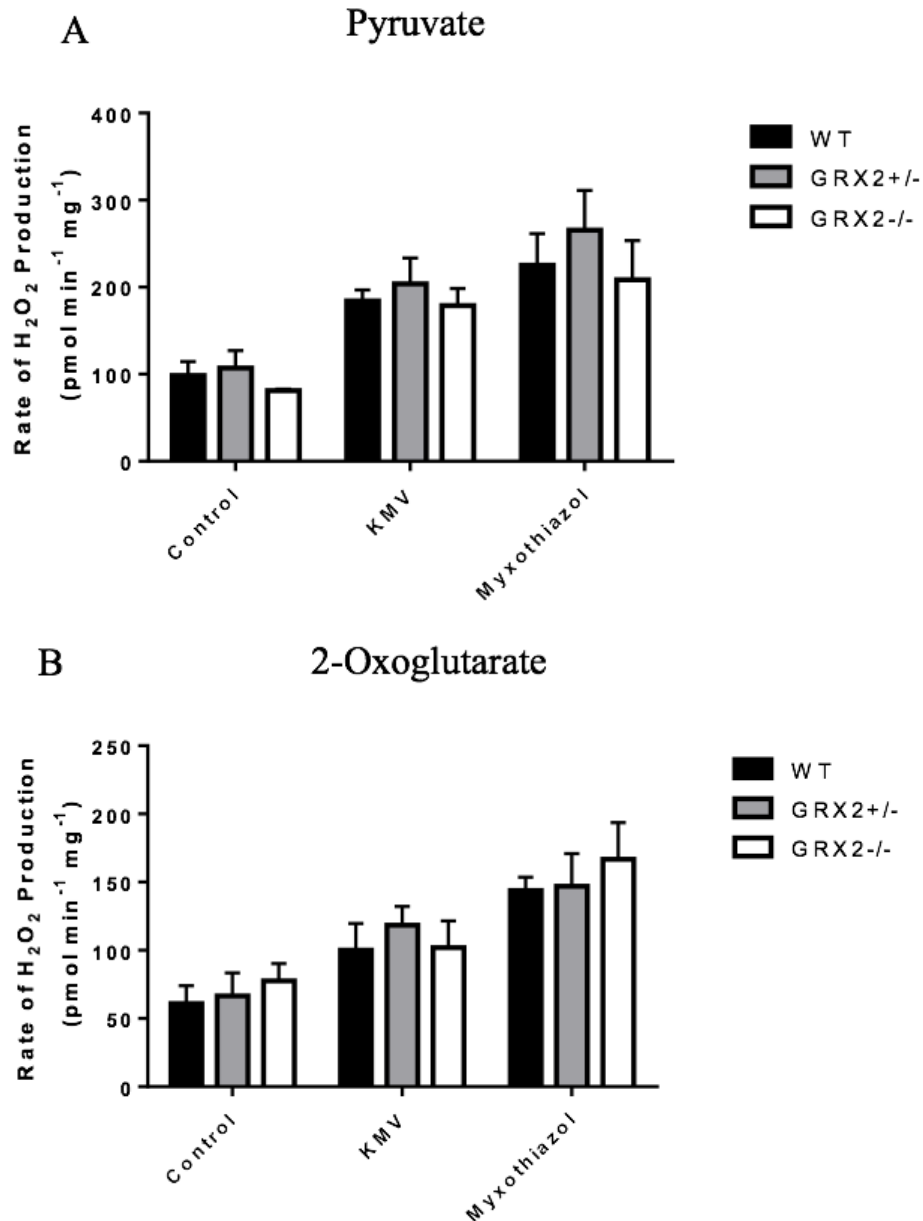


Figure 3.10: Production of $O_2^{\bullet-}/H_2O_2$ in cardiac mitochondria supplemented with pyruvate or 2-oxoglutarate

Cardiac mitochondria (0.1 mg/ml) were supplemented with 50 μ M malate and either 50 μ M (A) pyruvate or (B) 50 μ M 2-oxoglutarate. Mitochondria were inhibited with either 10 mM KMV or 4 μ M myxothiazol to examine the source of $O_2^{\bullet-}/H_2O_2$. The rate of $O_2^{\bullet-}/H_2O_2$ production was measured using AUR at 565/600 nm. N=4-6, mean + SEM, one-way ANOVA with a Fisher's LSD post-hoc test.

complexes in cardiac mitochondria via immunoblotting. There was no significant difference in either complex between WT and GRX2 deficient mice (Fig. 3.11). In the liver, increased S-glutathionylation and inactivation of PDH and OGDH caused by GRX2 loss may induce increases in their abundance. This effect may not be present in cardiac mitochondria, which may experience less S-glutathionylation of Krebs cycle enzymes in GRX2 deficiency.

3.2.3. $O_2^{\bullet-}/H_2O_2$ release by liver and cardiac mitochondria supplemented with succinate

Complexes I, II, and III are significant sources of $O_2^{\bullet-}/H_2O_2$ and complexes I and II are also known targets for S-glutathionylation, while complex III may also be a target (86, 121, 140). Thus, we decided to examine the effect of GRX2 deficiency on succinate-driven $O_2^{\bullet-}/H_2O_2$ production. Using succinate supplemented mitochondria also has the added advantage of examining $O_2^{\bullet-}/H_2O_2$ production exclusively by the respiratory complexes since succinate cannot be metabolized any further by the Krebs cycle following its oxidation to fumarate. Liver mitochondria from GRX2^{+/-} mice displayed a significant increase in $O_2^{\bullet-}/H_2O_2$ release during succinate oxidation (Fig. 3.12A). However, this trend did not hold for mitochondria isolated from GRX2^{-/-} mice (Fig. 3.12A). In addition, rotenone, atpenin A5, and myxothiazol, inhibitors for complexes I, II, and III, respectively, had little to no effect on succinate-driven $O_2^{\bullet-}/H_2O_2$ production. Indeed, inhibition of complex I with rotenone, as well as complex II with atpenin A5, had little effect on the rate of $O_2^{\bullet-}/H_2O_2$ production in liver mitochondria (Fig. 3.12A). Inhibition of complex III with myxothiazol did induce a minor decrease in $O_2^{\bullet-}/H_2O_2$ production which confirms that complex III is a significant source of ROS in liver mitochondria (62). The low levels of $O_2^{\bullet-}/H_2O_2$ produced from succinate supplementation, as well as the minor effect of these ETC inhibitors, indicates that the ETC complexes, particularly complexes I and II, are not a major source of $O_2^{\bullet-}/H_2O_2$ in liver mitochondria.

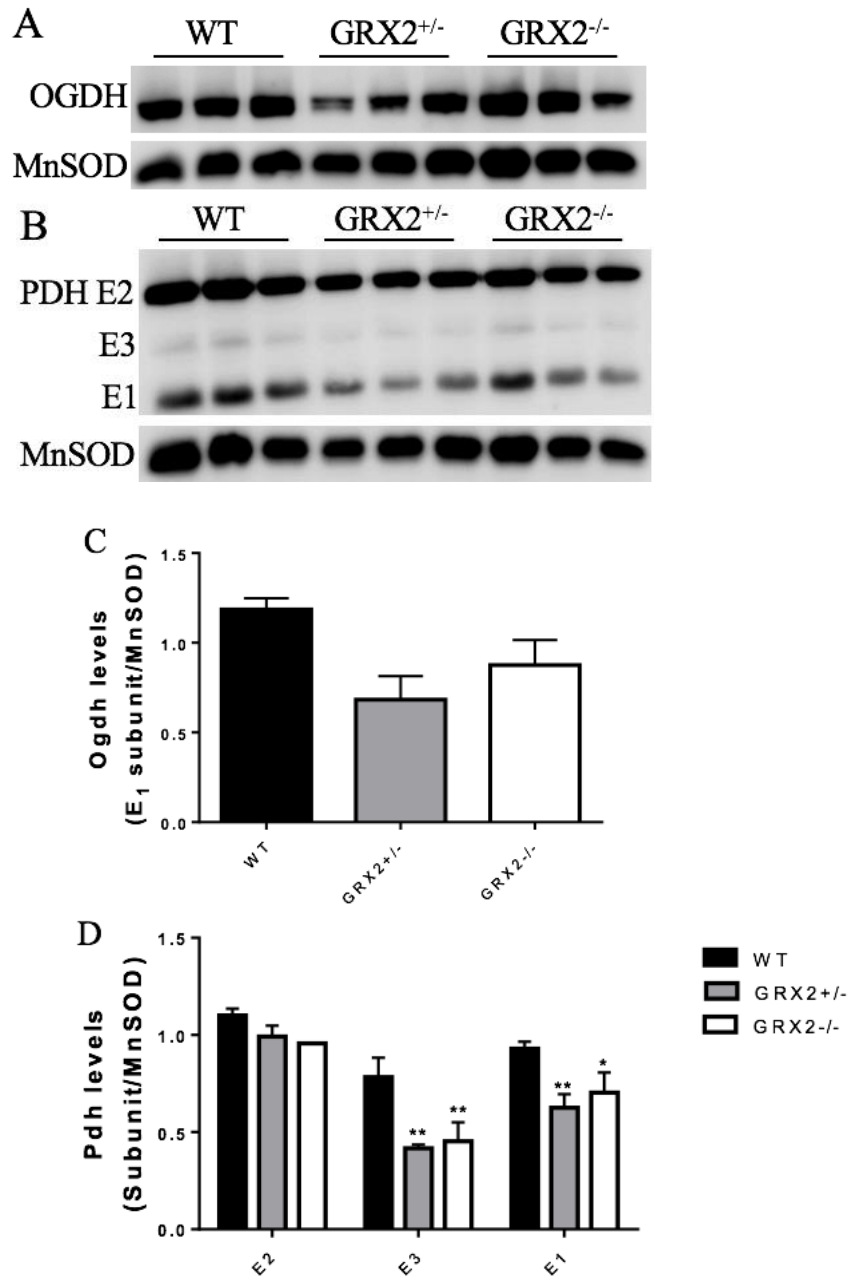


Figure 3.11: Immunoblot of OGDH and PDH cardiac abundance between genotypes

A) Immunoblot with cardiac mitochondrial samples using anti-OGDH B) Immunoblot with cardiac mitochondrial samples using anti-PDH cocktail. C) Densitometry analysis was performed on OGDH blot with ImageJ analysis. D) Densitometry analysis was performed on PDH blot with ImageJ analysis. MnSOD was used as a loading control. N=3, mean + SEM, one-way ANOVA with a Fischer's LSD post-hoc test.

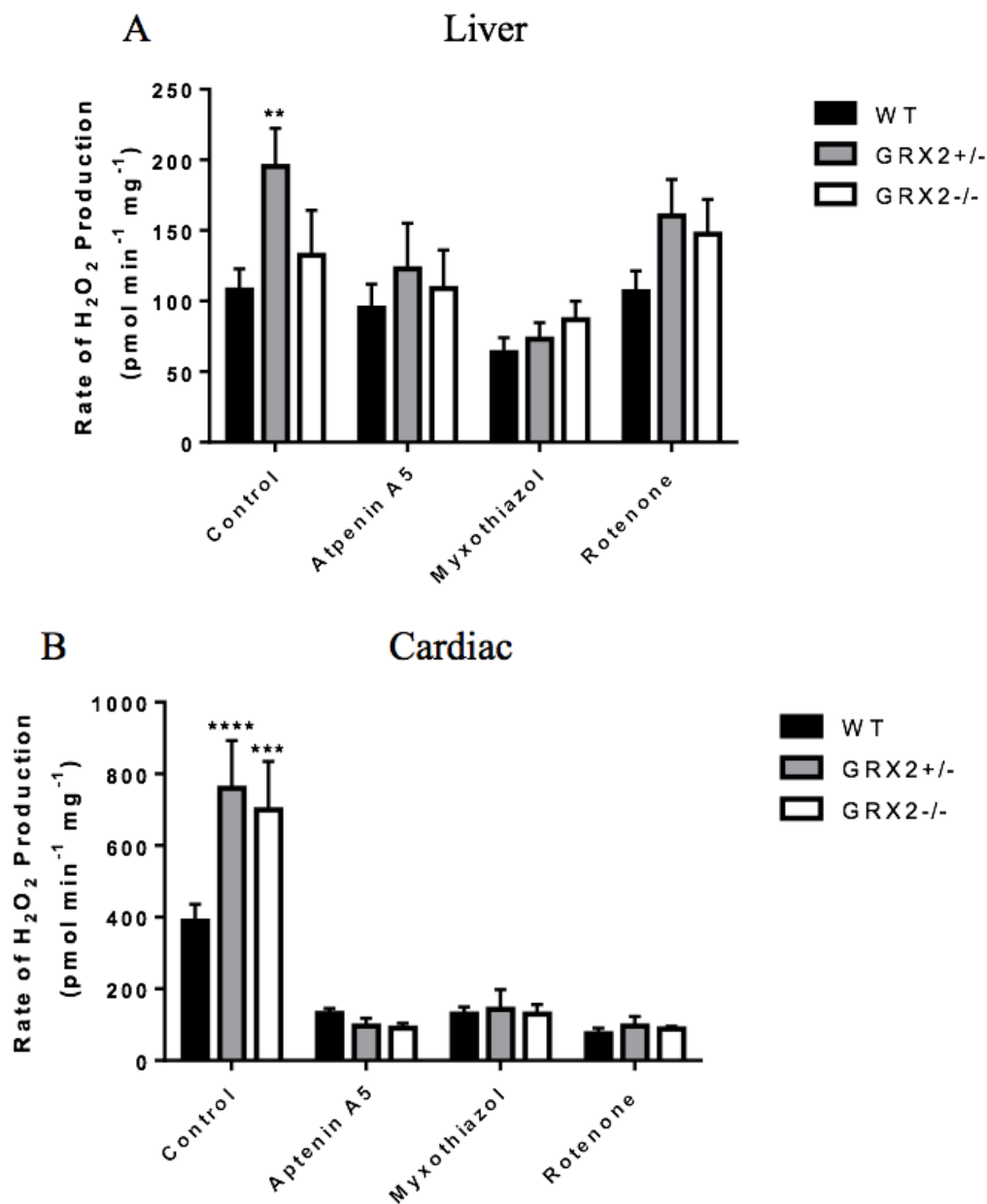


Figure 3.12: Sources of $O_2^{\bullet-}/H_2O_2$ production in succinate supplemented mitochondria

(A) Liver mitochondria (0.03 mg/ml) or (B) cardiac mitochondria (0.01 mg/ml) were supplemented with 50 μM succinate. Mitochondria were inhibited with either 40 μM atpenin A5, 4 μM myxothiazol or 4 μM rotenone to examine the source of $O_2^{\bullet-}/H_2O_2$. The rate of $O_2^{\bullet-}/H_2O_2$ production was measured using AUR at 565/600 nm. N=5, mean + SEM, one-way ANOVA with a Fisher's LSD post-hoc test

The results above indicate that succinate is a poor substrate for $O_2^{\bullet-}/H_2O_2$ production in liver mitochondria. By contrast, succinate served as an excellent substrate for $O_2^{\bullet-}/H_2O_2$ release in cardiac mitochondria (Fig. 3.12B). $O_2^{\bullet-}/H_2O_2$ production displayed a significant increase (almost 2-fold higher) in cardiac mitochondria isolated from GRX2^{+/-} and GRX2^{-/-} mice (Fig. 3.12B). In addition, succinate-induced $O_2^{\bullet-}/H_2O_2$ production by cardiac mitochondria was inhibited by rotenone, atpenin A5, and myxothiazol. Rotenone is a competitive inhibitor for complex I that binds the UQ binding pocket, preventing reverse electron flow from complex II. Since the use of rotenone induced a significant decrease in $O_2^{\bullet-}/H_2O_2$ production during succinate oxidation, we can deduce that reverse electron flow from succinate to complex I is a major source of $O_2^{\bullet-}/H_2O_2$ in cardiac tissue. Similar reasoning can apply to complex III - myxothiazol blocks the UQH₂ binding site of complex III preventing the accumulation of semiquinone radical, a vital source of ROS in mitochondria. It is possible that some decrease in ROS production may be due to membrane potential collapse by myxothiazol, but it has been established that myxothiazol does decrease ROS production by decreasing the formation of semiquinone in complex III (62). Indeed, myxothiazol supplementation almost completely abolished mitochondrial $O_2^{\bullet-}/H_2O_2$ production (Fig. 3.12B). Atpenin A5, on the other hand, selectively binds the UQ binding site upstream from the FAD center in complex II. Similar to rotenone and myxothiazol, atpenin A5 treatment almost completely abolished mitochondrial $O_2^{\bullet-}/H_2O_2$ release (Fig. 3.12B). The FAD center serves as the electron donating site for $O_2^{\bullet-}/H_2O_2$ production in complex II. Therefore, if complex II was a significant source of ROS, blocking the UQ binding site with atpenin A5 would augment $O_2^{\bullet-}/H_2O_2$ production during succinate oxidation. Since this is not the case, it can be concluded that complexes I and III are high capacity sites for ROS production in cardiac mitochondria.

3.2.4. Tissue specific effect of substrates in $O_2^{\bullet-}/H_2O_2$ production

In C57Bl/6N WT mice, it was observed that there were tissue specific effects in terms of the capacity of different substrates to stimulate $O_2^{\bullet-}/H_2O_2$ release from mitochondria. For example, it was observed that 2-oxoglutarate and pyruvate served as better substrates for $O_2^{\bullet-}/H_2O_2$ production in liver mitochondria (Fig. 3.7) in comparison to cardiac mitochondria (Fig. 3.10). By contrast, opposite trends were observed when succinate served as the oxidizable substrate (Fig. 3.12). Overall, this suggests that liver and cardiac mitochondria utilize different enzymes as high capacity sites for $O_2^{\bullet-}/H_2O_2$ production. To examine this effect further, the $O_2^{\bullet-}/H_2O_2$ production rates for liver and cardiac mitochondria oxidizing pyruvate, 2-oxoglutarate, or succinate was compared (Fig. 3.13). It was observed that pyruvate and 2-oxoglutarate were ~2-3-fold more effective than succinate at generating $O_2^{\bullet-}/H_2O_2$ in liver mitochondria. By contrast, succinate was ~4-fold more effective at stimulating $O_2^{\bullet-}/H_2O_2$ release in cardiac mitochondria in comparison to pyruvate or 2-oxoglutarate (Fig. 3.13). The capacity of succinate to stimulate $O_2^{\bullet-}/H_2O_2$ production in cardiac and liver mitochondria was also compared. As shown in Figure 3.13B, succinate was ~4x more for effective and inducing $O_2^{\bullet-}/H_2O_2$ emission from cardiac mitochondria. Opposite findings were made with 2-oxoglutarate and pyruvate. Indeed, pyruvate and 2-oxoglutarate were ~2-fold more effective at stimulating $O_2^{\bullet-}/H_2O_2$ formation in liver mitochondria (Fig. 3.13C & 3.13D). Collectively, these findings demonstrate that liver and cardiac mitochondria utilize different enzyme combinations as high capacity sites for $O_2^{\bullet-}/H_2O_2$ production. Moreover, these findings confirm a recent publication by Slade *et al.* which demonstrated that OGDH and complex III are the main sources of $O_2^{\bullet-}/H_2O_2$ in the liver whereas complex I and III are the chief sites in cardiac tissue (43, 63).

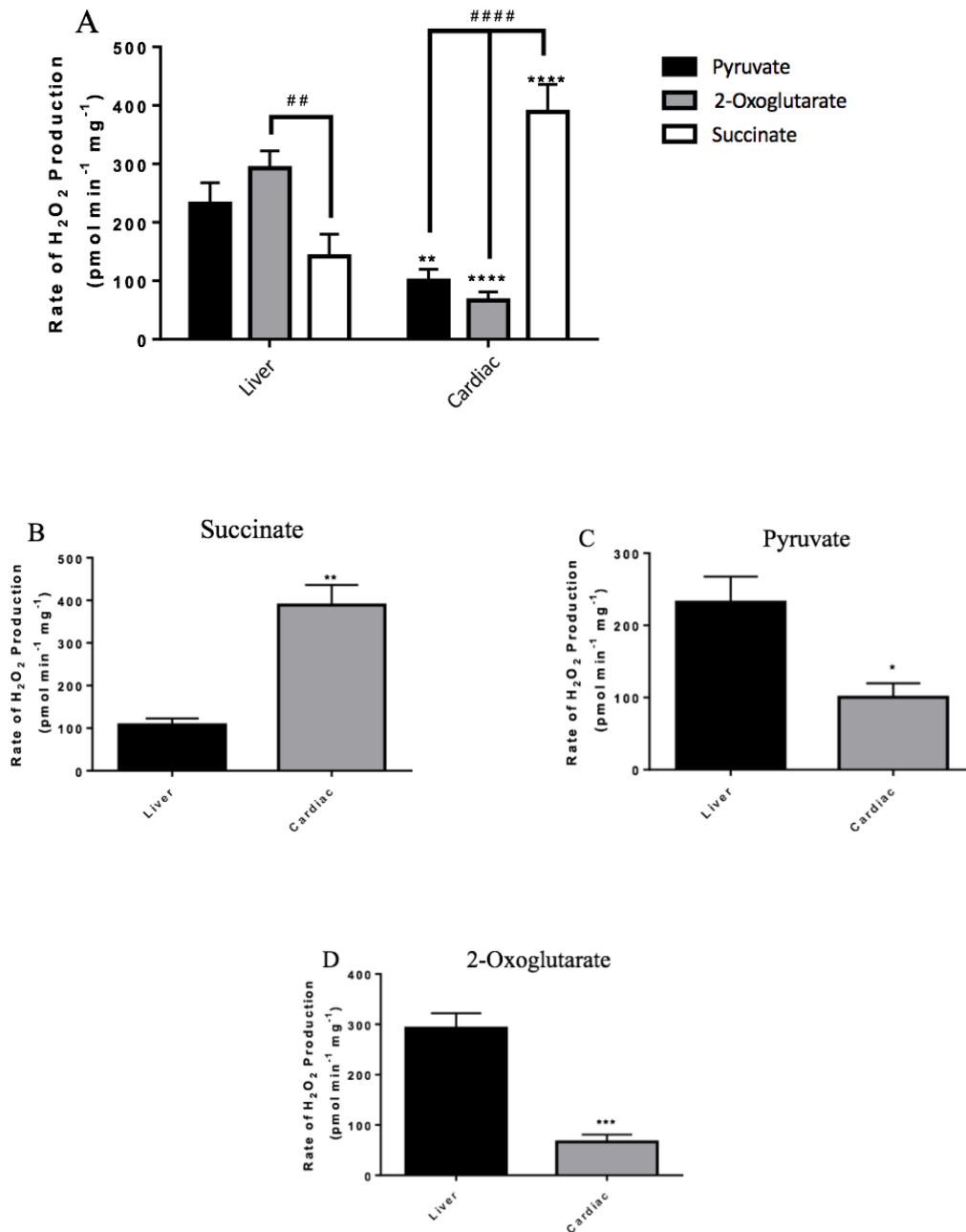


Figure 3.13: Tissue specific effects of different substrates on wildtype mice

(A) Wildtype C57Bl/6N mitochondria supplemented 50 μ M of various substrates. (B) Wildtype C57Bl/6N mitochondria supplemented with 50 μ M succinate. Wildtype C57Bl/6N mitochondria supplemented with 50 μ M malate and either 50 μ M (C) pyruvate or (D) 2-oxoglutarate. AUR fluorescence was measured at 565/600 nm. Stars represent significant differences between tissues while hashes represent significant differences within tissues, between genotypes. N=4-6, mean + SEM, (A) two-way ANOVA with a Fisher's LSD post-hoc test, (B, C, & D) unpaired t-test. This figure shows replotted data from the previous data to highlight key differences.

3.2.5. *GRX2 loss on proton gradient driven $O_2^{\bullet-}/H_2O_2$ production*

The polarity of the mitochondrial inner membrane has been shown to play an integral role in influencing mitochondrial ROS production in various tissue types. In addition, protein S-glutathionylation and GRX2 have been shown to modulate proton return to the matrix and the strength of the mitochondrial membrane potential (134, 141). Therefore, we decided to examine the impact of GRX2 deficiency on $O_2^{\bullet-}/H_2O_2$ production in mitochondria displaying differences in the rate of proton return to the matrix. In order to vary proton return, mitochondria were subjected to different respiratory states (states 2-4) which correspond to the stepwise addition of substrate, ADP, and oligomycin to a reaction chamber. Mitochondria were also supplemented with FCCP, a protonophore, to test the impact of proton gradient uncoupling on ROS production. The addition of pyruvate and malate induces state 2 respiration which corresponds to an increase in membrane potential. The addition of ADP stimulates state 3 respiration which augments proton return to the matrix through complex V lowering the membrane potential. Introducing oligomycin to the system causes the mitochondria to enter state 4 respiration. Oligomycin binds to the F_0 subunit of ATP synthase, blocking the return of protons to the matrix, which leads to hyperpolarization of the inner membrane. The addition of FCCP increases proton return to the matrix, dissipating the membrane potential. According to the prevailing theories, increasing the proton gradient should lead to an increase in the rate of mitochondrial ROS production, due to a slowing of electron transfer through the respiratory chain and an over-reduction of electron donating sites in the complexes. Likewise, decreasing the potential should lead to a decreased rate of mitochondrial ROS production. To our surprise induction of proton return with ADP or FCCP augmented $O_2^{\bullet-}/H_2O_2$ production in liver and cardiac mitochondria (Fig. 3.14). The addition of oligomycin did lead to an increase in $O_2^{\bullet-}/H_2O_2$ production in both tissues, which may be

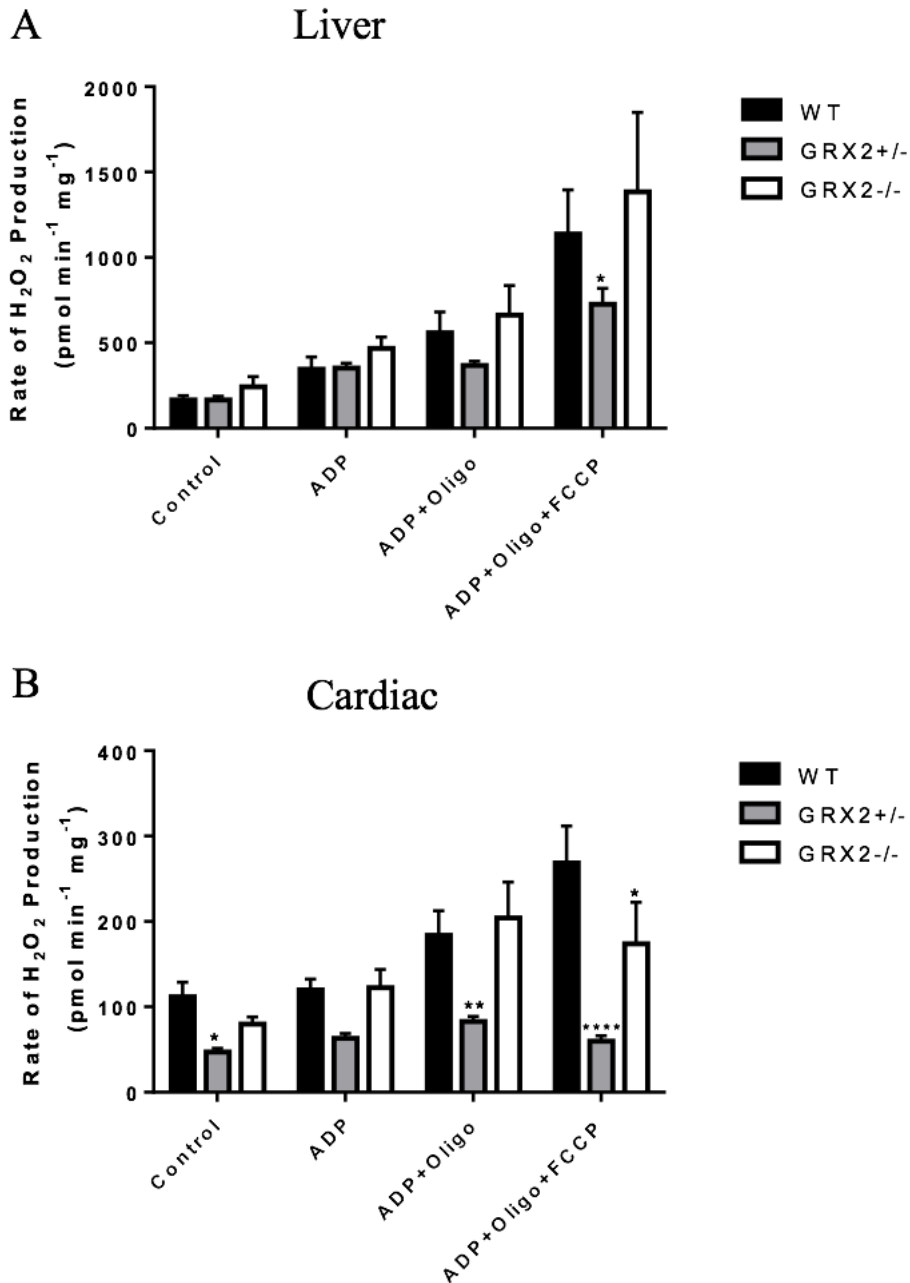


Figure 3.14: Production of $O_2^{\bullet-}/H_2O_2$ during state 3 respiratory conditions between genotypes

(A) Liver mitochondria (0.03 mg/ml) or (B) cardiac mitochondria (0.01 mg/ml) were incubated with 50 μ M malate and pyruvate, and then either 1 mM ADP, 1 mM ADP + 4 μ g/ml oligomycin or 1 mM ADP + 4 μ g/ml oligomycin + 4 μ M FCCP to examine $O_2^{\bullet-}/H_2O_2$ production. The rate of $O_2^{\bullet-}/H_2O_2$ production was measured using AUR at 565/600 nm. N=3-5, mean + SEM, one-way ANOVA with a Fischer's LSD post-hoc test.

associated with the hyperpolarization of the mitochondrial inner membrane (Fig. 3.14). Our results indicate that there may not necessarily be a relationship between the mitochondrial membrane potential and the rate of $O_2^{\bullet-}/H_2O_2$ production.

In the liver mitochondria (Fig. 3.14A), there was a significant decrease in the rate of $O_2^{\bullet-}/H_2O_2$ production for GRX2^{+/-} when the proton gradient was dissipated with FCCP. A more intense difference between genotypes was noticed in the cardiac mitochondria, where GRX2^{+/-} mice showed decreased rates of $O_2^{\bullet-}/H_2O_2$ production in state 2 and 4 respiration, and both GRX2^{+/-} and GRX2^{-/-} mice showed decreased respiration when treated with FCCP. This decrease in $O_2^{\bullet-}/H_2O_2$ production is possibly due to changes in S-glutathionylation in the mitochondrial matrix.

3.3. Mitochondrial respiration

The bioenergetics of isolated mitochondrial samples was assessed for the liver and cardiac tissue to look for any changes in respiration caused by GRX2 deficiency, as well as to ensure that the mitochondria remained functional after isolation. In liver tissue, GRX2^{+/-} mice showed significant increases in both state 2 and 3 respiration (Fig. 3.15A) However, in cardiac tissue there was a significant decrease in state 3 respiration for both GRX2^{+/-} and GRX2^{-/-} mice (Fig. 3.15B). This decrease in state 3 respiration in cardiac mitochondria deficient in GRX2 was observed in a previous study (117), and is likely due to increased S-glutathionylation of complex I. The loss of GRX2, leading to increased complex I S-glutathionylation, likely decreases the activity of complex I, diminishing the flow of electrons through the ETC, causing reduced oxygen consumption.

The RCR is a measurement of the mitochondrial coupling state. Typical RCR values vary from 3 to 15 (142), which indicate that the mitochondria are functional and undamaged from the isolation procedure. RCR values for each genotype in cardiac tissue were measured and found to

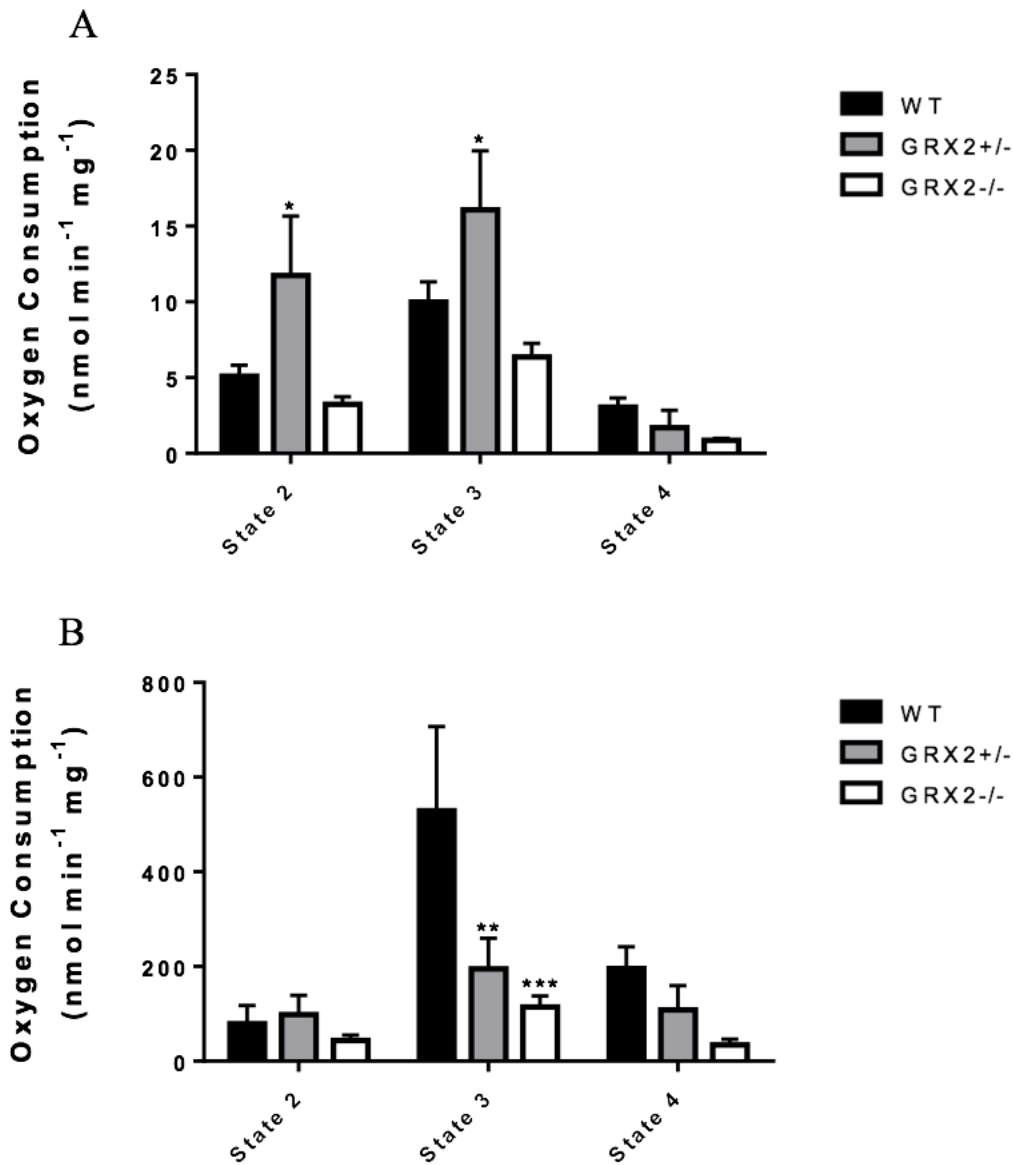


Figure 3.15: Changes in respiratory states due to loss of GRX2

(A) The oxygen consumption of 0.5 mg/ml of liver mitochondria from each genotype was measured with a clarke electrode. All rates were normalized to the rate of oxygen consumption with the addition of 4 μ M antimycin A. (B) The oxygen consumption was measured under the same conditions with 0.1-0.2 mg/ml of cardiac mitochondria from each genotype. N=4, mean + SEM, one-way ANOVA with a Fischer's LSD post-hoc test.

be consistently approximately 3, indicating the mitochondria were functioning properly (Fig. 3.16). In the liver tissue, WT and GRX2^{+/-} mice had consistent RCR values, however, GRX2^{-/-} mice had a significantly increased RCR, almost twice as large as WT mice (Fig. 3.16). This may indicate that the loss of GRX2 in liver tissue causes increased mitochondrial coupling, due to decreases in proton leak. This may be due to changes in the S-glutathionylation profile of the mitochondria.

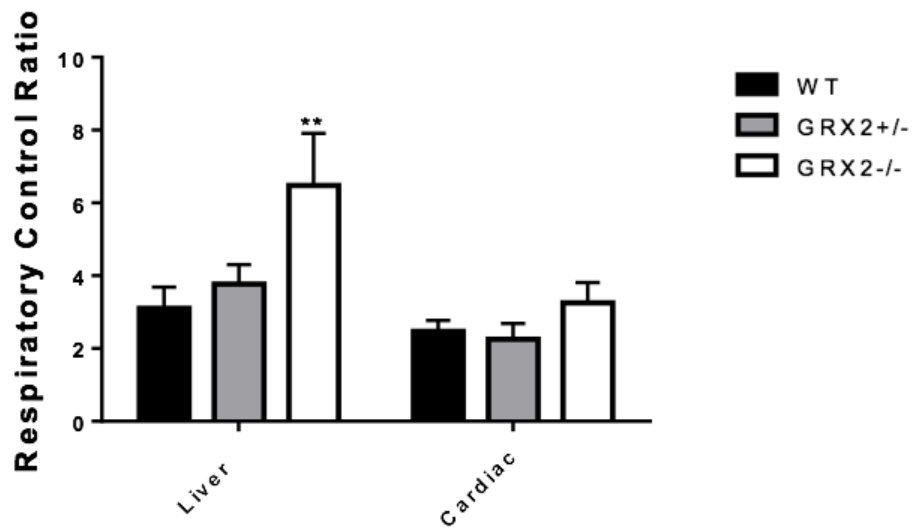


Figure 3.16: Deregulated S-glutathionylation in the liver may lead to decreased proton leak

The RCR of mitochondria from each genotype was measured as the ratio of state 3: state 4 respiration. RCR values were compared within tissues. N=4, mean + SEM, one-way ANOVA with a Fischer's LSD post-hoc test.

4. Discussion

4.1. Summary

The purpose of this investigation was to examine the role of the thiol oxidoreductase GRX2 in the regulation of $O_2^{\bullet-}/H_2O_2$ production from various sites in liver and cardiac mitochondria. Using mice deficient for GRX2, mitochondria isolated from liver and cardiac tissue were examined for rates of $O_2^{\bullet-}/H_2O_2$ production using various substrate and inhibitor combinations. It was initially found that the major sources of $O_2^{\bullet-}/H_2O_2$ production differ between cardiac and liver mitochondria. In liver mitochondria, the major sources of $O_2^{\bullet-}/H_2O_2$ included Krebs cycle enzyme OGDH and complex III of the ETC. Meanwhile, in cardiac mitochondria, complexes I and III of the ETC served as the high capacity sites for ROS release. It was also found that GRX2 deficiency affected $O_2^{\bullet-}/H_2O_2$ production differently in liver and cardiac mitochondria. Most of the GRX2 deficiency effects were associated with decreased $O_2^{\bullet-}/H_2O_2$ release from OGDH and PDH in liver mitochondria. By contrast, in cardiac mitochondria, the absence of GRX2 significantly augmented succinate induced $O_2^{\bullet-}/H_2O_2$ production by the ETC.

Measurement of the rate of $O_2^{\bullet-}/H_2O_2$ production in liver mitochondria with different substrates allowed for the identification of the high capacity sites for ROS production in this tissue. Pyruvate or 2-oxoglutarate were excellent substrates for $O_2^{\bullet-}/H_2O_2$ production, while supplementation with succinate induced low rates of $O_2^{\bullet-}/H_2O_2$ production. Inhibition of OGDH with KMV induced a large decrease in $O_2^{\bullet-}/H_2O_2$ production. Myxothiazol, a complex III inhibitor, also induced a small decrease in ROS production. These results indicate the Krebs cycle complexes OGDH, and likely PDH, along with complex III, are the major sources of ROS in liver mitochondria. The loss of GRX2 in liver mitochondria metabolizing pyruvate was found to cause decreased $O_2^{\bullet-}/H_2O_2$ production. This is likely due to increased S-glutathionylation of Krebs cycle

enzymes PDH and OGDH, which have already been shown to decrease $O_2^{\bullet-}/H_2O_2$ production following S-glutathionylation of the E2 subunit (44, 61). The protein abundance of PDH and OGDH was also found to be increased in liver mitochondria. It is likely that chronic deregulation of protein S-glutathionylation reactions due to GRX2 deficiency induces mitochondrial stress signals to increase PDH and OGDH in an effort to maintain Krebs cycle flux.

Mitochondria isolated from cardiac tissue show a very different profile from that of the liver. When supplemented with pyruvate or 2-oxoglutarate, the rates of $O_2^{\bullet-}/H_2O_2$ production from cardiac mitochondria are much lower than the liver. When metabolizing these substrates, KMV had little effect on $O_2^{\bullet-}/H_2O_2$ production, and the use of myxothiazol increased ROS production. Rates of $O_2^{\bullet-}/H_2O_2$ production by cardiac mitochondria oxidizing succinate on the other hand were ~4x higher than the rate of ROS release during pyruvate or 2-oxoglutarate metabolism. Inhibition of the complexes in the ETC during succinate supplementation lead to drastic decreases in $O_2^{\bullet-}/H_2O_2$ production. All this evidence suggests that complexes I and III are the major sources of ROS in cardiac mitochondria. GRX2 deficiency in cardiac mitochondria had no effect on $O_2^{\bullet-}/H_2O_2$ production during pyruvate and 2-oxoglutarate oxidation. However, cardiac mitochondria from GRX2^{+/-} or GRX2^{-/-} mice displayed a significant increase $O_2^{\bullet-}/H_2O_2$ production when succinate was being metabolized. This may be caused by increased S-glutathionylation of complex I in cardiac mitochondria, which has previously been shown to lead to increased $O_2^{\bullet-}/H_2O_2$ production from the complex (121). GRX2 deficiency also leads to decreased state 3 respiration in cardiac mitochondria, as S-glutathionylation of complex I has been shown to decrease its activity (117, 123).

The combined results of this study indicate that GRX2 plays an important role in regulating the production of $O_2^{\bullet-}/H_2O_2$ in mitochondria by altering the S-glutathionylation profile. The effects

of GRX2 and S-glutathionylation on ROS production are different between cardiac and liver tissue, as the amount of ROS emitted from mitochondrial sites of production differs between the two tissues.

4.2. Importance of GRX2 in health and development

4.2.1. GRX2 is required to regulate cell metabolism and survival

The role of GRX2 in cellular models has been thoroughly examined to determine its significance in maintaining mitochondrial function. GRX2 has been found to have a protective effect in HeLa cells when challenged with doxorubicin, an anti-cancer drug which is known to increase the production of ROS (112). Silencing GRX2 expression via short interfering RNA, led to the dramatic sensitization of HeLa cells to cell death by doxorubicin treatment, decreasing the median effective dosage from 40 μM to 0.7 μM (112). These results suggest that the presence of GRX2 is required to restore the redox status of one or more targets in the mitochondria, preventing cell death during increased levels of oxidative stress (112).

The function of GRX2 in protecting cells from cell death through prevention of oxidative stress has been also been examined in cells overexpressing GRX2. Overexpression of GRX2 in HeLa cells was found to decrease susceptibility to apoptosis following doxorubicin treatment (118). Indeed, GRX2 overexpression inhibited cytochrome *c* release, preventing the induction of intrinsic apoptotic signaling cascades (118). Increased expression of GRX2 was found to prevent the doxorubicin-mediated loss of cardiolipin, the lipid which anchors cytochrome *c* to the mitochondrial inner membrane (118). Other studies suggest that the ability of GRX2 to prevent apoptosis induced by oxidative stress lies in its ability to preserve the function of complex I. Wu *et al.* (143) found that in human epithelial lens cells, that GRX2 protected cells from H_2O_2 mediated apoptosis, which correlated with increased complex I activity. By contrast, in GRX2

knock down cells, the activity of complex I was significantly diminished following a H₂O₂ challenge (143). Using primary cell culture of epithelial lens cells collected from GRX2 knock out mice, further proof was found that GRX2 protects complex I function (135). Treating these cells with H₂O₂ showed that the loss of GRX2 induces mitochondrial inner membrane leakage, decreased complex I activity and ATP production, and a weakened ability to detoxify H₂O₂ (135). Results from this thesis agree with these findings, as the loss of GRX2 was found to increase the production of ROS from complex I in cardiac cells, likely due to increased S-glutathionylation of the complex.

Cellular studies have also been used to examine the function of GRX2 in protection against disease. GRX2 has been studied for its role in neuronal dopamine-induced apoptosis, a phenomenon seen in neurodegenerative diseases, such as Parkinson's disease. Using a primary culture of granule neurons from BALB/c mice, the overexpression of GRX2 was found to reduce dopamine induced apoptosis by stabilizing nuclear factor NF- κ B, which resulted in the expression of genes related to the immune response, stress, inflammation, and the inhibition of apoptosis (144). This was mediated by GRX2 induced expression of Ref-1, a redox controlled factor that activates NF- κ B (144). The ability of GRX2 to maintain a reduced mitochondrial matrix may also be important in the prevention of amyotrophic lateral sclerosis. The overexpression of GRX2 in both murine and human neuronal cell lines has been shown to prevent the aggregation of mutant SOD1 in mitochondria (145). Mutant SOD1 has been suggested as a possible cause for the degeneration of motor neurons, and its aggregation results in the impairment of oxidative phosphorylation (145). Finally, GRX2 has also been found to protect oligodendrocytes from nitrosative stress by scavenging nitric oxide (146). The role of GRX2 in maintaining functionality in the mitochondrial matrix has been linked to the prevention of many cellular dysfunctions. The

evidence discussed above is indicative of the importance of GRX2 and S-glutathionylation in the mitochondria. It is possible that GRX2 plays a major role in healthy cellular function and its loss can be detrimental. Exploring the mechanisms by which GRX2 exerts its control may lead to further understanding of certain diseases.

4.2.2. Understanding the physiological function of GRX2 using mouse models

GRX2 is required to protect from oxidative stress and maintain mitochondrial function through reversible S-glutathionylation reactions. To understand its physiological function, transgenic animals either deficient or overexpressing GRX2 have been utilized in a number of studies. Most of this work has focused on the function of GRX2 in regulating cardiac physiology and protecting heart tissue from oxidative stress. For instance, it was found that the overexpression of GRX2 protected cardiac tissue from doxorubicin-induced heart damage by preserving mitochondrial respiration, ATP production, and preventing the release of pro-apoptotic factors from the intermembrane space of mitochondria (111). Mice with increased GRX2 expression were also protected from a decline in left ventricular function and damage to cardiac tissue (111). Treatment of GRX2 transgenic mice with iBid, an inducer of apoptosis, also showed decreased release of cardiolipin when compared to WT mice (111). This indicates that regulation of protein S-glutathionylation in cardiac tissue is essential for maintaining its physiological function. In the present study, it was demonstrated that GRX2 deficiency augments succinate-induced ROS production which is associated with a substantial decrease in phosphorylating respiration. Cardiac tissue relies heavily on a steady supply of ATP to maintain its hemodynamic function. In addition, cardiomyocytes are quite vulnerable to the over production of ROS which can lead to oxidative stress and damage. Therefore, it is likely that the absence of GRX2 results in cardiac dysfunction by compromising the delivery of ATP while simultaneously exposing healthy heart cells to high

ROS levels. These effects are likely associated with the inability of GRX2 to catalyze reversible S-glutathionylation reactions.

The results from this thesis indicate that GRX2 is required for the regulation of ROS production in mitochondria. Many previous studies have highlighted the importance of GRX2 in maintaining proper health and development. Mice with a whole body GRX2 knock out have been extensively profiled and found to show certain detrimental characteristics. In a previous study, GRX2^{-/-} mice were found to display a slight decrease in body weight when compared to their WT littermates (134). This was related to deregulated proton leaks in skeletal muscle mitochondria which resulted in increased overall mitochondrial respiration and carbon catabolism (134). It needs to be emphasized though that GRX2 deficient mice do not display any changes in linear growth or food intake in comparison to WT litter mates (134). GRX2 deficient mice were also found to have significantly heavier hearts than WT mice (117). Upon closer examination, GRX2^{-/-} mouse hearts were found to display left ventricular hypertrophy and fibrosis by 9 weeks of age (117). It was also found that left ventricular hypertrophy developed as early as 6 weeks of age, which was not associated with an increase in hypertension (117). In the same study, it was also found that hearts from GRX2^{-/-} mice rely heavily on glucose as a source of ATP indicating that mice develop metabolic inflexibility which is normally associated with mitochondrial dysfunction, a hallmark of cardiac disease (117). At the molecular level, GRX2 deficient mice were found to have a lower GSH/GSSG ratio than WT mice, which was associated with an increase in the total number of S-glutathionylated proteins (117). In the present study, it was also found that GRX2 knockout leads to hyper-glutathionylation of the mitochondrial proteome in cardiac and liver tissue (134, 135). In addition, a previous report showed that elimination of GRX2 induces mitochondrial fragmentation and alterations in the expression of the respiratory complexes, including complex I, and the

availability of cytochrome *c* (117). GRX2 is well known to target complex I in cardiac tissue for regulation by reversible S-glutathionylation (121). Without GRX2 present to regulate S-glutathionylation reactions, increased S-glutathionylation of complex I causes significant increases in ROS production (121). Since complex I is an integral source of $O_2^{\bullet-}/H_2O_2$ in cardiac mitochondria, deregulation of its S-glutathionylation due to a loss in GRX2 function is the likely cause for oxidative damage to cardiac tissue. In this thesis, cardiac mitochondria from GRX2^{-/-} mice displayed decreased state 3 respiration, an observation that is consistent with other reports showing GRX2 and protein S-glutathionylation are vital for regulating complex I activity and mitochondrial respiration. This change in mitochondrial respiration has been previously noted, and further research has also found that GRX2^{-/-} mice have decreased ATP production (117). Modulation of mitochondrial bioenergetics in cardiac tissue, causing increased ROS production and decreased oxidative phosphorylation efficiency, are likely the cause of the ventricular hypertrophy and hypertension noted in these mice. This evidence indicates that the presence of GRX2 is required for normal cardiac function, as S-glutathionylation reactions must be regulated in the mitochondria to prevent unwanted changes in mitochondrial physiology.

The loss of GRX2 expression in the mouse model has not been found to cause any subsequent upregulation of related enzymes in the oxidoreductase family. This study, as well as others (113), found no compensatory increase in GRX1. This is expected since GRX1 resides in the mitochondrial intermembrane space and thus would not be able to compensate for a loss in GRX2 function. Another more likely candidate for GRX2 compensation would be TRX2, a member of the thioredoxin-fold family that has been implicated in driving S-glutathionylation reactions. However, it has also been shown that the loss of GRX2 does not lead to compensatory increases in TRX1 or TRX2 in mitochondria isolated from lens, muscle, or cardiac tissue (117,

134, 135). It should be noted though that several studies have documented that TRX2 does not catalyze S-glutathionylation since it lacks the GSH motif required to remove GSH from a target protein (147). It is possible that the loss of GRX2 may lead to regulation of S-glutathionylation reactions by GST. Isoforms of GST are present in the mitochondrial matrix (148), but little is known about whether these enzymes have the ability to perform reversible S-glutathionylation reactions in the matrix of mitochondria.

A GRX2 whole body knock out model has also been used in the study of cataract formation. Previous studies in mouse epithelial lens cells have indicated that GRX2 is required to maintain the functionality of complex I during oxidative stress, preserving mitochondrial oxidative phosphorylation (135). Compared to WT mice, GRX2^{-/-} mice were shown to induce the formation of age-related cataract development approximately three months sooner (113). The lenses of the GRX2 null mice contained lower levels of protein thiols and GSH than WT mouse lenses, with a significant increase in S-glutathionylation proteins (113). The inappropriate addition of GSH to proteins may lead to protein destabilization, and the eventual formation of water-insoluble protein aggregates that cause clouding of the lens (113). The mitochondrial function in the lenses of GRX2 null mice was also affected. Mitochondrial preparations from the GRX2 null lens showed decreased complex I activity as well as decreased overall ATP production (113). These results indicate that multiple tissues require the activity of GRX2 to maintain properly functioning mitochondria, and to allow the tissue to perform its physiological function.

4.2.3. The role of GRX2 in embryogenesis

In addition to its role in maintaining mitochondrial function, GRX2 has also been shown to be required for proper embryonic development. GRX2 has been implicated in the cardiac, vascular and brain development. In the zebrafish model, GRX2 has been found to be necessary for

the migrations of cardiac neural crest cells into the primary heart field (116). The knockdown of GRX2 led to impaired migration of these cells, causing obstructed blood flow and reduced pumping efficacy due to disrupted looping of the cardiac tube (116). It was suggested that this impairment is caused by disruptions in the reversible S-glutathionylation of actin by GRX2 (116). GRX2 deficiency also causes delayed and disordered blood vessel network development (115). Investigation of this phenomenon led to the discovery that for proper blood vessel development, the presence of GRX2 is required for the deglutathionylation of a certain cysteine residue on NAD⁺-dependant protein deacetylase sirtuin-1 (115). This mechanism was also confirmed in HeLa cells, demonstrating that it is applicable to humans as well as zebrafish. Lastly, the role of GRX2 was also studied in zebrafish brain development. Silencing the expression of GRX2 in a zebrafish model led to increased apoptosis in neurons, as well as the loss of the ability to develop an axonal scaffold (114). In a zebrafish and human cell model, it was demonstrated that GRX2 is required for the thiol redox regulation of collapsin response mediator protein 2, which is needed for axon growth guidance (114). These studies further highlight the important role of GRX2 in numerous thiol redox reactions that are required throughout the body for health and development.

4.3. Production of O₂[•]/H₂O₂ during pyruvate/2-oxoglutarate oxidation

4.3.1. Liver mitochondria metabolizing pyruvate/2-oxoglutarate

The results of this thesis indicate that the majority of O₂[•]/H₂O₂ produced in liver mitochondria comes OGDH of the Krebs cycle and complex III of the ETC. PDH is also an important source but produces less ROS than OGDH and complex III. Previous studies examining the main sources of ROS production in liver mitochondria agree with these findings. Findings by Slade *et al.* (62) showed that while complex III is the main source of O₂[•]/H₂O₂ production, OGDH also produces a significant amount. Complexes I and III are traditionally viewed as the main

sources of ROS production in mitochondria (86). However, identification of PDH and OGDH as important sources of mitochondrial $O_2^{\bullet-}/H_2O_2$ has challenged this view. Indeed, PDH and OGDH have been found to be important sources of ROS production in liver, muscle, and brain mitochondria (44, 128). In fact, in skeletal muscle, PDH and OGDH have been found to produce 4x and 8x more ROS than complex I during the oxidation of Krebs cycle-linked substrates (128). Although PDH and OGDH have analogous structures, their ROS production potentials are not equal. In skeletal muscle, PDH is found to produce about half as much ROS as OGDH (128). In liver mitochondria, OGDH accounts for ~35% of the ROS emission whereas PDH produces ~7% of the total amount of $O_2^{\bullet-}/H_2O_2$ (62). In this thesis, the inhibition of OGDH with KMV in liver mitochondria led to a ~85% decrease in $O_2^{\bullet-}/H_2O_2$ production when pyruvate or 2-oxoglutarate served as the substrate. It is important to emphasize that malate was also included in the reaction mixtures to complete the Krebs cycle and ensure that any acetyl-CoA formed by PDH can be condensed with oxaloacetate allowing for further oxidation. Therefore, as in previous studies, OGDH is a far more significant source for $O_2^{\bullet-}/H_2O_2$ than PDH.

Mitochondrial $O_2^{\bullet-}/H_2O_2$ production depends on the concentration and redox state of the electron donating site. Both OGDH and PDH were also more abundant in liver mitochondria isolated from GRX2^{-/-} mice. Therefore, we decided to normalize the amount of $O_2^{\bullet-}/H_2O_2$ production to the abundance of each complex since the overall concentration of both enzymes will influence the rate of ROS release. Normalizing the results to overall PDH and OGDH content revealed that a deficiency in GRX2 results in a significant decrease in $O_2^{\bullet-}/H_2O_2$ production. It is likely that this is associated with the increased S-glutathionylation of OGDH and PDH, since it has been established in two previous studies that GRX2 is required to deglutathionylate both enzymes (44, 61). The compensatory increase in PDH and OGDH protein abundance is either

related to mitochondrial stress signaling to the nucleus or an increase in mitochondrial proliferation.

It was shown nearly a decade ago that OGDH can be S-glutathionylated on the lipoic acid site of its E2 subunit (130). This S-glutathionylation was found to occur when mitochondria were challenged with high levels of H₂O₂ (130). Hydrogen peroxide has a high activation energy which prevents it from spontaneously oxidizing most protein cysteine thiols. However, at high enough concentrations, H₂O₂ can oxidize protein cysteine thiols forming highly nucleophilic SOH. Sulfenic acid is very unstable and can undergo a range of modifications – during oxidative stress sulfenic acids can either be irreversibly oxidized by H₂O₂ further or can be covalently modified by lipid peroxidation degradation products like 4-HNE (99). The vicinal thiols on the lipoic acid of the E2 subunit in OGDH and PDH are highly sensitive oxidative deactivation by H₂O₂ (22). Moreover, oxidative deactivation of OGDH occurs in several neurological and metabolic disorders (99). S-glutathionylation of OGDH is required to protect the enzyme complex from irreversible oxidative deactivation (130). In addition, the GSH moiety can be removed by the action of GRX2 (22). On top of this protective function of S-glutathionylation, recent work by our group has found that this redox sensitive modification can also regulate ROS emission from OGDH. OGDH has been shown to alter its production of O₂^{•-}/H₂O₂ depending on its state of S-glutathionylation (132). S-glutathionylation of the lipoic acid residues of OGDH leads to decreased production of O₂^{•-}/H₂O₂ during forward electron flow, as GSH blocks the flow of electrons from the oxidation of 2-oxoglutarate, to the E3 subunit, where O₂^{•-}/H₂O₂ is produced by the flavin site (132). Based on this, it seems likely that the loss of GRX2 leads to hyperglutathionylation of matrix proteome, including the S-glutathionylation of OGDH, decreasing its production of O₂^{•-}/H₂O₂. Since OGDH

is a major source of ROS in liver mitochondria, this change causes a large decrease in the overall production of $O_2^{\bullet-}/H_2O_2$.

Fisher-Wellman *et al.* showed in two studies that depletion of mitochondrial GSH or NADPH augments $O_2^{\bullet-}/H_2O_2$ production by PDH (127). It was hypothesized that this regulation may actually occur through the S-glutathionylation of PDH (127). However, in the same study, the authors used GSH depleting agents to study ROS production by PDH and were thus unable to determine if the change in $O_2^{\bullet-}/H_2O_2$ production was related to the depletion of a critical antioxidant, GSH, or via redox sensing by PDH. Our group provided the first evidence that PDH can undergo S-glutathionylation, an observation that should not be surprising given that PDH is highly homologous to OGDH (61). S-glutathionylation of PDH also lowers the production of $O_2^{\bullet-}/H_2O_2$ in the forward electron transfer (61). Moreover, in the same study it was found that GRX2 can remove GSH from PDH. Therefore, it is likely that the loss of GRX2 also induces the S-glutathionylation of PDH, decreasing its $O_2^{\bullet-}/H_2O_2$ production and contributing to the overall decrease of ROS production in the mitochondria. However, as PDH is a less significant source of $O_2^{\bullet-}/H_2O_2$ than OGDH in liver tissue (44), it is likely that its inhibition has a lesser effect on the overall ROS production as compared to the S-glutathionylation of OGDH. The loss of GRX2 is likely to affect the S-glutathionylation status of both OGDH and PDH, as both complexes have been shown to be deglutathionylated by GRX2 (61, 132).

4.3.2. Cardiac mitochondria metabolizing pyruvate/2-oxoglutarate

The results of this experiment indicate that both pyruvate and 2-oxoglutarate are poor substrates for inducing $O_2^{\bullet-}/H_2O_2$ production in isolated cardiac mitochondria. Utilization of either of these substrates induced $O_2^{\bullet-}/H_2O_2$ production rates approximately 5x lower than in liver mitochondria. This indicates that OGDH and PDH are not likely to be important sources of $O_2^{\bullet-}$

/H₂O₂ production in cardiac mitochondria. A previous study by the Mailloux group (44) also found that liver mitochondria generated approximately ~3-4.5x more ROS than cardiac mitochondria, in the presence of either pyruvate or 2-oxoglutarate. Since the Krebs cycle is not found to be an important source of ROS in cardiac mitochondria, inhibition of OGDH with KMV did not lead to a decrease in O₂[•]/H₂O₂ production. The inhibition of complex III with myxothiazol led to an increase in O₂[•]/H₂O₂ production. This indicates that complexes upstream of complex III may be important sites of ROS production, such as complexes I and II. Myxothiazol binds to the UQH₂ binding site of complex III, preventing the complex from accepting electrons. This leads to reverse electron transfer to complexes I and II, indicating a significant amount of ROS is being produced from either of these sites.

The loss of GRX2 in cardiac mitochondria did not lead to any significant change in O₂[•]/H₂O₂ production during supplementation with pyruvate or 2-oxoglutarate. Unlike liver mitochondria, there was also no changes in OGDH and PDH abundance between WT and GRX2 deficient mice. Therefore, we did not normalize O₂[•]/H₂O₂ production rates to enzyme content in this tissue. It's possible that increased S-glutathionylation of Krebs cycle complexes does not have a very noticeable effect on overall ROS production rates in cardiac mitochondria, as they do not produce significant amounts of ROS in this tissue.

4.4. Production of O₂[•]/H₂O₂ during succinate supplementation

4.4.1. Liver mitochondria metabolizing succinate

The supplementation of isolated liver mitochondria with succinate was determined not to be an effective method of inducing O₂[•]/H₂O₂ production. The rates of O₂[•]/H₂O₂ production in liver mitochondria were about ~3x lower in comparison to pyruvate or 2-oxoglutarate. This data supports the previously discussed notion that enzyme complexes PDH and OGDH are important

sources of $O_2^{\bullet-}/H_2O_2$ production in liver mitochondria. Electrons from succinate are passed to UQ via complex II of the ETC, therefore bypassing both PDH and OGDH, eliminating their ability to produce $O_2^{\bullet-}/H_2O_2$. Since the supplementation with succinate led to a significant decrease in $O_2^{\bullet-}/H_2O_2$ production, we can deduce that complexes I and II are not significant sources of $O_2^{\bullet-}/H_2O_2$ in liver mitochondria. It is likely that the $O_2^{\bullet-}/H_2O_2$ being produced with succinate supplementation is from complex III, which has previously been discussed to be a significant $O_2^{\bullet-}/H_2O_2$ source in liver mitochondria (62). The use of ETC inhibitors in liver mitochondria supplemented with succinate also provides data which supports these conclusions. Mxyothiazol, an inhibitor of the UQH₂ binding site of complex III, induced a small decrease in $O_2^{\bullet-}/H_2O_2$ production. Both atpenin A5, a complex II UQ inhibitor, and rotenone, a complex I UQ inhibitor, did not alter the rate of $O_2^{\bullet-}/H_2O_2$ production in WT mice. These results indicate that when liver mitochondria are metabolizing succinate, complex III may be a significant source of $O_2^{\bullet-}/H_2O_2$ production, while both complexes I and II are not.

We also noted a significant increase in $O_2^{\bullet-}/H_2O_2$ production in GRX2^{+/-} mouse liver tissue, as compared to WT, during succinate supplementation. This is possibly due to increased S-glutathionylation of complex I, which has been shown to lead to increased production of $O_2^{\bullet-}/H_2O_2$ (121). While complex I was not found in the liver to be a significant source of $O_2^{\bullet-}/H_2O_2$ in the liver, it's possible that increased S-glutathionylation induced increased rates of $O_2^{\bullet-}/H_2O_2$ production during reverse electron flow from complex II. Previous research with GRX2 deficient mice has shown that they present with increased S-glutathionylation of complex I, leading to decreased activity (117). It is possible that since succinate results in such low rates of ROS production in the liver mitochondria, that it is difficult to know if the increase seen in heterozygotes is truly significant, or if it is based in error. A larger n value could fix this problem. However, it is

also possible that there is a compensatory response occurring in the GRX2 KO mice preventing the increase of ROS production, which is not present in the heterozygous mice.

4.4.2. *Cardiac mitochondria metabolizing succinate*

Cardiac mitochondria supplemented with succinate showed a robust increase in $O_2^{\bullet-}/H_2O_2$ production as compared to pyruvate or 2-oxoglutarate. These results indicate that succinate is an effective stimulator of $O_2^{\bullet-}/H_2O_2$ production in cardiac mitochondria. This is likely because sites of ROS production in the ETC have been found to be more significant sources of $O_2^{\bullet-}/H_2O_2$ production in cardiac mitochondria when compared to sites in the Krebs cycle. Since succinate enters the ETC at complex II, it is able to stimulate $O_2^{\bullet-}/H_2O_2$ production from complexes II and III, as well as by complex I via reverse electron transport by UQH₂. Inhibitors of ETC complexes were also used in cardiac mitochondria to pinpoint sites of $O_2^{\bullet-}/H_2O_2$ production. All three inhibitors: rotenone, atpenin A5, and mxyothiazol, had a noticeable effect, inducing large decreases in the rates of $O_2^{\bullet-}/H_2O_2$ production. Interpretation of these results lead to the conclusion that complexes I and III are significant sources of $O_2^{\bullet-}/H_2O_2$ production in cardiac mitochondria, as blocking electron transfer to these sites led to large decreases in overall $O_2^{\bullet-}/H_2O_2$ production. Complex II was found not to be a significant source of $O_2^{\bullet-}/H_2O_2$ production in cardiac tissue, as blocking electron flow out of the complex by atpenin A5 led to a decrease in $O_2^{\bullet-}/H_2O_2$ production, whereas an increase would be expected if complex II was a major site of $O_2^{\bullet-}/H_2O_2$ production. Previous research in brain mitochondria has shown similar results, with complexes I and III being the major sites of ROS production (149). Combined with the results from this thesis, it appears that tissues with high-oxygen requirements, such as brain and cardiac tissue, rely heavily on complexes I and III for ROS production. As complex I is known to be an important site in the mitochondria for regulation of ROS production (117, 121, 123), this likely allows high-oxygen

tissues to control their ROS production and oxidative phosphorylation efficiency by altering the glutathionylation state of complex I.

GRX2 deficient mice also showed significant increases in $O_2^{\bullet-}/H_2O_2$ production as compared to WT mice during succinate supplementation. Both GRX2^{-/-} and GRX2^{+/-} mouse cardiac mitochondria showed levels of $O_2^{\bullet-}/H_2O_2$ production approximately twice as large as WT mice. This increase in $O_2^{\bullet-}/H_2O_2$ due to the loss of GRX2, like in the liver tissue, is also likely due to increases in the S-glutathionylation status of complex I. Since complex I is a much more significant source of ROS in cardiac tissue, rates of $O_2^{\bullet-}/H_2O_2$ production are very significantly increased when S-glutathionylated in the absence of GRX2. The increased S-glutathionylation of complex I is very likely in GRX2 deficient mice as they showed decreased state 3 respiration, likely due to the decreased activity of complex I which occurs when S-glutathionylated (121). Recent evidence in yeast studies have indicated that complex III may also contain sites for S-glutathionylation (140). It is possible that, like complex I, increased S-glutathionylation of complex III may increase $O_2^{\bullet-}/H_2O_2$ production, however this is only speculative as no studies have yet examined S-glutathionylation of complex III in mammals and its effects on ROS production.

4.5. Proton gradient on $O_2^{\bullet-}/H_2O_2$ production

The theory that mild uncoupling of mitochondria may reduce ROS induced damage has been widely examined, and still there is much debate about the veracity of this hypothesis. In this study, there seemed to be no correlation between the proton gradient and the rate of $O_2^{\bullet-}/H_2O_2$ production in liver or cardiac tissue. The addition of FCCP, which dissipates the mitochondrial membrane potential, led to an increase in $O_2^{\bullet-}/H_2O_2$ production in both tissues. This contrasts with the theory that decreases in membrane potential should lead to reduced ROS production. However,

there is much evidence that does not support this theory. Previous research has indicated that ROS production from complex I-linked substrates is not sensitive to decreases in the proton gradient mediated by chemical uncouplers in liver or heart tissue (150). However, some studies have found a correlation (76). The evidence for the regulation of ROS production by mild uncoupling through UCP 1/2/3 has been widely disputed (151). Therefore, the results obtained in this study support the emerging theory that membrane potential does not play a role in controlling the amount of ROS produced in the mitochondria.

4.6. Conclusions

The present study demonstrates that protein S-glutathionylation reactions mediated by GRX2 are integral for the regulation of mitochondrial $O_2^{\bullet-}/H_2O_2$ production. In addition, the evidence presented herein indicates that S-glutathionylation reactions target different enzymes in different tissues. For example, GRX2 deficiency decreased pyruvate and 2-oxoglutarate driven $O_2^{\bullet-}/H_2O_2$ release in liver, an effect that was absent in cardiac mitochondria. This indicates that PDH and OGDH are targets for regulation by GRX2 in liver mitochondria. By contrast, GRX2 deletion augmented succinate driven ROS production in cardiac mitochondria, which is most likely related to the S-glutathionylation of complex I. Therefore, we can surmise that GRX2 targets high capacity sites of ROS production for regulation by S-glutathionylation. Loss of this function compromises the regulation of mitochondrial $O_2^{\bullet-}/H_2O_2$ production which can either limit mitochondrial ROS signaling or induce oxidative stress due to over production. In aggregate, the results collected in this study illustrate that redox signals are vital for regulating mitochondrial $O_2^{\bullet-}/H_2O_2$ production. Based on this, we hypothesize that mitochondrial S-glutathionylation reactions are required to regulate mitochondrial ROS signaling. Furthermore, our results demonstrate that GRX2-mediated

S-glutathionylation reactions target different enzymes in different tissues to properly modulate ROS production.

4.7. Future Directions

Based upon the results obtained in this thesis, future directions for this work will include:

1. Challenging the GRX2 deficient mice with a high fat diet and examining changes in ROS production as compared to WT mice
2. Cardiac ischemia reperfusion modelling and doxorubicin challenging of GRX2 deficient cardiac mitochondria
3. Investigation of how S-glutathionylation reactions modulate the production of mitochondrial ROS in skeletal muscle

5. References

1. Nelson, D. L., and Cox, M. M. (2013) *Lehninger Principles of Biochemistry 6th ed.*, 10.1016/j.jse.2011.03.016
2. Arora, K. K., Filburn, C. R., and Pedersen, P. L. (1991) Glucose phosphorylation. Site-directed mutations which impair the catalytic function of hexokinase. *J. Biol. Chem.* **266**, 5359–5362
3. Massa, M. L., Gagliardino, J. J., and Francini, F. (2011) Liver glucokinase: An overview on the regulatory mechanisms of its activity. *IUBMB Life.* **63**, 1–6
4. Achari, a, Marshall, S. E., Muirhead, H., Palmieri, R. H., and Noltmann, E. a (1981) Glucose-6-phosphate isomerase. *Philos. Trans. R. Soc. Lond. B. Biol. Sci.* **293**, 145–157
5. Evans, P. R., Farrants, G. W., and Hudson, P. J. (1981) Phosphofructokinase: structure and control. *Philos. Trans. R. Soc. Lond. B. Biol. Sci.* **293**, 53–62
6. Harris, J. Ieuan, and M. W. (1976) 1 glyceraldehyde-3-phosphate dehydrogenase. *Enzym.* **13**, 1–49
7. Banks R, Blake C, Evans P, Haser R, and Rice D (1979) Sequence, structure and activity of phosphoglycerate kinase: a possible hinge-bending enzyme. *Nature.* **279**, 773–777
8. Jurica, M. S., Mesecar, A., Heath, P. J., Shi, W., Nowak, T., and Stoddard, B. L. (1998) The allosteric regulation of pyruvate kinase by fructose-1,6-bisphosphate. *Structure.* **6**, 195–210
9. Rich, P. R. (2003) The molecular machinery of Keilin's respiratory chain. *Biochem. Soc. Trans.* **31**, 1095–1105
10. Violante, S., IJlst, L., Te Brinke, H., De Almeida, I. T., Wanders, R. J. A., Ventura, F. V., and Houten, S. M. (2013) Carnitine palmitoyltransferase 2 and carnitine/acylcarnitine translocase are involved in the mitochondrial synthesis and export of acylcarnitines. *FASEB J.* **27**, 2039–2044
11. Ghisla, S., and Thorpe, C. (2004) Acyl-CoA dehydrogenases: A mechanistic overview. *Eur. J. Biochem.* **271**, 494–508
12. Agnihotri, G., and Liu, H. W. (2003) Enoyl-CoA hydratase: Reaction, mechanism, and inhibition. *Bioorganic Med. Chem.* **11**, 9–20
13. Fisher, H. F. (1985) [3] L-Glutamate Dehydrogenase from Bovine Liver. *Methods Enzymol.* **113**, 16–27
14. Kirsch, J. F., Eichele, G., Ford, G. C., Vincent, M. G., Jansonius, J. N., Gehring, H., and Christen, P. (1984) Mechanism of action of aspartate aminotransferase proposed on the basis of its spatial structure. *J. Mol. Biol.* **174**, 497–525

15. Liaw, S. H., and Eisenberg, D. (1994) Structural model for the reaction mechanism of glutamine synthetase, based on five crystal structures of enzyme-substrate complexes. *Biochemistry*. **33**, 675–681
16. Curthoys, N. P., and Watford, M. (1995) Regulation of glutaminase activity and glutamine metabolism. *Annu. Rev. Nutr.* **15**, 133–159
17. Felig, P. (1973) The glucose-alanine cycle. *Metabolism*. **22**, 179–207
18. Sidney, M., and Morris, J. (1992) Regulation of enzymes of the urea cycle and arginine metabolism. *Annu. Rev. Nutr.* **12**, 81–101
19. Patel, M. S., Nemeria, N. S., Furey, W., and Jordan, F. (2014) The pyruvate dehydrogenase complexes: Structure-based function and regulation. *J. Biol. Chem.* **289**, 16615–16623
20. Wiegand, G., and Remington, S. J. (1986) Citrate Synthase: Structure, Control, and Mechanism. *Annu. Rev. Biophys. Biophys. Chem.* **15**, 97–117
21. Beinert, H., Kennedy, M. C., and Stout, C. D. (1996) Aconitase as Iron–Sulfur Protein, Enzyme, and Iron-Regulatory Protein. *Chem. Rev.* **96**, 2335–2374
22. McLain, A. L., Szweda, P. A., and Szweda, L. I. (2011) α -Ketoglutarate dehydrogenase: a mitochondrial redox sensor. *Free Radic. Res.* **45**, 29–36
23. Bridger, W. A. (1974) 18. Succinyl-Coa Synthetase. *Enzymes*. **10**, 581–606
24. Banaszak, L. J., and Bradshaw, R. A. (1975) 6 Malate Dehydrogenases. *Enzymes*. **11**, 369–396
25. Mimaki, M., Wang, X., McKenzie, M., Thorburn, D. R., and Ryan, M. T. (2012) Understanding mitochondrial complex I assembly in health and disease. *Biochim. Biophys. Acta-Bioenergetics*. **1817**, 851–862
26. Zickermann, V., Kerscher, S., Zwicker, K., Tocilescu, M. A., Radermacher, M., and Brandt, U. (2009) Architecture of complex I and its implications for electron transfer and proton pumping. *Biochim. Biophys. Acta - Bioenerg.* **1787**, 574–583
27. Dröse, S., Stepanova, A., and Galkin, A. (2016) Ischemic A/D transition of mitochondrial complex I and its role in ROS generation. *Biochim. Biophys. Acta - Bioenerg.* **1857**, 946–957
28. Sun, F., Huo, X., Zhai, Y., Wang, A., Xu, J., Su, D., Bartlam, M., and Rao, Z. (2005) Crystal structure of mitochondrial respiratory membrane protein Complex II. *Cell*. **121**, 1043–1057
29. Yankovskaya, V., Horsefield, R., Tornroth, S., Luna-Chavez, C., Miyoshi, H., Leger, C., Byrne, B., Cecchini, G., and Iwata, S. (2003) Architecture of succinate dehydrogenase and reactive oxygen species generation. *Science (80-.)*. **299**, 700–704

30. Cecchini, G., Schröder, I., Gunsalus, R. P., and Maklashina, E. (2002) Succinate dehydrogenase and fumarate reductase from *Escherichia coli*. *Biochim. Biophys. Acta.* **1553**, 140–157
31. Iwata, S. (1998) Complete Structure of the 11-Subunit Bovine Mitochondrial Cytochrome bc1 Complex. *Science (80-.)*. **281**, 64–71
32. Mitchell, P. (1975) The protonmotive Q cycle: A general formulation. *FEBS Lett.* **59**, 137–139
33. Balsa, E., Marco, R., Perales-Clemente, E., Szklarczyk, R., Calvo, E., Landázuri, M. O., and Enríquez, J. A. (2012) NDUFA4 is a subunit of complex IV of the mammalian electron transport chain. *Cell Metab.* **16**, 378–386
34. Yamashita, T., and Voth, G. A. (2012) Insights into the mechanism of proton transport in cytochrome c oxidase. *J. Am. Chem. Soc.* **134**, 1147–1152
35. Sazanov, L. A. (2015) A giant molecular proton pump: structure and mechanism of respiratory complex I. *Nat. Rev. Mol. Cell Biol.* **16**, 375–388
36. MITCHELL, P., and MOYLE, J. (1967) Chemiosmotic Hypothesis of Oxidative Phosphorylation. *Nature.* **213**, 137–139
37. Mitchell, P. (2011) Chemiosmotic coupling in oxidative and photosynthetic phosphorylation. *Biochim. Biophys. Acta - Bioenerg.* **1807**, 1507–1538
38. Busiello, R. A., Savarese, S., and Lombardi, A. (2015) Mitochondrial uncoupling proteins and energy metabolism. *Front. Physiol.* **6**, 36
39. Kim, E. H., Koh, E. H., Park, J.-Y., and Lee, K.-U. (2010) Adenine nucleotide translocator as a regulator of mitochondrial function: implication in the pathogenesis of metabolic syndrome. *Korean Diabetes J.* **34**, 146–53
40. Berg, J. M., Tymoczko, J. L., and Stryer, L. (2006) Biochemistry. 5th edition. in *Biochemistry textbook*, p. 1120, 10.1007/s13398-014-0173-7.2
41. Boyer, P. D. (1997) The ATP synthase - a splendid molecular machine. *Annu. Rev. Biochem.* **66**, 717–749
42. Yoshida, M., Muneyuki, E., and Hisabori, T. (2001) ATP synthase--a marvellous rotary engine of the cell. *Nat. Rev. Mol. Cell Biol.* **2**, 669–77
43. Murphy, M. P. (2009) How mitochondria produce reactive oxygen species. *Biochem. J.* **417**, 1–13
44. Mailloux, R. J., Gardiner, D., and O'Brien, M. (2016) 2-oxoglutarate dehydrogenase is a more significant source of O₂•⁻/H₂O₂ than pyruvate dehydrogenase in cardiac and liver tissue. *Free Radic. Biol. Med.* 10.1016/j.freeradbiomed.2016.06.014

45. St-Pierre, J., Buckingham, J. A., Roebuck, S. J., and Brand, M. D. (2002) Topology of superoxide production from different sites in the mitochondrial electron transport chain. *J. Biol. Chem.* **277**, 44784–90
46. Staniek, K., and Nohl, H. (2000) Are mitochondria a permanent source of reactive oxygen species? *Biochim. Biophys. Acta - Bioenerg.* **1460**, 268–275
47. Bienert, G. P., and Chaumont, F. (2014) Aquaporin-facilitated transmembrane diffusion of hydrogen peroxide. *Biochim. Biophys. Acta - Gen. Subj.* **1840**, 1596–1604
48. Winterbourn, C. C. (2008) Reconciling the chemistry and biology of reactive oxygen species. *Nat. Chem. Biol.* **4**, 278–286
49. Gardner, P. R., Raineri, I., Epstein, L. B., and White, C. W. (1995) Superoxide radical and iron modulate aconitase activity in mammalian cells. *J. Biol. Chem.* **270**, 13399–13405
50. Nulton-Persson, A. C., and Szwed, L. I. (2001) Modulation of Mitochondrial Function by Hydrogen Peroxide. *J. Biol. Chem.* **276**, 23357–23361
51. Kehrer, J. P. (2000) The Haber-Weiss reaction and mechanisms of toxicity. *Toxicology.* **149**, 43–50
52. Finkel, T. (2011) Signal transduction by reactive oxygen species. *J. Cell Biol.* **194**, 7–15
53. Dinkova-Kostova, A. T., and Abramov, A. Y. (2015) The emerging role of Nrf2 in mitochondrial function. *Free Radic. Biol. Med.* **88**, 179–188
54. Papa, S., and Skulachev, V. P. (1997) Reactive oxygen species , mitochondria , apoptosis and aging
55. Sena, L. A., Li, S., Jairaman, A., Prakriya, M., Ezponda, T., Hildeman, D. A., Wang, C. R., Schumacker, P. T., Licht, J. D., Perlman, H., Bryce, P. J., and Chandel, N. S. (2013) Mitochondria Are Required for Antigen-Specific T Cell Activation through Reactive Oxygen Species Signaling. *Immunity.* **38**, 225–236
56. Tormos, K. V., Anso, E., Hamanaka, R. B., Eisenbart, J., Joseph, J., Kalyanaraman, B., and Chandel, N. S. (2011) Mitochondrial complex III ROS regulate adipocyte differentiation. *Cell Metab.* **14**, 537–544
57. Kil, I. S., Lee, S. K., Ryu, K. W., Woo, H. A., Hu, M. C., Bae, S. H., and Rhee, S. G. (2012) Feedback Control of Adrenal Steroidogenesis via H₂O₂-Dependent, Reversible Inactivation of Peroxiredoxin III in Mitochondria. *Mol. Cell.* **46**, 584–594
58. Leloup, C., Turrel-Cuzin, C., Magnan, C., Karaca, M., Castel, J., Carneiro, L., Colombani, A. L., Ktorza, A., Casteilla, L., and Pénicaud, L. (2009) Mitochondrial reactive oxygen species are obligatory signals for glucose-induced insulin secretion. *Diabetes.* **58**, 673–681
59. Brand, M. D. (2016) Mitochondrial generation of superoxide and hydrogen peroxide as the

- source of mitochondrial redox signaling. *Free Radic. Biol. Med.* 10.1016/j.freeradbiomed.2016.04.001
60. Moreno-Sánchez, R., Hernández-Esquivel, L., Rivero-Segura, N. A., Marín-Hernández, A., Neuzil, J., Ralph, S. J., and Rodríguez-Enríquez, S. (2013) Reactive oxygen species are generated by the respiratory complex II - Evidence for lack of contribution of the reverse electron flow in complex I. *FEBS J.* **280**, 927–938
 61. O'Brien, M., Chalker, J., Slade, L., Gardiner, D., and Mailloux, R. J. (2017) Protein S-glutathionylation alters superoxide/hydrogen peroxide emission from pyruvate dehydrogenase complex. *Free Radic. Biol. Med.* **106**, 302–314
 62. Slade, L., Chalker, J., Kuksal, N., Young, A., Gardiner, D., and Mailloux, R. J. (2017) Examination of the superoxide/hydrogen peroxide forming and quenching potential of mouse liver mitochondria. *Biochim. Biophys. Acta - Gen. Subj.* 10.1016/j.bbagen.2017.05.010
 63. Chen, Y.-R., and Zweier, J. L. (2014) Cardiac mitochondria and reactive oxygen species generation. *Circ. Res.* **114**, 524–37
 64. Mailloux, R. J., McBride, S. L., and Harper, M. (2013) Unearthing the secrets of mitochondrial ROS and glutathione in bioenergetics. *Trends Biochem. Sci.* **38**, 592–602
 65. Fernandez-Checa, J. C., Kaplowitz, N., Garcia-Ruiz, C., and Colell, A. (1998) Mitochondrial glutathione: importance and transport. *Semin Liver Dis.* **18**, 389–401
 66. Booty, L. M., King, M. S., Thangaratnarajah, C., Majd, H., James, A. M., Kunji, E. R. S., and Murphy, M. P. (2015) The mitochondrial dicarboxylate and 2-oxoglutarate carriers do not transport glutathione. *FEBS Lett.* **589**, 621–628
 67. Garcia, J., Han, D., Sancheti, H., Yap, L. P., Kaplowitz, N., and Cadenas, E. (2010) Regulation of mitochondrial glutathione redox status and protein glutathionylation by respiratory substrates. *J. Biol. Chem.* **285**, 39646–39654
 68. Murphy, M. P. (2012) Mitochondrial Thiols in Antioxidant Protection and Redox Signaling: Distinct Roles for Glutathionylation and Other Thiol Modifications. 10.1089/ars.2011.4289
 69. Johansson, C., Lillig, C. H., and Holmgren, A. (2004) Human Mitochondrial Glutaredoxin Reduces S-Glutathionylated Proteins with High Affinity Accepting Electrons from Either Glutathione or Thioredoxin Reductase. *J. Biol. Chem.* **279**, 7537–7543
 70. Lundberg, M., Johansson, C., Chandra, J., Enoksson, M., Jacobsson, G., Ljung, J., Johansson, M., and Holmgren, A. (2001) Cloning and Expression of a Novel Human Glutaredoxin (Grx2) with Mitochondrial and Nuclear Isoforms. *J. Biol. Chem.* **276**, 26269–26275
 71. Cox, A. G., Winterbourn, C. C., and Hampton, M. B. (2010) Mitochondrial peroxiredoxin

- involvement in antioxidant defence and redox signalling. *Biochem. J.* **425**, 313–325
72. Trujillo, M., Clippe, A., Manta, B., Ferrer-Sueta, G., Smeets, A., Declercq, J. P., Knoop, B., and Radi, R. (2007) Pre-steady state kinetic characterization of human peroxiredoxin 5: Taking advantage of Trp84 fluorescence increase upon oxidation. *Arch. Biochem. Biophys.* **467**, 95–106
 73. Fu, Y., Cheng, W. H., Porres, J. M., Ross, D. A., and Lei, X. G. (1999) Knockout of cellular glutathione peroxidase gene renders mice susceptible to diquat-induced oxidative stress. *Free Radic. Biol. Med.* **27**, 605–611
 74. García-Ruiz, C., Colell, A., Morales, A., Kaplowitz, N., and Fernández-Checa, J. C. (1995) Role of oxidative stress generated from the mitochondrial electron transport chain and mitochondrial glutathione status in loss of mitochondrial function and activation of transcription factor nuclear factor-kappa B: studies with isolated mitochondria and. *Mol. Pharmacol.* **48**, 825–834
 75. Jastroch, M., Divakaruni, A. S., Mookerjee, S., Treberg, J. R., and Brand, M. D. (2010) Mitochondrial proton and electron leaks. *Essays Biochem.* **47**, 53–67
 76. Korshunov, S. S., Skulachev, V. P., and Starkov, A. A. (1997) High protonic potential actuates a mechanism of production of reactive oxygen species in mitochondria. *FEBS Lett.* **416**, 15–18
 77. Mailloux, R. J., and Harper, M. (2011) Uncoupling proteins and the control of mitochondrial reactive oxygen species production. *Free Radic. Biol. Med.* **51**, 1106–1115
 78. Brand, M. D., Buckingham, J. A., Esteves, T. C., Green, K., Lambert, A. J., Miwa, S., Murphy, M. P., Pakay, J. L., Talbot, D. A., and Echtay, K. S. (2004) Mitochondrial superoxide and aging: uncoupling-protein activity and superoxide production. *Biochem Soc Symp.* **71**, 203–213
 79. Toime, L. J., and Brand, M. D. (2010) Uncoupling protein-3 lowers reactive oxygen species production in isolated mitochondria. *Free Radic. Biol. Med.* **49**, 606–11
 80. Salvayre, A. N., Troly, M., and Upresa, C. (2017) A role for uncoupling protein-2 as a regulator of mitochondrial hydrogen peroxide generation. **11**, 809–815
 81. Teshima, Y., Akao, M., Jones, S. P., and Marbán, E. (2003) Uncoupling protein-2 overexpression inhibits mitochondrial death pathway in cardiomyocytes. *Circ. Res.* **93**, 192–200
 82. Vidal-Puig, a J., Grujic, D., Zhang, C. Y., Hagen, T., Boss, O., Ido, Y., Szczepanik, a, Wade, J., Mootha, V., Cortright, R., Muoio, D. M., and Lowell, B. B. (2000) Energy metabolism in uncoupling protein 3 gene knockout mice. *J. Biol. Chem.* **275**, 16258–16266
 83. Glatz, J. F. C., Moonen-kornips, E., Nabben, M., Hoeks, J., Briede, J. J., Hesselink, M. K. C., and Schrauwen, P. (2008) The effect of UCP3 overexpression on mitochondrial ROS

- production in skeletal muscle of young versus aged mice. **582**, 4147–4152
84. Trenker, M., Malli, R., Fertschai, I., Levak-Frank, S., and Graier, W. F. (2007) Uncoupling proteins 2 and 3 are fundamental for mitochondrial Ca²⁺ uniport. *Nat. Cell Biol.* **9**, 445–452
 85. Schrauwen, P., Hoeks, J., Schaart, G., Kornips, E., Binas, B., Van De Vusse, G. J., Van Bilsen, M., Luiken, J. J., Coort, S. L., Glatz, J. F., Saris, W. H., and Hesselink, M. K. (2003) Uncoupling protein 3 as a mitochondrial fatty acid anion exporter. *FASEB J.* **17**, 2272–2274
 86. Brand, M. D. (2016) Mitochondrial generation of superoxide and hydrogen peroxide as the source of mitochondrial redox signaling. *Free Radic. Biol. Med.* 10.1016/j.freeradbiomed.2016.04.001
 87. Schagger, H. (2000) Supercomplexes in the respiratory chains of yeast and mammalian mitochondria. *EMBO J.* **19**, 1777–1783
 88. Acín-Pérez, R., Fernández-Silva, P., Peleato, M. L., Pérez-Martos, A., and Enriquez, J. A. (2008) Respiratory Active Mitochondrial Supercomplexes. *Mol. Cell.* **32**, 529–539
 89. Acin-perez, R., and Enriquez, J. A. (2014) Biochimica et Biophysica Acta The function of the respiratory supercomplexes : The plasticity model ☆☆. *BBA - Bioenerg.* **1837**, 444–450
 90. Porras, C. A.-M., and Bai, Y. (2015) Respiratory supercomplexes: plasticity and implications. *Front. Biosci.* **20**, 621–34
 91. Maranzana, E., Barbero, G., Falasca, A. I., Lenaz, G., and Genova, M. L. (2013) Mitochondrial respiratory supercomplex association limits production of reactive oxygen species from complex I. *Antioxid. Redox Signal.* **19**, 1469–80
 92. Maranzana, E., Barbero, G., Falasca, A. I., Lenaz, G., and Genova, M. L. (2013) Mitochondrial Respiratory Supercomplex Association Limits. 10.1089/ars.2012.4845
 93. Shelton, M. D., Chock, P. B., and Mieyal, J. J. (2005) Glutaredoxin: role in reversible protein s-glutathionylation and regulation of redox signal transduction and protein translocation. *Antioxid. Redox Signal.* **7**, 348–366
 94. Lowther, W. T., and Haynes, A. C. (2011) Reduction of Cysteine Sulfinic Acid in Eukaryotic, Typical 2-Cys Peroxiredoxins by Sulfiredoxin. *Antioxid. Redox Signal.* **15**, 99–109
 95. Rehder, D. S., and Borges, C. R. (2010) Cysteine sulfenic acid as an intermediate in disulfide bond formation and nonenzymatic protein folding. *Biochemistry.* **49**, 7748–7755
 96. Jensen, K. S., Pedersen, J. T., Winther, J. R., and Teilum, K. (2014) The pKa value and accessibility of cysteine residues are key determinants for protein substrate discrimination by glutaredoxin. *Biochemistry.* **53**, 2533–2540

97. Klaus, A., Zorman, S., Berthier, A., Polge, C., Ramirez, S., Michelland, S., Sève, M., Vertommen, D., Rider, M., Lentze, N., Auerbach, D., and Schlattner, U. (2013) Glutathione S-Transferases Interact with AMP-Activated Protein Kinase: Evidence for S-Glutathionylation and Activation In Vitro. *PLoS One*. 10.1371/journal.pone.0062497
98. Gallogly, M. M., and Mieyal, J. J. (2007) Mechanisms of reversible protein glutathionylation in redox signaling and oxidative stress. *Curr. Opin. Pharmacol.* **7**, 381–391
99. Mailloux, R. J., and Willmore, W. G. (2014) S-glutathionylation reactions in mitochondrial function and disease. *Front. cell Dev. Biol.* **2**, 68
100. Chen, Y.-R., Chen, C.-L., Pfeiffer, D. R., and Zweier, J. L. (2007) Mitochondrial complex II in the post-ischemic heart: oxidative injury and the role of protein S-glutathionylation. *J. Biol. Chem.* **282**, 32640–54
101. Dröse, S., Brandt, U., and Wittig, I. (2014) Mitochondrial respiratory chain complexes as sources and targets of thiol-based redox-regulation. *Biochim. Biophys. Acta - Proteins Proteomics.* **1844**, 1344–1354
102. McGarry, D. J., Chen, W., Chakravarty, P., Lamont, D. L., Wolf, C. R., and Henderson, C. J. (2015) Proteome-wide identification and quantification of S-glutathionylation targets in mouse liver. *Biochem. J.* **469**, 25–32
103. Pai, H. V., Starke, D. W., Lesnefsky, E. J., Hoppel, C. L., and Mieyal, J. J. (2007) What is the Functional Significance of the Unique Location of Glutaredoxin 1 (GRx1) in the Intermembrane Space of Mitochondria? *Antioxid. Redox Signal.* **9**, 2027–2034
104. Mannervik, B., and Axelsson, K. (1980) Role of cytoplasmic thioltransferase in cellular regulation by thiol-disulphide interchange. *Biochem. J.* **190**, 125–130
105. Gladyshev, V. N., Liu, A., Novoselov, S. V., Krysan, K., Sun, Q. A., Kryukov, V. M., Kryukov, G. V., and Lou, M. F. (2001) Identification and Characterization of a New Mammalian Glutaredoxin (Thioltransferase), Grx2. *J. Biol. Chem.* **276**, 30374–30380
106. Lillig, C. H., Berndt, C., Vergnolle, O., Lönn, M. E., Hudemann, C., Bill, E., and Holmgren, A. (2005) Characterization of human glutaredoxin 2 as iron-sulfur protein: a possible role as redox sensor. *Proc. Natl. Acad. Sci. U. S. A.* **102**, 8168–73
107. Lönn, M. E., Hudemann, C., Berndt, C., Cherkasov, V., Capani, F., Holmgren, A., and Lillig, C. H. (2008) Expression Pattern of Human Glutaredoxin 2 Isoforms: Identification and Characterization of Two Testis/Cancer Cell-Specific Isoforms. *Antioxid. Redox Signal.* **10**, 547–558
108. Mashamaite, L. N., Rohwer, J. M., and Pillay, S. (2015) The glutaredoxin mono- and di-thiol mechanisms for deglutathionylation are functionally equivalent: implications for redox systems biology. 10.1042/BSR20140157

109. Starke, D. W., Chock, P. B., and Mieyal, J. J. (2003) Glutathione-thiyl radical scavenging and transferase properties of human glutaredoxin (thioltransferase): Potential role in redox signal transduction. *J. Biol. Chem.* **278**, 14607–14613
110. Johansson, C., Kavanagh, K. L., Gileadi, O., and Oppermann, U. (2007) Reversible sequestration of active site cysteines in a 2Fe-2S-bridged dimer provides a mechanism for glutaredoxin 2 regulation in human mitochondria. *J. Biol. Chem.* **282**, 3077–3082
111. Diotte, N. M., Xiong, Y., Gao, J., Chua, B. H. L., and Ho, Y. S. (2009) Attenuation of doxorubicin-induced cardiac injury by mitochondrial glutaredoxin 2. *Biochim. Biophys. Acta - Mol. Cell Res.* **1793**, 427–438
112. Lillig, C. H., Lönn, M. E., Enoksson, M., Fernandes, A. P., and Holmgren, A. (2004) Short interfering RNA-mediated silencing of glutaredoxin 2 increases the sensitivity of HeLa cells toward doxorubicin and phenylarsine oxide. *Proc. Natl. Acad. Sci. U. S. A.* **101**, 13227–32
113. Wu, H., Yu, Y., David, L., Ho, Y. S., and Lou, M. F. (2014) Glutaredoxin 2 (Grx2) gene deletion induces early onset of age-dependent cataracts in mice. *J. Biol. Chem.* **289**, 36125–36139
114. Brautigam, L., Schutte, L. D., Godoy, J. R., Prozorovski, T., Gellert, M., Hauptmann, G., Holmgren, a., Lillig, C. H., and Berndt, C. (2011) Vertebrate-specific glutaredoxin is essential for brain development. *Proc. Natl. Acad. Sci.* **108**, 20532–20537
115. Bräutigam, L., Jensen, L. D. E., Poschmann, G., Nyström, S., Bannenberg, S., Dreij, K., Lepka, K., Prozorovski, T., Montano, S. J., Aktas, O., Uhlén, P., Stühler, K., Cao, Y., Holmgren, A., and Berndt, C. (2013) Glutaredoxin regulates vascular development by reversible glutathionylation of sirtuin 1. *Proc. Natl. Acad. Sci. U. S. A.* **110**, 20057–62
116. Berndt, C., Poschmann, G., Stühler, K., Holmgren, A., and Bräutigam, L. (2014) Zebrafish heart development is regulated via glutaredoxin 2 dependent migration and survival of neural crest cells. *Redox Biol.* **2**, 673–678
117. Mailloux, R. J., Xuan, J. Y., McBride, S., Maharsy, W., Thorn, S., Holterman, C. E., Kennedy, C. R. J., Rippstein, P., Silva, J., Nemer, M., Lou, M., and Harper, M. (2014) Glutaredoxin-2 Is Required to Control Oxidative Phosphorylation in Cardiac Muscle by Mediating Deglutathionylation Reactions *. **289**, 14812–14828
118. Enoksson, M., Fernandes, A. P., Prast, S., Lillig, C. H., Holmgren, A., and Orrenius, S. (2005) Overexpression of glutaredoxin 2 attenuates apoptosis by preventing cytochrome c release. *Biochem. Biophys. Res. Commun.* **327**, 774–779
119. Balijepalli, S., Annepu, J., Boyd, M. R., and Ravindranath, V. (1999) Effect of thiol modification on brain mitochondrial complex I activity. *Neurosci. Lett.* **272**, 203–206
120. Beltrán, B., Orsi, a, Clementi, E., and Moncada, S. (2000) Oxidative stress and S-nitrosylation of proteins in cells. *Br. J. Pharmacol.* **129**, 953–960

121. Taylor, E. R., Hurrell, F., Shannon, R. J., Lin, T. K., Hirst, J., and Murphy, M. P. (2003) Reversible glutathionylation of complex I increases mitochondrial superoxide formation. *J. Biol. Chem.* **278**, 19603–19610
122. Hurd, T. R., Requejo, R., Filipovska, A., Brown, S., Prime, T. A., Robinson, A. J., Fearnley, I. M., and Murphy, M. P. (2008) Complex I within oxidatively stressed bovine heart mitochondria is glutathionylated on Cys-531 and Cys-704 of the 75-kDa subunit: Potential role of Cys residues in decreasing oxidative damage. *J. Biol. Chem.* **283**, 24801–24815
123. Beer, S. M., Taylor, E. R., Brown, S. E., Dahm, C. C., Costa, N. J., Runswick, M. J., and Murphy, M. P. (2004) Glutaredoxin 2 catalyzes the reversible oxidation and glutathionylation of mitochondrial membrane thiol proteins: Implications for mitochondrial redox regulation and antioxidant defense. *J. Biol. Chem.* **279**, 47939–47951
124. Quinlan, C., Orr, A., Perevoshchikova, I., Treberg, J., Ackrell, B., and Brand, M. (2012) Mitochondrial Complex II Can Generate Reactive Oxygen Species at High Rates in Both the Forward and Reverse. *J. Biol. Chem.* **287**, 27255–64
125. Starkov, A. A. (2004) Mitochondrial Alpha-Ketoglutarate Dehydrogenase Complex Generates Reactive Oxygen Species. *J. Neurosci.* **24**, 7779–7788
126. Tretter, L., and Tam-Vizi, V. (2004) Generation of reactive oxygen species in the reaction catalyzed by alpha-ketoglutarate dehydrogenase. *J. Neurosci.* **24**, 7771–7778
127. Fisher-Wellman, K. H., Gilliam, L. A. A., Lin, C. Te, Cathey, B. L., Lark, D. S., and Darrell Neuffer, P. (2013) Mitochondrial glutathione depletion reveals a novel role for the pyruvate dehydrogenase complex as a key H₂O₂-emitting source under conditions of nutrient overload. *Free Radic. Biol. Med.* **65**, 1201–1208
128. Quinlan, C. L., Goncalves, R. L. S., Hey-Mogensen, M., Yadava, N., Bunik, V. I., and Brand, M. D. (2014) The 2-oxoacid dehydrogenase complexes in mitochondria can produce superoxide/hydrogen peroxide at much higher rates than complex I. *J. Biol. Chem.* **289**, 8312–8325
129. Nulton-Persson, A. C., Starke, D. W., Mieyal, J. J., and Szweda, L. I. (2003) Reversible inactivation of alpha-ketoglutarate dehydrogenase in response to alterations in the mitochondrial glutathione status. *Biochemistry.* **42**, 4235–4242
130. Applegate, M. A. B., Humphries, K. M., and Szweda, L. I. (2008) Reversible inhibition of alpha-ketoglutarate dehydrogenase by hydrogen peroxide: Glutathionylation and protection of lipoic acid. *Biochemistry.* **47**, 473–478
131. McLain, A. L., Cormier, P. J., Kinter, M., and Szweda, L. I. (2013) Glutathionylation of alpha-ketoglutarate dehydrogenase: The chemical nature and relative susceptibility of the cofactor lipoic acid to modification. *Free Radic. Biol. Med.* **61**, 161–169
132. Mailloux, R. J., Craig Ayre, D., and Christian, S. L. (2016) Induction of mitochondrial reactive oxygen species production by GSH mediated S-glutathionylation of 2-oxoglutarate

- dehydrogenase. *Redox Biol.* **8**, 285–297
133. Echtay, K. S., Roussel, D., St-pierre, J., Jekabsons, M. B., Cadenas, S., Stuart, J. A., Harper, J. A., Roebuck, S. J., Morrison, A., Pickering, S., Clapham, J. C., and Brand, M. D. (2002) Superoxide activates mitochondrial uncoupling proteins
 134. Mailloux, R. J., Xuan, J. Y., Beauchamp, B., Jui, L., Lou, M., and Harper, M. (2013) Glutaredoxin-2 Is Required to Control Proton Leak through. **288**, 8365–8379
 135. Wu, H., Lin, L., Giblin, F., Ho, Y., and Lou, M. F. (2011) Free Radical Biology & Medicine Glutaredoxin 2 knockout increases sensitivity to oxidative stress in mouse lens epithelial cells ☆. *Free Radic. Biol. Med.* **51**, 2108–2117
 136. Miyadera, H., Shiomi, K., Ui, H., Yamaguchi, Y., Masuma, R., Tomoda, H., Miyoshi, H., Osanai, A., Kita, K., and Omura, S. (2003) Atpenins, potent and specific inhibitors of mitochondrial complex II (succinate-ubiquinone oxidoreductase). *Proc. Natl. Acad. Sci. U. S. A.* **100**, 473–7
 137. Lambert, A. J., and Brand, M. D. (2004) Inhibitors of the quinone-binding site allow rapid superoxide production from mitochondrial NADH:ubiquinone oxidoreductase (complex I). *J. Biol. Chem.* **279**, 39414–39420
 138. Angelides, K. J., Akiyama, S. K., and Hammes, G. G. (1979) Subunit stoichiometry and molecular weight of the pyruvate dehydrogenase multienzyme complex from *Escherichia coli*. *Proc. Natl. Acad. Sci. U. S. A.* **76**, 3279–83
 139. Robitaille, S., Mailloux, R. J., and Chan, H. M. (2016) Methylmercury alters glutathione homeostasis by inhibiting glutaredoxin 1 and enhancing glutathione biosynthesis in cultured human astrocytoma cells. *Toxicol. Lett.* **256**, 1–10
 140. Rachel Gergondey, Camille Garcia, Christophe H. Marchand, Stephane D. Lemaire, Jean-Michel Camadro, F. A. (2017) Modulation of the specific glutathionylation of mitochondrial proteins in the yeast *Saccharomyces cerevisiae* under basal and stress conditions. *Biochem. J.* **474**, 1175–1193
 141. Mailloux, R. J., Seifert, E. L., Collins, S., and Harper, M. (2011) Glutathionylation Acts as a Control Switch for Uncoupling. **286**, 21865–21875
 142. Nicholls, D. G., and Ferguson, S. J. (2003) *Bioenergetics*, 10.1016/B978-012518121-1/50011-7
 143. Wu, H., Xing, K., and Lou, M. F. (2010) Glutaredoxin 2 prevents H₂O₂-induced cell apoptosis by protecting complex I activity in the mitochondria. *Biochim. Biophys. Acta - Bioenerg.* **1797**, 1705–1715
 144. Daily, D., Vlamis-Gardikas, A., Offen, D., Mittelman, L., Melamed, E., Holmgren, A., and Barzilai, A. (2001) Glutaredoxin Protects Cerebellar Granule Neurons from Dopamine-induced Apoptosis by Dual Activation of the Ras-Phosphoinositide 3-Kinase and Jun N-

terminal Kinase Pathways. *J. Biol. Chem.* **276**, 21618–21626

145. Ferri, A., Fiorenza, P., Nencini, M., Cozzolino, M., Pesaresi, M. G., Valle, C., Sepe, S., Moreno, S., and Carrì, M. T. (2010) Glutaredoxin 2 prevents aggregation of mutant SOD1 in mitochondria and abolishes its toxicity. *Hum. Mol. Genet.* **19**, 4529–4542
146. Lepka, K., Volbracht, K., Bill, E., Schneider, R., Rios, N., Hildebrandt, T., Ingwersen, J., Prozorovski, T., Lillig, C. H., Horssen, J. van, Steinman, L., Hartung, H.-P., Radi, R., Holmgren, A., Aktas, O., and Berndt, C. (2017) Iron-sulfur glutaredoxin 2 protects oligodendrocytes against damage induced by nitric oxide release from activated microglia. *Glia.* **65**, 1521–1534
147. Casagrande, S., Bonetto, V., Fratelli, M., Gianazza, E., Eberini, I., Massignan, T., Salmona, M., Chang, G., Holmgren, A., and Ghezzi, P. (2002) Glutathionylation of human thioredoxin: A possible crosstalk between the glutathione and thioredoxin systems. *Proc Natl Acad Sci U S A.* **99**, 9745–9749
148. Raza, H., Robin, M.-A., Fang, J.-K., and Avadhani, N. G. (2002) Multiple isoforms of mitochondrial glutathione S-transferases and their differential induction under oxidative stress. *Biochem. J.* **366**, 45–55
149. Gusdon, A. M., Fernandez-bueno, G. A., Wohlgemuth, S., Fernandez, J., Chen, J., and Mathews, C. E. (2015) Respiration and substrate transport rates as well as reactive oxygen species production distinguish mitochondria from brain and liver. *BMC Biochem.* **16**, 1–17
150. Tahara, E. B., Navarete, F. D. T., and Kowaltowski, A. J. (2009) Tissue-, substrate-, and site-specific characteristics of mitochondrial reactive oxygen species generation. *Free Radic. Biol. Med.* **46**, 1283–1297
151. Shabalina, I. G., and Nedergaard, J. (2011) Mitochondrial ('mild') uncoupling and ROS production: physiologically relevant or not? *Biochem. Soc. Trans.* **39**, 1305–9